Alma Mater Studiorum - Università di Bologna

DOTTORATO DI RICERCA IN

MECCANICA E SCIENZE AVANZATE DELL'INGEGNERIA

Ciclo 34

Settore Concorsuale: 09/C1 - MACCHINE E SISTEMI PER L'ENERGIA E L'AMBIENTE

Settore Scientifico Disciplinare: ING-IND/08 - MACCHINE A FLUIDO

DESIGN AND OFF-DESIGN MODELLING OF ADVANCED POWER-TO-GAS ENERGY STORAGE SYSTEMS

Presentata da: Francesco Catena

Coordinatore Dottorato

Marco Carricato

Supervisore

Andrea De Pascale

Co-supervisore

Francesco Melino

Esame finale anno 2022

Abstract

Power-to-Gas storage systems have the potential to address grid-stability issues that arise when an increasing share of power is generated from sources that have a highly variable output. Although the proof-of-concept of these has been promising, the behaviour of the processes in off-design conditions is not easily predictable.

The primary aim of this PhD project was to evaluate the performance of an original Power-to-Gas system, made up of innovative components. To achieve this, a numerical model has been developed to simulate the characteristics and the behaviour of the several components when the whole system is coupled with a renewable source. The developed model has been applied to a large variety of scenarios, evaluating the performance of the considered process and exploiting a limited amount of experimental data. The model has been then used to compare different Power-to-Gas concepts, in a real scenario of functioning.

Several goals have been achieved. In the concept phase, the possibility to thermally integrate the high temperature components has been demonstrated. Then, the parameters that affect the energy performance of a Power-to-Gas system coupled with a renewable source have been identified, providing general recommendations on the design of hybrid systems; these parameters are: 1) the ratio between the storage system size and the renewable generator size; 2) the type of coupled renewable source; 3) the related production profile. Finally, from the results of the comparative analysis, it is highlighted that configurations with a highly oversized renewable source with respect to the storage system show the maximum achievable profit.

Contents

List of Figures

Chapter 4

Chapter 5

Chapter 6

List of Tables

Chapter 6

Nomenclature

Abbreviations

AC	After-cooler
C	Compression
C	Tuning coefficient
CCS	Carbon capture and storage
CE	Co-electrolysis
CR	Conversion rate
E2F	Electric-to-fuel
G2P	Gas-to-power
HE	Heat exchanger
HRS	Heat recovery section
HT	High temperature
HTE	High temperature electrolyzer
HTM	High temperature methanation
HX	Heat exchanger
IC	Inter-cooler
Liq	Liquid
LT	Low temperature
LTE	Low temperature electrolyzer
LTM	Low temperature methanation
NG	Natural gas
NP-RES	Non-programmable renewable energy source
O&M	Operation and maintenance
PC	Pre-cooler
PEM	Proton exchange membrane
PEMFC	Proton exchange membrane fuel cell
PEV	Plug-in electric vehicle
PtH_2	Power-to-hydrogen
PtM	Power-to-methane
P2G	Power-to-Gas
R	Reactor
SCS	Solution combustion synthesis
SE	Steam electrolysis
Sep	Separation
SNG	Synthetic natural gas

SOE	Solid oxide electrolyzer
SOEC	Solid oxide electrolyte cell
Syn	Synthesis gas
TRL	Technology readiness level
V2G	Vehicle-to-grid

Symbols

A	Area [m^2]
C	Cost [€]
c	Specific heat [J/kgK]
E	Electric energy [kW]
F	Faraday constant [C/kmol]
f	Utilization factor [-]
g	Gibbs free energy [kJ/kmol]
GHSV	Gas hourly space velocity [h^{-1}]
h	Specific molar enthalpy [kJ/kmol]
HHV	Higher heating value [kJ/kg]
I	Electric current [A]
i	Time step [-]
IR	Index of recovery [-]
J	Electric current density [A/m^2]
LHV	Lower heating value [kJ/kg]
$\dot{m}$	Mass flow rate [kg/s]
n	Iterative index [-]
$\dot{n}$	Molar flow rate [kmol/s]
OCV	Open circuit voltage [V]
P	Electrical power [kW]
p	Pressure [bar]
$\dot{Q}$	Thermal power [kW]
R	Power size ratio [-]
s	Specific molar enthalpy [kJ/kmolK]
T	Temperature [°C]
t	Time step [-]
U	Global heat transfer coefficient [W/m^2K]
V	Voltage [V]
WI	Wobbe index [kJ/Sm^3]

x	Molar fraction [$\%_{vol}$]
Z	Valency number of ions [-]

Greek symbols

Δ	Difference [-]
η	Efficiency [-]
ρ	Density [kg/m^3]

Subscripts and superscripts

E	electricity
el	electrical
eq	equivalent
exp	experimental
fc	fuel cell
in	inlet
max	maximum
min	minimum
out	outlet
p	pressure
tn	thermoneutral
tot	total
u	utilization
I	first law
II	second law

Chapter 1 - Introduction

1.1 – State-of-the-art

The mission of the 2030 Climate Target Plan [1] is to provide a practical, independent and objective analysis of pathways to achieve a low-carbon economy in Europe, in line with the energy security, environmental and economic goals of the European Union. In order to meet these climate targets, a possible solution is to increase the penetration of renewable energy sources into the electrical system. However, renewable generation is affected by environmental, seasonal and daily cycles that can limit their use or efficiency. As such, renewable sources cannot always consistently produce energy at all hours of the day. This intermittency leads to issues related to the management of local and regional electric networks, due to the several hours and even days of electricity surplus and deficit. Indeed, as pointed out by Karimi et al. [2], despite its development, photovoltaic penetration shows several issues, such as the voltage stability, the power quality and the reliability, and additional challenges will need to be dealt with in the future. Moreover, in the study of Eltawil and Zhao [3], the operation of grid-connected photovoltaic generators has been evaluated, demonstrating that the intermittent power generation results in management issues. Likewise, as reported by Jung et al. [4], wind generators are affected by a short-term non-programmable and intermittent power production and by a long-term variability too.

As the share of these sources in power generation increases, electric energy has to be stored to be made available when needed. Therefore, the long-term and large-scale storage demand for high energy density, low costs and little self-discharging will rise in the near future. A solution to these needs can be represented by the so-called Power-to-Gas (P2G) technology [5] (i.e. the process of converting the surplus of renewable electrical energy into a gaseous fuel), which allows to store electric power by producing renewable gases (such as hydrogen, methane and methanol - see Fig. 1.1). Complementary to green power, this technology is able to produce green or clean gases contributing to meet the climate targets; indeed, green gases could represent a feedstock for several industrial processes, reducing at the same time carbon emissions too. In addition, the P2G technology is a pivotal element for the coupling of the electric and gas infrastructures, encouraging the integration of renewable sources into well established and high performing energy storage and distribution systems. As shown by Kilkis et al. [6], the Power-to-X technologies (multiplicity of electricity conversion, energy storage and reconversion pathways that use surplus electric power) offer a wide range of opportunities to integrate variable renewable energy sources into useful forms of energy that are demanded at the specific moment or a later use; among these technologies, the P2G

concept can offer the benefit of allowing renewable power to be converted into a synthetic fuel as a way of integrating the power and gas grids.

Regarding this storage concept for a later electricity production, the system is usually made up of an electrolyzer, in order to produce hydrogen through the electrolysis of water, a storage system and a Gas-to-Power (G2P) system. At the same time, also the production of Synthetic natural Gas (SNG) as energy vector is gaining attention in recent times, due to the possibility of introducing the SNG into the local natural gas network [7]; in this case, an additional hydrogen upgrading section to convert the reactants into a methane rich fuel is requested. Regarding the methanation section, carbon dioxide is also required as reactant: in this way, the P2G storage system is able to recycle carbon dioxide, towards the mitigation of climate change issues involved by the power generation and other industrial sectors. Indeed, the amount of carbon dioxide required by the P2G system can be provided by power plants run on conventional fuels, by other carbon intensive industrial sectors (e.g. cement and ammonia production processes) or by biomass conversion processes (as shown by Wei and Jinlong [8]). As a consequence, a P2G technology coupled with carbon capture and storage (CCS) systems [9] can be also considered a potential pathway for decarbonization of power and industrial sectors.

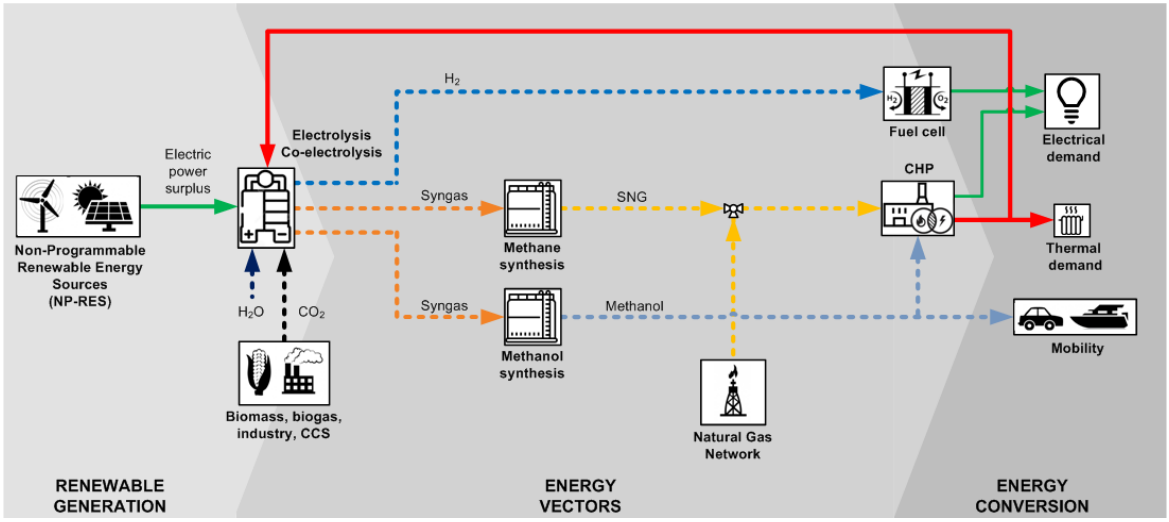

Fig. 1.1. The main pathways of the Power-to-Gas technology concept.

One of the key elements requiring proper design for a P2G application is the electrolyzer. On this matter, Anwar et al. [10] have presented a recent literature review on the developments for hydrogen production through water electrolysis, focusing on the current status of water electrolysis for energy storage and highlighting the different developments between low and high temperature electrolyzers. Indeed, low temperature water electrolyzers (LTE), operating below 100 °C and based on Proton Exchange Membrane (PEM) or Potassium Hydroxide (KOH) electrolyte technologies, are currently commercial products [11]. High temperature

steam electrolyzers (HTE), typically operating in the range 600 – 900 °C and based on the Solid Oxide Electrolyte Cell (SOEC) technology [12], instead, are still at the pre-commercial stage for multi-kW-range size (e.g. see the HELMETH EU project [13] or the HEPP project [14]). Nevertheless, HTE expected efficiency is very promising: values nearly 100 % (if thermal integration is considered) are mentioned in a recent study of Li et al. [15], remarkably higher with respect to the LTE efficiency level (average values can be estimated around 55 – 70 % [16]). The overall P2G system efficiency, based on HTE, has been targeted to values around 70 – 75 % on HHV basis in the work of Wang et al. [17]. In order to demonstrate the advantages of HTE technology, a few pilot plants have been developed in recent years, even if the large part of pilot and demonstration plants still use LTE, as summarized in an overview of P2G projects by Liao et al. [18].

In the case of SNG as final product of the considered P2G process, a methanation section is also required. Regarding the methanation technologies, several concepts are currently available (fixed-bed reactors, structured reactors or fluidized-bed reactors), as shown in the literature review of Rönsch et al. [19], in which fundamentals and current projects are presented.

In the recent literature, different features of renewable systems based on the P2G technology have been investigated. In [20], Nastasi et al. have carried out a sensitivity analysis among several buildings provided with photovoltaic panels, with the aim to compare processes of a hydrogen storage and an electrical one, showing that the choice of the hydrogen technology to be installed is affected by the system scale. A novel P2G process, based on the carbon dioxide recycling from gas-fired power plant emissions into SNG, has been proposed by Momeni et al. [21]; the system has been assessed from the technical, economic and environmental points of view, pointing out that an optimized system could reduce the SNG cost and could lead to a high reduction of CO_2 emissions. Instead, Xiong et al. [22] have evaluated how the P2G technologies could provide spatial and temporal flexibility to the energy production by integrating the electrical grid to the gas infrastructure; indeed, in the study it is highlighted that the introduction of P2G systems could bring flexibility to the electric system, leading to a better use of renewable energy sources. Furthermore, Liu et al. [23] have proposed a multi-objective operational strategy of an integrated system, considering the thermal demand and the P2G storage, with the aim to obtain the maximum environmental relief. Moreover, in the work of Wang et al. [24], a method of coupling the natural gas system and the power system using P2G and gas turbines has been proposed, in order to improve the absorption capacity of hydropower and reduce the amount of surplus water. Finally, Zhai et al. [25] have analysed how to use a P2G facility to increase the grid connected ratio of new power generation; this work proposes a solution to this issue, concluding that P2G technology is effective in stabilizing the volatility and shows significant economic benefits.

In this context, the PhD project is based on the evaluation of the behaviour of an innovative P2G system at various loading conditions, considering the variability of the electric energy supply. The aim of the research is the development of a mathematical model for the design and off-design operations of the P2G process. In particular, the project focuses on an innovative P2G process based on a high temperature co-electrolyzer (simultaneous electrolysis of water and carbon dioxide) with a SOEC technology. The developed model allows to evaluate the behaviour of the P2G process in design condition and it is able to predict the characteristics of each component when the operating point of the system is modified. The detail of the novelty of the proposed research project is discussed in the following paragraph.

1.2 – Research project contribution

The primary aim of this research is to characterize and evaluate the performance of an original Power-to-Gas system, made up of innovative components. To achieve this, a numerical model has been developed to simulate the characteristics and the behaviour of the several components when the whole system is coupled with a renewable source.
The considered P2G system is made up of a high temperature section and a low temperature section. The high temperature section represents the core of the whole system and it is composed by two innovative components:

- a high temperature co-electrolyzer of SOEC technology, in which co-electrolysis reactions of water and carbon dioxide occur;
- a high temperature methanation sub-section, based on an experimental structured catalyst, producing a rough synthetic natural gas.

The low temperature section has been implemented in order to improve the quality of the produced SNG. In more detail, this section is composed by:

- a low temperature methanation section, based on a conventional catalytic technology;
- a SNG processing section.

In addition, a pre-heating section has been implemented in order to achieve significant energy savings by means of internal heat recovery.
Even if the considered P2G system shows some components that have already achieved the technology maturity (conventional methanation section, heat exchangers, pumps, compressors and the other plant auxiliaries), it can be considered that the development level of the proposed storage solution is currently in a range of TRL (Technology Readiness Level) values between 3 and 5 (3: experimental proof of concept; 4: technology validated in laboratory; 5: technology validated in relevant environment). This level of innovation refers

both to specific key components and to the whole system, with particular attention to the following innovative features:

- the whole high temperature section, that includes: 1) the high temperature SOEC co-electrolyzer, a key component of the system, whose functioning in co-electrolysis mode is still not a technology standard for sizes as large as those considered in this study [17] - [26]; 2) the high temperature methanator, fundamental in order to obtain a SNG stream with a high content of methane; it is based on an experimental reactor tested in the CNR-ITAE laboratory on small scale [27] - [28], that differs from the conventional methanation technologies operating at low temperatures;
- the specific operating conditions of the SOEC, in the study considered operating up to intermediate temperature levels (600 °C), on average less high [29] than the typical operating range (800 – 1000 °C);
- the thermal integration between the SOEC and the downstream experimental reactor represents a potential innovation, promising from the thermodynamic performance point of view;
- the development of an energy storage system of P2G technology, based on the high temperature electrolysis on large scale, that could achieve energy conversion efficiencies higher with respect to the conventional P2G configurations, based on low temperature electrolyzers of PEM technology.

In a first approach, the thermodynamic performance of the proposed P2G process have been evaluated through different parameters in design condition. In this first step, the novelty stands in the development and analysis of the P2G system, considering the possibility to thermally integrate the electrolysis with the methanation process, as a first step towards a physical integration between the two components.
In this first study, the analysis has been carried out in design condition, considering all the sub-sections working at their set-points of operating temperature and pressure. In order to evaluate the behaviour of the several components in off-design conditions, a numerical code has been developed. The originality of the developed model is represented by the possibility to predict the performance of any P2G process in conditions far from the design point, on the basis of a limited set of experimental data. This particular feature makes the model capable of being applied to a large variety of scenarios, in which the aim is to evaluate the characteristics and the performance of the considered process, exploiting a limited amount of data.
Finally, an innovative comparison between different P2G concepts, in a scenario in which also G2P systems and electrical demands are considered, has been proposed. In more detail, the aim of this line of research is to compare the behaviour of different storage paths when integrated in a real scenario of functioning, with a real renewable production and a real electrical demand. The P2G concepts that have been considered differ in the used energy

vector: one concept is based on the SNG and the other concept is based on the hydrogen; this distinction adopted in the study is essential in order to figure out the behaviour in a real application of the two main energy vectors involved in the energy transition.

1.3 – Structure of the manuscript

The thesis is divided into three main parts.

Part I. The first part presents the proposed Power-to-Gas concept and a description of the developed model, outlining the fundamental key aspects concerning the Power-to-Gas conversion process. In particular, Chapter 2 introduces the concept and the architecture of the Power-to-Gas solution analysed during the PhD project. Chapter 3, instead, focuses on the developed numerical model, considering both the design and off-design modelling.

Part II. In this section, a thermodynamic analysis has been carried out in order to assess the influence of the main operating parameters and of the plant configuration on the P2G process performance. In particular, in Chapter 4 parametric analyses on the behaviour of the P2G system in design conditions have been carried out, starting from a reference case, analysing several operating temperatures of the main components of the system, by means of the in-house developed numerical model. In addition, a further thermodynamic analysis has been carried out, in which the operating pressure of the main components has been varied. In particular, the thermodynamic model has been modified, evaluating and comparing different configurations of the system layout, in which the pressurization section has been placed differently. Then, in Chapter 5 the P2G system has been analysed in off-design conditions in two different steps. In the first step, a specific renewable generation scenario has been selected, characterized by a set renewable source and by an assigned size in terms of power size. Then, in the second step, several operating scenarios have been analysed, by means of a parametric evaluation, in order to expand the obtained results and make them applicable in a wider range of situations.

Part III. Chapter 6 describes the comparison between different Power-to-Gas concepts in a microgrid application, carried out during the PhD period abroad, at the École Polytechnique Fédérale de Lausanne (EPFL) – Valais offices. In more detail, the two different concepts (hydrogen-based and SNG-based) have been compared from the thermodynamic point of view. Then, a decision-making parameter has been defined in order to establish the best solution among the obtained results.

1.4 – Acknowledgments

The PhD research project has been supported by Ricerca di Sistema (RdS-CNR), an Italian ministerial founding for research on electric systems.

Chapter 2 – The proposed Power-to-Gas concept

The Power-to-Gas (P2G) solution as a storage for the electrical energy produced by non-programmable renewable energy sources (NP-RES) represents a field of investigation by several recent sector studies and is also the subject of different pilot activities (recent discussions on the state-of-the-art of P2G technology can be found in studies carried-out by Eveloy and Gebreegziabher [30] and by Wulf et al. [31]). Energy storage of the P2G type is extremely promising also in the scenario of the Italian energy system, provided of a highly structured infrastructure for the distribution of the natural gas and a considerable penetration rate of renewable sources.

In particular, this introductory chapter refers to the main components and the flows of the studied innovative P2G system. This is an advanced P2G system, not yet industrially available and it represents the starting point of the PhD project. The proposed architecture is also the subject of the analyses carried-out in the current study campaign.

2.1 System's architecture

The scheme of the studied P2G system is shown in Fig. 2.1. Basically, this system converts the flow of electrical power (P_{el}), coming from a generic Non-Programmable Renewable Energy Source (NP-RES), into a stream of Synthetic Natural Gas (SNG)[1], to be introduced into the natural gas (NG) network. In particular, the considered P2G concept consists of a series of processes (see Fig. 2.1); to this regard, the three key sub-sections of the P2G system are:

1) a co-electrolyzer of Solid Oxide Electrolyte Cell (SOEC) technology. In this component, the simultaneous electrolysis reactions of water and carbon dioxide occur, producing an intermediate synthesis gas (*Syn* in the figure), including hydrogen and carbon oxide as main species;
2) a methanation section. This is the area related to the production of the SNG, made up of several reactors of different technologies in series, as it will be described in the following; the purpose of this section is to convert the intermediate synthesis gas produced by the co-electrolyzer into a blend with a high methane content, therefore as similar as possible to the natural gas composition;
3) a SNG processing section. This section is made up of several plant auxiliaries needed to introduce the produced SNG into the NG distribution network.

Therefore, as a whole, the system requires as input:

[1] Due to the renewable source, the gas produced by these P2G-type systems is also commonly referred to as *green gas*, while the term *syngas* refers more generically to a synthesis gas of heterogenous composition and not necessarily derived from a renewable source.

- an electrical energy source (in this case represented by the NP-RES, that produces the energy surplus to be stored);
- an external water supply flow;
- an external carbon dioxide supply flow, which can be the by-product of combustion capture processes.

In addition, due to the thermal operating conditions of the components, the system requires one or more external thermal inputs, not shown in the figure, which represent an additional and significant energy cost of the P2G system, as it will be detailed below.

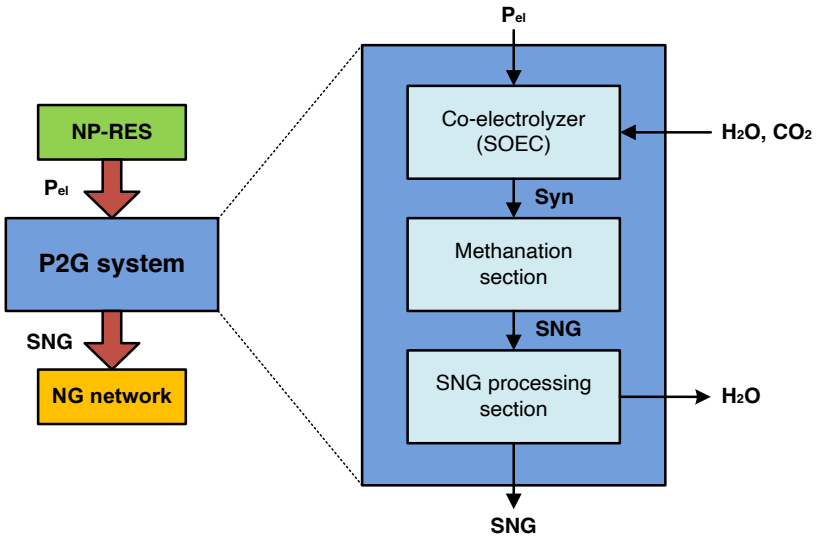

Fig. 2.1. Scheme of the proposed P2G concept.

The simplified block diagram of Fig. 2.2 highlights some features of the proposed solution and the most innovative components of the P2G system. Indeed, in the figure, the different methanation steps are illustrated and, in particular, the distinction of the temperature levels among the components is shown. It should be highlighted that this simplified representation does not contain all the involved flows: e.g., for the sake of simplicity, details on the thermal exchanges among the components have been overlooked, but they will be described in the following.

In more detail, the P2G system is made up of two main sections:

- a high-temperature (HT) section (highlighted in the red box in Fig. 2.2);
- a downstream low-temperature (LT) section (in blue in the figure).

In particular, the HT section represents the innovative core of the system, due to the components currently still under development; the key components of this section are:

- a solid oxide co-electrolyzer (SOEC in Fig. 2.2). This technology requires high operating temperatures, typically in the range of 600 – 900 °C [32]; currently, this solid oxide cell technology is in a pre-commercial development phase for MW-size, necessary for large-scale electrical storage;
- a methanation section at high temperature (HTM – High Temperature Methanation). The HTM considered in this study is based on the ongoing researches carried-out at the CNR (National Research Council) of Messina on high-temperature methanation by means of structured catalysts; this experimental reactor, developed in the CNR laboratory and tested in the operating range of 250 – 600 °C [27] - [28] on a small-scale, is taken as a reference for a future upscaling of the system.

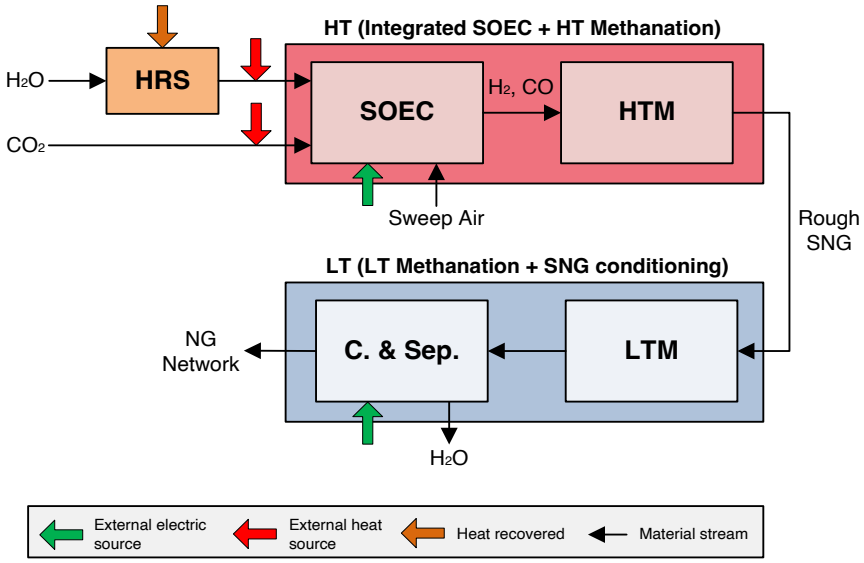

Fig. 2.2. Simplified block diagram of the P2G system; different thermal levels (HT: high temperature section; LT: low temperature section) and methanation processes (HTM: high temperature methanation; LTM: low temperature methanation) are highlighted.

The LT section of Fig. 2.2, instead, is made up of less innovative components but necessary for the functioning of the system and for the integration with the NG distribution network. In particular, the low temperature section is composed by:

- a methanation section at low temperature (LTM – Low Temperature Methanation). This section is based on a conventional catalytic methanation technology (TREMP™ [33]); this sub-section has been introduced in order to improve the quality of the rough SNG produced by the upstream section;
- a conditioning and separation (C. & Sep.) section. In this area, basically, the SNG is compressed, cooled and separated from the residual water, before the introduction into the NG network.

In addition, the considered P2G system includes a complex heat recovery section (HRS in Fig. 2.2), with the purpose to preheat the reactants by means of several streams within the process, outgoing from different components operating at high temperature levels. In the figure, for the sake of simplicity, only the overall heat recovery has been highlighted (in orange in the figure) and the streams from which the recovery starts are not shown. As it will be described in detail, the HRS block, structured in several heat exchangers, contributes to the optimal operating temperature achievement of the several downstream components (SOEC, HTM, LTM and C. & Sep.). The HRS block plays a leading role, considering the difference between the temperature levels of the several components of the system (especially for the high operating temperatures of the SOEC). Without internal heat recoveries, heating-up the reactants of the SOEC to temperatures in the order of several hundred degrees, would represent a significant additional energy consumption if fully supplied by external energy sources (combustors, electric heaters or other types of heat exchanges).

2.2 Layout of the energy storage system's model

The above-described P2G system implies an even more complex architecture, made up of several sub-components and plant auxiliaries, in addition to the key components. A general layout of the energy storage system is shown in Fig. 2.3. The multiple interconnections among the components can be noticed, affecting the overall performance of the system; the hypothesis, the internal settings of each component and additional details of the model will be illustrated in the next chapter. The plant scheme highlights the basic components (heat exchangers, reactors, separators, heaters, compressors, etc.) implemented in order to simulate the four main sections of the whole system:

1) the co-electrolyzer;
2) the methanation sections (HTM and LTM, in the figure gathered together);
3) the pre-heating section with the HRS;
4) the SNG processing section.

In particular, in the layout, the points of heat exchange and the main heat exchangers are highlighted, in order to simulate both the external thermal inputs and the cooling heat flows. In the figure, the HRS has been detailed, showing a configuration composed by several heat exchangers, on the basis of the considered thermodynamic configuration. Indeed, the internal heat recovery is introduced with the HRS to partially preheat the SOEC inlet water stream, using heat available at different downstream sections of the P2G system. In more detail, heat is recovered from the SOEC outlet cathode and anode streams and from all the methanation reactors cooling sections. The pre-heating heat exchangers arrangement in the heat recovery line has been established considering the temperature levels of the available heat flows. In particular, it has been decided to locate the pre-heating section in the more demanding water

line. Nevertheless, a residual external heat source is included to feed the SOEC with reactants at the operating temperature (HE_{H2O} and HE_{CO2}).

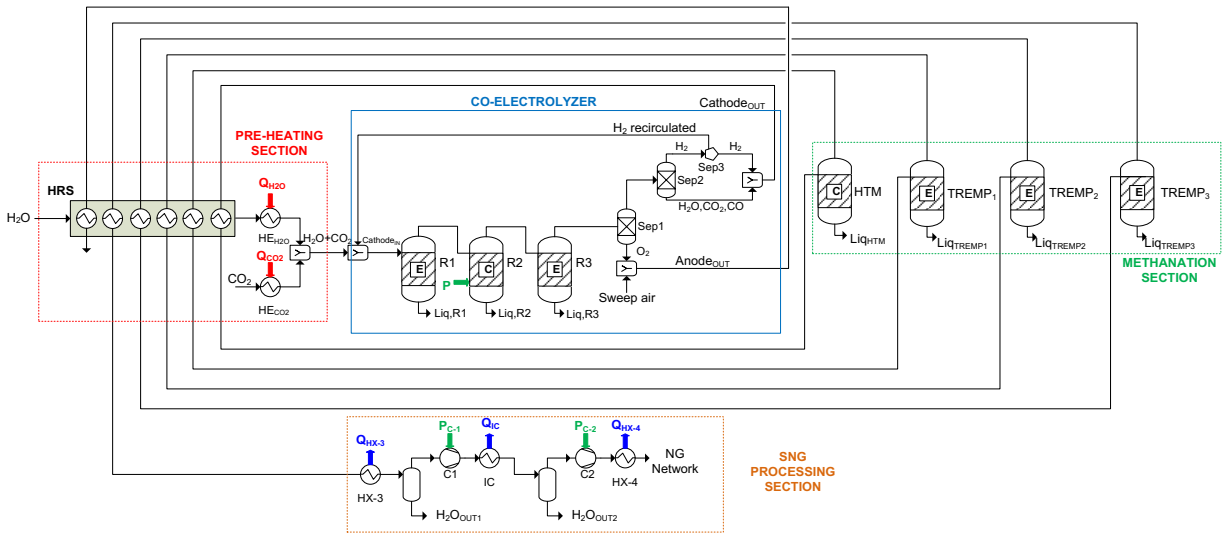

Fig. 2.3. General layout of the studied P2G system.

2.3 Innovative features of the investigated P2G system

Even though the considered P2G system shows some components that have already achieved the technology maturity (low temperature methanation section, heat exchangers, pumps, compressors and the other plant auxiliaries), it can be considered that the development level of the proposed storage solution is currently in a range of TRL (Technology Readiness Level) values between 3 and 5 (3: experimental proof of concept; 4: technology validated in laboratory; 5: technology validated in relevant environment). This level of innovation refers both to specific key components and to the whole system, with particular attention to the following innovative features:

- the whole HT section, that includes: 1) the high temperature SOEC co-electrolyzer, a key component of the system, whose functioning in co-electrolysis mode is still not a technology standard for sizes as large as those considered in this study [26] - [17]; 2) the high temperature methanator (HTM), fundamental in order to obtain a SNG stream with a high content of methane; it is based on an experimental reactor tested in the CNR-ITAE laboratory on small scale [27] - [28], that differs from the conventional methanation technologies operating at low temperatures;
- the specific operating conditions of the SOEC, in the study considered operating up to intermediate temperature levels (600 °C), on average less high [29] than the typical operating range (800 – 1000 °C);

- the thermal integration between the SOEC and the downstream HTM represents a potential innovation, promising from the thermodynamic performance point of view;
- the development of an energy storage system of P2G technology, based on the high temperature electrolysis on large scale, that could achieve energy conversion efficiencies higher with respect to the conventional P2G configurations, based on low temperature electrolyzers of PEM (Proton Exchange Membrane) technology.

Chapter 3 – The Power-to-Gas model

This chapter describes the assumptions, the structure and the settings of the physical-mathematical model developed in order to simulate the overall P2G system. The characterization of complex systems' performance, as the one object of the study, requires a detailed thermodynamic, thermochemical and electrochemical modelling of the several components and sub-sections; this type of investigation may be made possible by means of tools for lumped parameters thermodynamic analysis.
In this framework, the innovative step of this work is the numerical prediction of off-design performance for a P2G process including a SOEC operated in co-electrolysis mode. Indeed, the aim of the study mainly stands in the development of a calculation model for the off-design operations of the P2G process, focussing on a particular and innovative P2G system based on a high temperature co-electrolyzer of SOEC technology coupled with an advanced experimental methanator, which allows to operate at relatively high temperatures. Initially, the model has been developed in order to analyse to system behaviour in design conditions, considering all the sub-sections working at their set-points of operating temperature and pressure. In order to evaluate the behaviour of the several components in off-design conditions, a numerical code has been developed. In more detail, the code has been developed in commercial tool environments and it is able to predict the operating point shift of the several components during the off-design operations.

3.1 - Design modelling

In this first part of the work, the system model has been developed only for the analyses of set-point operations (design analysis, i.e. when the input electric power is set constantly at the design value). The design model has been developed in Aspen HYSYS™ environment [34], a chemical process simulator used to mathematically model chemical processes. This software is a commercial tool with a lumped-parameters approach for the numerical modelling of complex energy systems, able to perform steady-state thermochemical analysis of the process. Standard units from Aspen HYSYS™ library have been used to model common components, like separators, heat exchangers, pumps and compressors; specific sub-models have been implemented for the key components of the P2G system.
The system model is made up of several sub-sections:

1) the co-electrolysis section (SOEC);
2) the methanation section, divided into two sub-sections (HTM and LTM);
3) the SNG processing section;

4) the pre-heating section, which includes an internal heat recovery section (HRS), in order to partially pre-heat the water stream.

In the following paragraphs, the configuration of the P2G system is presented; the developed lumped parameters model for the whole P2G system, including sub-models for the SOEC, the methanation sections, the SNG processing section and the pre-heating section, will be described in detail.

3.1.1 - The co-electrolysis section

The first key component of the innovative P2G system is the high temperature co-electrolyzer of SOEC technology. Aspen HYSYS™ does not contain a single pre-built co-electrolyzer model. Therefore, in the developed SOEC model (Fig. 3.1), the co-electrolyzer has been designed as a combination of prebuilt units, according to [35], using three reactors (*R1*, *R2* and *R3* in Fig. 3.1) in order to simulate the main internal reactions.
In particular, co-electrolysis reactions - Eq. 3.1 and Eq. 3.2 - of water and carbon dioxide occur in the conversion reactor *R2*:

Eq. 3.1. $H_2O \rightarrow H_2 + {}^1/_2\, O_2$

Eq. 3.2. $CO_2 \rightarrow CO + {}^1/_2\, O_2$

Moreover, the equilibrium reverse water-gas shift reaction Eq. 3.3 is considered by means of reactors *R1* and *R3*:

Eq. 3.3. $CO_2 + H_2 \leftrightarrow CO + H_2O$

In addition, for SOEC under pressurized conditions, methane formation may also take place [36] through the following reaction Eq. 3.4:

Eq. 3.4. $CO + 3H_2 \leftrightarrow CH_4 + H_2O$

Generally, in the modelling process it is considered that firstly the reactants reach the chemical equilibrium through the reverse water-gas shift reaction and then the co-electrolysis reactions occur. Finally, the produced syngas achieves the equilibrium according to Eq. 3.3 and Eq. 3.4 before leaving the cathode compartment [37] - [38] - [39]. The reactor *R2* is associated to the

energy input from the NP-RES. The energy input (indicated as *P* in the figure) represents the electric power from NP-RES and used for the electrochemical reactions.

The *R3* outlet stream (*R3,out* in Fig. 3.1) corresponds to the outlet flows of the anodic compartment and of the cathodic compartment; the physical separation between the two sides of the electrolytic cell is modelled by a flow separator component (*Sep1*).

The output stream from the anodic compartment is also modelled including a sweep air flow. Pre-heated sweep air stream (by means of the heat exchanger *Heater*) at the anode compartment is included in the model, in order to simulate the oxygen removal from the anode side of the SOEC stack and to account for the residual heat content. As shown in the figure, the heat exchanger *Heater* has been actually also flanked by an internal recovery which partially preheats the incoming air, by means of the air stream exiting the SOEC from the anodic compartment. The sweep air stream has been set in order to achieve the 50 % of oxygen molar fraction at the anode outlet stream [37].

A small percentage of hydrogen is recirculated from the cathode outlet to the inlet, to ensure reducing atmosphere and, thus, to avoid re-oxidation in the electrode [40]. The required amount of hydrogen, set in the model equal to 5 % in volume of the inlet stream, is separated (by means of the separator *Sep2* and the flow splitter shown in Fig. 3.1, according to [41]) and then recirculated to the feed stream. It should be pointed out that the liquid outlet streams at each reactor (*Liq,R1*, *Liq,R2* and *Liq,R3* in the figure) are default settings of the software and calculated as zero in this sub-section.

Finally, in Fig. 3.1, three manipulators of two different types (*Adjust* and *Set*) have been shown. The *Adjust* manipulator, indicated as *Sweep Air regulator* in the figure, set the oxygen molar fraction at the anode outlet stream varying the *Sweep Air* mass flow, by means of several iterations within the Secant method. The *Set* manipulator *H2 recirculated regulator* and the *Adjust* manipulator *Hydrogen molar fraction* are linked: the *Set* manipulator set the percentage of hydrogen to be separated from the stream *H2* and this value is regulated by the *Adjust* manipulator in order to achieve the 5 % of hydrogen in volume of the inlet stream.

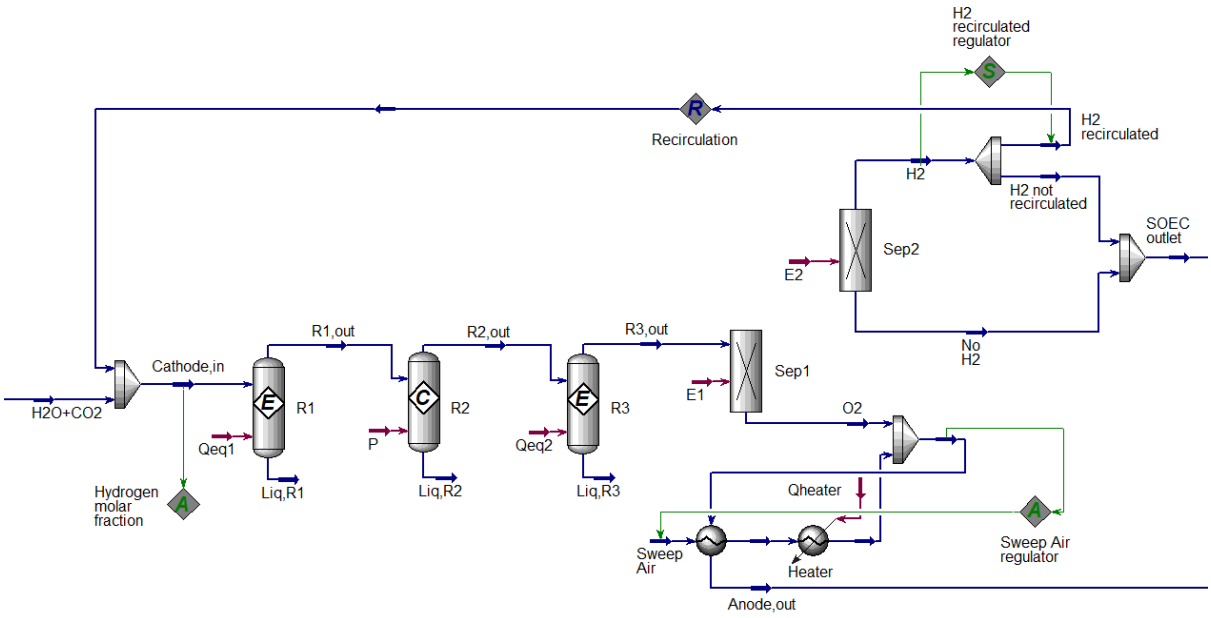

Fig. 3.1. Co-electrolyzer sub-model developed on Aspen HYSYS™.

Boundary conditions

The P2G system design power size considered in the study corresponds to a SOEC stack power size equal to 1 MW of absorbed electric power. As a result, the thermodynamic analysis of the system and of its variants has been carried out with a proper setting of the inlet H_2O and CO_2 mass flow rates, in order to keep the SOEC power size constant.

Moreover, in order to detect the optimum set-point conditions of the P2G feeding, a preliminary parametric analysis of the P2G system inlet stream composition has been carried out. The feeding composition in terms of H_2O/CO_2 ratio has been varied, reducing stepwise the water fraction and increasing the CO_2 fraction. In order to establish the optimal inlet stream composition, the stoichiometric conditions at the inlet of the HTM section (i.e. at the co-electrolyzer cathode outlet) have been targeted. The FEED parameter calculated using the HTM inlet volume fractions, in stoichiometric conditions is defined as [42]:

Eq. 3.5. $$FEED = \frac{[H_2]-[CO_2]}{[CO]+[CO_2]} = 3$$

The above reported FEED stoichiometric value leads to SNG with a higher methane concentration, at the methanation outlet. Results of the parametric assessment of inlet composition effects, presented in detail in a previous preliminary study on the system [43], show that only the P2G inlet composition with 80 % H_2O and 20 % CO_2 provides FEED values close to 3. Thus, this H_2O/CO_2 feeding ratio is used as setpoint in this study.

In the model, the streams of water and carbon dioxide (*H2O+CO2* in Fig. 3.1), coming from the HRS section of the system, are pre-heated up to the operating temperature of the SOEC with specific external thermal inputs, before entering the co-electrolyzer.

In this study, the operating temperature of the SOEC (reactants temperature at the inlet of the SOEC) is within the range of 600 - 850 °C. The upper limit of this range is in line with high performance SOEC operating conditions, in accordance to the available literature [44] - [45]. Furthermore, experimental pilot plants [13] confirm the viability of the value set, in this study, for the SOEC operating temperature. In more detail, an experimental test – conducted for 700 h of operation – has been carried out with the SOEC operating range between 845 and 855 °C, in order to evaluate the outlet stream composition. The lower limit, instead, has been chosen in order to investigate possible thermal synergies within the system; in more detail, the thermal synergy can be achieved operating both the co-electrolyzer and the methanation sections within relatively high temperature ranges (in particular, the co-electrolysis operation at intermediate temperature has been demonstrated by Lo Faro et al. [29]).

The operating pressure of the SOEC has been varied from a scenario with operating conditions at ambient pressure to a scenario of maximum pressurization; in this study, the maximum value has been set equal to 8 bar (it will be described in detail in the paragraph of the off-design model): this value is in line with current state-of-the-art of pressurized SOEC technology (even if higher values are also expected in the future – see the HELMETH project [13]) and it corresponds to the experimental data provided in the study by Meharan et al. [46] on a prototypal SOEC co-electrolyzer.

Regarding the conversion efficiency of the reactions, the conversion rate target of electrolysis reactions is assumed equal or higher than the 80 % in [13]: in this study, a conservative value equal to the 80 % is set.

The set-point parameters in design conditions implemented in the co-electrolyzer model are summarized in Tab. 3.1.

Tab. 3.1. Set-point parameters of the co-electrolyzer model in design conditions.

Parameter	Value	Units
Electric power input	1	MW
Operating temperature	600 - 850	°C
Operating pressure	1 - 8	bar
Reactants (H_2O+CO_2) inlet temperature	25	°C
Sweep air inlet temperature	25	°C
Inlet H_2O fraction	80	$\%_{vol}$
Inlet CO_2 fraction	20	$\%_{vol}$
H_2O electrolysis reaction conversion rate	80	%
CO_2 electrolysis reaction conversion rate	80	%
H_2 fraction recirculated	5	$\%_{vol}$
O_2 fraction in the anode stream	50	$\%_{vol}$

3.1.2 - The methanation section

The methanation section implemented in the model (Fig. 3.2) is able to simulate the streams, the heat exchanges and the chemical reactions of hydrogen, carbon oxide and carbon dioxide to methane. In this implementation, it has been considered that the reactants (H_2, CO and CO_2) come from the co-electrolyzer (after the passage through the HRS).

This section lumped-parameters model includes two key sub-sections, as already mentioned:

- a high temperature methanation (HTM) sub-section, based on the experimental data of the methanation reactor developed by the CNR of Messina [27] - [28], producing a rough SNG stream (containing methane and other elements);
- a low temperature methanation (LTM) sub-section, based on a conventional catalytic methanation technology (TREMP™ [33]); this sub-section has been implemented in the model in order to improve the methane content in the SNG stream.

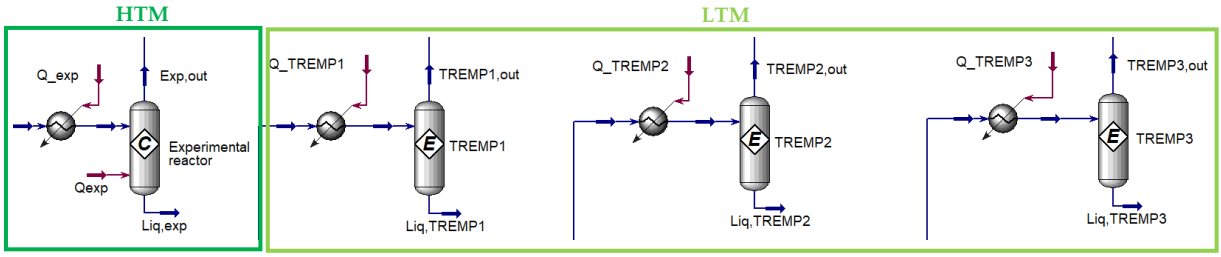

Fig. 3.2. Methanation sub-section developed on Aspen HYSYS™.

High temperature methanation (HTM) sub-section

In the proposed P2G system, the SOEC outlet syngas – rich in H_2, CO_2 and CO – is converted into a methane rich fuel, by means of the downstream high temperature methanation reactor (*Experimental reactor* in Fig. 3.2). This reactor, as it has been said, is based on a structured catalyst developed and tested by the CNR of Messina at laboratory scale [27] - [28], considering its scaling at a large size.

The CNR experimental reactor set-up consists in a quartz tubular fixed-bed reactor (horizontally placed in a furnace) under atmospheric pressure. The reactor contains a structured catalyst (diameter 1 cm, length 1.5 cm in the laboratory scale), the catalytic layer (50 wt.% Ni/GDC) was deposited on the cordierite monolith (500 cps) by SCS reaching a total loading of 0.5 g/cm^3. Details on the catalyst features and on the experimental setup have been previously provided [27] - [28]. Briefly, the temperature dependence (250 – 600 °C) of the catalytic performance was evaluated with a supply of 11.1 % CO_2 / 8.9 % CO /68.9 % H_2 / 11.1 % N_2 at Gas Hourly Space Velocity (GHSV) of 10000, 30000 and 50000 h^{-1}. In these tests, the incoming molar fractions remain unchanged regardless of the flow analyzed. On the basis of the outlet flow composition, the reactor conversion rate (CR) has been calculated as:

Eq. 3.6. $$CR = \frac{\dot{n}_{CH4,out}}{(\dot{n}_{CO}+\dot{n}_{CO2})_{in}}$$

where $\dot{n}_{CH4,out}$ represents the outlet molar flow of CH_4 and $(\dot{n}_{CO} + \dot{n}_{CO2})_{in}$ is the inlet molar flow of CO and CO_2. The trend of CR as a function of the temperature and of the inlet flow has been analyzed (see Fig. 3.3a). It can be noted that, for the used structured catalyst, the production of methane is very low for temperatures below 300 °C and it increases with the operating temperature; CR value is maximum for temperatures ranging around 400 - 500 °C, while it tends to reduce for temperature values above that interval, but it is still significant up to 600 °C. This upper range of values could be compatible with the SOEC operating conditions. It should be noted that during the carried-out tests, the experimental reactor temperature has shown a quite isothermal behavior along its length (Fig. 3.3b). As a consequence, in order to simulate the HTM process on Aspen HYSYS™ environment, an isothermal conversion reactor has been used, setting CO and CO_2 conversion into CH_4 according to the Sabatier methanation reactions Eq. 3.7 - Eq. 3.8:

Eq. 3.7. $$CO + 3H_2 \rightarrow CH_4 + H_2O$$

Eq. 3.8. $$CO_2 + 4H_2 \rightarrow CH_4 + 2H_2O$$

The input values of CR have been modeled on Aspen HYSYS™ as a function of the operating temperature, by interpolation of the available experimental data with a second order polynomial equation:

Eq. 3.9. $$CR = C_0 + C_1 T + C_2 T^2$$

where T is the operating temperature of the reactor, while C_0, C_1 and C_2 are the tuned coefficients of the interpolating function. Fig. 3.3a shows the experimental data and the interpolating curve obtained for the 10000 GHSV case (red triangles in the figure), corresponding to the operating condition with the maximum conversion rate, in the temperature range equal to 400 - 500 °C. The coefficients of the interpolating function plotted in Fig. 3.3a are: C_0 = -246.67; C_1 = 1.31; C_2 = -1.37·10^{-3}.

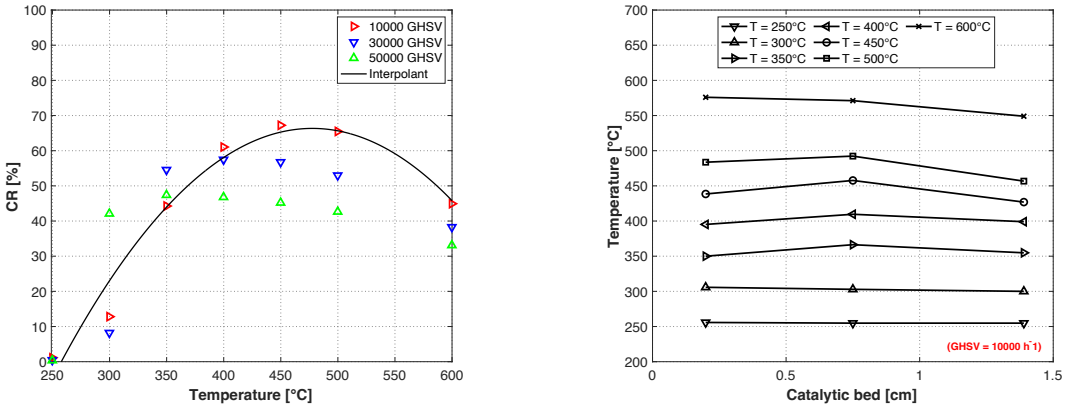

a) b)

Fig. 3.3. a) Experimental Conversion Rate (CR) of the HTM, as a function of the operating temperature for three different values of inlet flow and interpolating function; b) temperature profile of the catalytic bed [27] - [28].

Low temperature methanation (LTM) section

In order to simulate the LTM process, used to increase the methane content of the final output SNG, a methanation section with a multiple reactor arrangement, reproducing the Haldor-Topsøe TREMP™ [33] catalytic technology, is here considered. The TREMP™ technology is a well-known industrial process, usually operating in the temperature range of 200 - 700 °C, but the highest conversion efficiency values are typically achieved when operated close to the lowest values of the temperature range [42]; this process can be employed at large scale to produce SNG, starting from several rough fuels varying from biomass to coal.

In this work, a multi-stage methanation section has been considered, using three equilibrium reactors (*TREMP1*, *TREMP2* and *TREMP3* in Fig. 3.2) located downstream of the HTM experimental reactor (*Experimental reactor*, Fig. 3.2), in order to improve the overall system CH_4 production.

While the experimental reactor is modeled as isothermal, in order to match the experimental data [27] - [28], the TREMP reactors are modeled as adiabatic [33], i.e. the exothermic reactions will cause a temperature increase along the reactors from inlet to outlet. Thus, inter-cooling is included in the model between each reactor, in order to adjust the inlet temperature (LTM set temperature) for each equilibrium reactor. Also in this sub-section, the liquid outlet streams of each reactor (*Liq,exp*, *Liq,TREMP1*, *Liq,TREMP2* and *Liq,TREMP3* in Fig. 3.2) are calculated as zero by the software.

Boundary conditions

Regarding the temperature settings, the followed pattern highlights two different P2G concept: conventional and innovative. Indeed, regarding the conventional concept, the HTM temperature (set at 450 °C) corresponds to the point of maximum conversion rate. Instead, in the innovative concept, the temperature of the HTM has been shifted to operating points (600 °C) less conventional for the single components, with the aim to explore possible synergies among the sub-sections.

Preliminary parametric investigations reported in [43] have been carried out by means of the model, varying the operating temperature of the TREMP™ reactors in the range 200 – 500 °C. From the results, it has been pointed out that the lower the operating temperature at the inlet of the reactors, the higher the concentration of methane in the SNG stream, while, as the operating temperature of the TREMP™ reactors increases, the concentration of methane decreases until it reaches the minimum value for an operating temperature of 500 °C. Therefore, in this study, the operating temperature level of the LTM section reactors has been kept constant, both in the design and off-design conditions, setting the operating temperature at 200 °C.

Regarding the operating pressure set point of the reactors, both the HTM and LTM have been operated at the same pressure, on the basis of the upstream components. Therefore, depending on the SOEC conditions, the operating pressure of the methanation sections has been varied from a scenario of ambient pressure to a scenario of maximum pressurization (8 bar). The favorable effect of the pressure on the equilibrium of methanation reactions is also known.

The set-point parameters in design conditions implemented in the methanation section model are summarized in Tab. 3.2.

Tab. 3.2. Set-point parameters of the methanation section model in design conditions.

Parameter	Value	Units
HTM operating temperature	450 - 600	°C
HTM operating pressure	1 - 8	bar
LTM operating temperature	200	°C
LTM operating pressure	1 - 8	bar

3.1.3 - The SNG processing section

This model's section includes the plant main auxiliaries and energy-consuming components, necessary for the compression and dehumidification of the SNG produced by the upstream methanation section. The model implemented on Aspen HYSYS™ is shown in Fig. 3.4. The SNG coming from the LTM section (*LTM,out* in the figure) is first cooled by means of heat exchangers, to reduce the gas compression work; a gas outlet temperature value of 25 ° C has been set for all the heat exchangers in this section. In particular, the model includes a pre-cooler (*PC* in the figure), an inter-refrigerated compression with two compression blocks (*C1* and *C2*), an inter-cooling exchanger (*IC*), an after-cooler (*AC*) and two separator blocks, able to remove the residual water. The storage pressure has been set at 60 bar, corresponding to a typical value of the natural gas distribution network, considering high pressure networks [47]. The isentropic compression efficiency has been set at 80 %, in line with the state-of-the-art of medium technology natural gas compressors. Furthermore, the distribution of the pressure drop between the compressors of the model has been optimized, in order to minimize the total compression work. Therefore, the intermediate pressure has been calculated for each operating condition of inlet pressure, on the basis of the equal distribution of the enthalpy drop between the two compressors.

The set-point parameters in design conditions implemented in the SNG processing section model are summarized in Tab. 3.3.

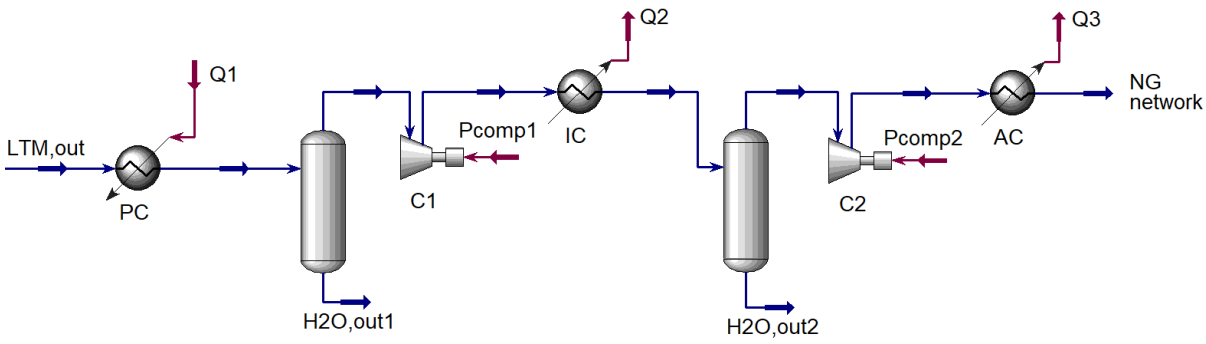

Fig. 3.4. SNG processing sub-section developed on Aspen HYSYS™.

Tab. 3.3. Set-point parameters of the SNG processing section model in design conditions.

Parameter	Value	Units
Pre-cooling temperature	25	°C
Inter-cooling temperature	25	°C
After-cooling temperature	25	°C
Isentropic compression efficiency	80	%
Inlet SNG stream pressure	1 - 8	bar
NG distribution network pressure	60	bar

3.1.4 - The pre-heating section

In order to include in the whole P2G system thermodynamic model also the thermal consumption to heat-up the SOEC reactants to the operating temperature, a section for the reactants pre-heating has also been implemented. This model's section includes the HRS, introduced to partially preheat the water stream at the input of the P2G system, exploiting the residual heat available from different downstream sections of the system. In particular, it has been decided to locate the pre-heating section in the more heat demanding water line. Nevertheless, a residual external heat source is included to feed the SOEC with reactants at the internal operating temperature. By means of the HRS section, heat is recovered from the outgoing streams from the cathode and anode of the SOEC and from all the methanation reactors. In more detail, two different configurations for the preheating section have been introduced, on the basis of the pressurization of the co-electrolyzer. The arrangement of the heat exchangers in the HRS line has been affected by the temperature levels of the available heat flows.

Regarding the configuration of the P2G system with the SOEC at ambient pressure (Fig. 3.5), the recovery section is made up of 6 heat exchangers: in order, the thermal recovery has been carried out from the anode stream, the outlet stream of the reactor *TREMP3*, the outlet stream of the reactor *TREMP2*, the outlet stream of the reactor *TREMP1*, the outlet stream of the HTM and the cathode stream at the outlet of the co-electrolyzer. Regarding, instead, the P2G system provided of a pressurized SOEC (Fig. 3.6), the optimal configuration shows 7 heat exchangers in the HRS. Indeed, in this configuration, an additional heat exchanger has been implemented in order to maximize the heat recovery of residual heat from the air stream at the outlet of the anode compartment. The arrangement of the heat exchangers in the HRS line of the two configurations (Fig. 3.5 and in Fig. 3.6) describes this particular section for systems at ambient pressure and pressurized systems; however, it must be pointed out that these configurations

could be modified on the basis of the components' temperature and the several analyzed configurations will be shown in Chapter 4 – Synthetic natural gas application: design analysis. Finally, in Fig. 3.6, it is shown that the pressurization of the water stream takes place in the liquid state, by means of a pump, while the compression of the carbon dioxide stream is carried out with a compressor, before the pre-heating from an external source.

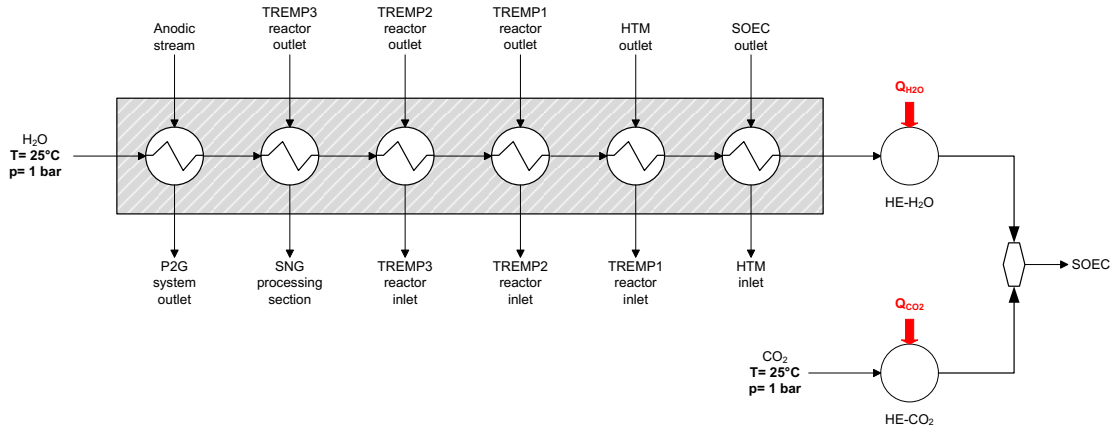

Fig. 3.5. Pre-heating section model developed on Aspen HYSYS™ – Ambient pressure configuration.

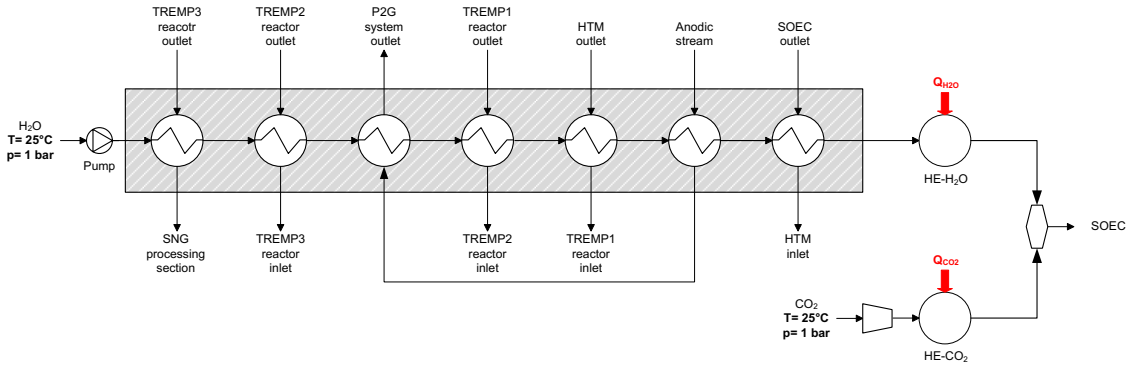

Fig. 3.6. Pre-heating section model developed on Aspen HYSYS™ – Pressurized configuration.

3.2 - Off-design modelling

In order to evaluate the performance of the whole P2G system in off-design conditions, starting from the thermodynamic design point above introduced, the overall thermodynamic model with lumped-parameters approach developed in Aspen HYSYS™ has been modified by implementing a specific numerical sub-model for the SOEC co-electrolyzer, developed in the Matlab™ environment [48]. The carried-out analysis is of quasi-static type; this assumption implies that the considered system has a time-dependent response, but the inertia effects have been neglected. As a consequence, the proposed model does not consider process dynamics.

This paragraph describes the semi-empirical model implemented to simulate the off-design operations of the SOEC co-electrolyzer, able to replicate its behavior in a simplified but realistic way, due to its calibration on the basis of available experimental data or literature data. The SOEC technology, considered in this study for the development of the high temperature co-electrolysis section of the system, if compared with other low-temperature electrolysis technologies, is currently still under development. Therefore, there are few references (scientific studies related to the modelling and/or experimental data for large-scale applications) in the state-of-the-art on the performance achievable in off-design conditions, i.e. when the electrical load differs significantly from the value assumed at the design point due to a power supply from NP-RES. In this framework, the originality of this study stands in the development of a numerical simulation tool that follows the variation of the electrical input of the whole integrated P2G system, through a generalization of the performance curves of a specific electrolyzer taken as a reference, whose experimental data are available. In particular, the approach described below is able to reproduce the off-design operations of a large-scale SOEC electrolyzer, operated in co-electrolysis mode, with the simultaneous input of water and carbon dioxide, as required by the considered system architecture.

The SOEC sub-model has to be integrated with the other components of the whole P2G system, which operate off-design conditions at the same time; therefore, the overall thermodynamic model has been specifically adapted. To simulate the off-design behavior of the other sub-sections, a simpler approach has been used (based on a lumped parameters method), by means of:

1) off-design maps and parameter correction, derived from manufacturers and/or from physical correlations;

2) simplifying hypothesis, with the assumption of constant values for different operating parameters (for a variable load).

In particular, specific modifications have been implemented for the off-design operations on the thermodynamic model developed on the Aspen HYSYS™ environment, specifically for the HRS section, the methanation sections and the SNG compression section, as detailed below.

3.2.1 - Integration of the SOEC numerical sub-model in the overall P2G thermodynamic model

In order to evaluate the performance of the whole P2G system in off-design conditions, the overall thermodynamic model with lumped-parameters approach developed in Aspen HYSYS™ has been modified by implementing a specific numerical sub-model for the SOEC co-electrolyzer, developed in the Matlab™ environment. Therefore, the product of this study is an integrated modelling environment based on the link between commercial computational software, external user-defined routines and empirical data for the model tuning.

The flow chart in Fig. 3.7 shows the connection between the whole P2G system model and the SOEC sub-model developed in this study; in particular, the steps of the calculation procedure in the integrated numerical environment, the data streams between the different considered codes and the iterations for the P2G system simulation are highlighted. In more detail, the overall calculation procedure requires the development of the system layout in Aspen HYSYS™ environment as a preliminary starting point; at this stage, each system component is modelled at the set point (design conditions), by means of the lumped-parameter approach described in the paragraph 3.1 - Design modelling. The thermodynamic analysis of the P2G system in design conditions is then performed (*DESIGN analysis* in Fig. 3.7, with nominal input electrical power of 1 MW assigned) in the Aspen HYSYS™ environment, in which the layout has been developed; the boundary conditions related to the design scenarios shown in Tab. 3.1, Tab. 3.2 and Tab. 3.3 are used as the thermodynamic set-point parameters of the different components. As a consequence, at this early stage, the lumped-parameters approach described in the paragraph 3.1 - Design modelling has been used to describe the SOEC design operations.

This first stage of the calculation procedure provides as output all the stream flows and enthalpy values, at the input and output of each component, corresponding to the reference inlet power condition (design point). These design data represent the reference thermodynamic data set for the calculation stage in off-design conditions. The *OFF-DESIGN analysis* block in Fig. 3.7 uses this data and, by means of specific routine (*SOEC sub-model* block) developed in the Matlab™ environment, is able to describe the electrochemical behavior of the SOEC as the electrical input varies.

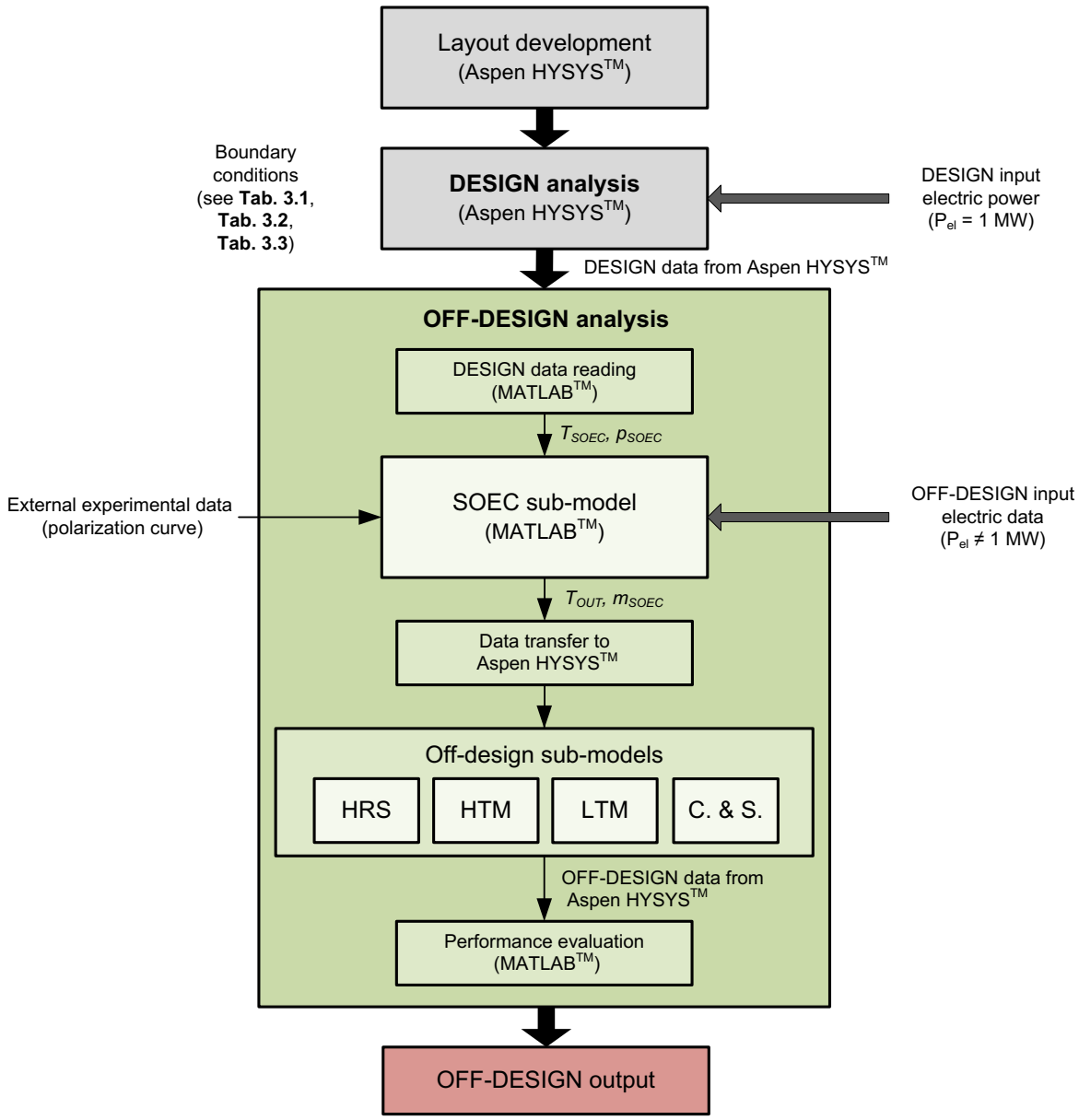

Fig. 3.7. Simplified flow chart of the whole numerical model for the design/off-design analysis of the P2G system; the numerical model includes the *SOEC sub-model*, in order to simulate the electrochemical behaviour of the component in off-design conditions.

The first step of the *OFF-DESIGN analysis* block consists in the DESIGN data reading in Matlab™ environment. With this purpose, a link between the Aspen HYSYS™ environment and the Matlab™ environment has to be established; the link, in this study, is based on the creation of a virtual server in Matlab™ environment through the function *actxserver* (as shown below), that returns a handle to the default interface of the server. Once the server has been created, the Matlab™ environment is able to open any Aspen HYSYS™ file and to interact with it; as it can be seen, data in Aspen HYSYS™ are divided on the basis of belonging to a specific class, namely the *Operations* (related to the components), the *Material Streams* and the *Energy Streams*.

```
%% Aspen HYSYS - Matlab link

% Matlab connection to Aspen HYSYS through Matlab activeX server
Hysys = actxserver('Hysys.Application.V11.0');
% Test name input in .hsc format
FileNamePath = 'Test_001';
% Considered Aspen HYSYS file opening
Simulation = Hysys.SimulationCases.Open([cd,strcat('\',FileNamePath,'.hsc')]);
% Opening the Aspen HYSYS interface
Simulation.Visible = true;
% Operations level
Components = Simulation.Flowsheet.Operations;
% Material streams level
Streams = Simulation.Flowsheet.MaterialStreams;
% Energy fluxes level
Fluxes = Simulation.Flowsheet.EnergyStreams;
```

When the data are transferred to the Matlab™ environment, they are used as input to the SOEC sub-model. This sub-model is based on the use of electrochemical experimental data (polarization curves), related to a reference SOEC co-electrolyzer (see Fig. 3.7), to evaluate the off-design performance. In particular, in this study reference has been made to an experimental work [49], in which a co-electrolyzer of SOEC technology has been tested in a limited set of operating conditions (pressure and temperature).

The calculation of the SOEC off-design operations is carried out with a set electrical input power to the SOEC (off-design electrical power), coming from NP-RES, and at given pressure and temperature conditions, defined in the *DESIGN analysis* block.

The empirical SOEC sub-model provides, as output, the electrochemical and thermodynamic data related to the variable load operations of the SOEC itself - mainly the reaction products outlet temperature, T_{OUT}, and the processed mass flow rate, $\dot{m}_{SOEC}$ - which affect the behavior of the other P2G sub-sections.

Thus, the output data of the SOEC sub-model are used as input for a new calculation iteration in the Aspen HYSYS™ environment, in which the lumped-parameters thermodynamic model of the overall P2G system is relaunched, in order to obtain all the inlet and outlet stream flows and the values of the thermodynamic properties in off-design conditions. In particular, the off-design evaluation of the system is carried out using the Aspen HYSYS™ software, by means of specific off-design settings for the HRS, HTM and LTM sub-sections and for the SNG processing section.

At the end of this general procedure with a double iteration in the Aspen HYSYS™ environment, the values of all the thermochemical quantities related to the partial load operations are transferred to a further data processing routine in the Matlab™ environment, by means of which the performance parameters of the whole P2G system are evaluated.

It must be pointed out that the proposed model has a generalized approach and it can be applied to every P2G concept involving an electrolyzer. Indeed, the input data of the electrolyzer sub-model can be related to every electrolyzer data set (including also a simple water electrolyzer of other technologies) and then be applied to a wide variety of devices. In

addition, as shown below, the code developed in Matlab™ environment requires the input and output definition (material, electrical, thermal and system general input and material output) of the considered system; once these parameters are defined, the procedure is completely automatic and adaptable to every layout developed in the Aspen HYSYS™ environment.

```
%% INPUT and OUTPUT definition

% Material INPUT
input_m1 = 'H2O';
input_m2 = 'CO2';
input_m3 = 'Sweep Air';
% Electrical INPUT
input_e1 = 'P_SOEC';
input_e2 = 'P_comp1';
input_e3 = 'P_comp2';
% Thermal INPUT
input_th1 = 'Q_H2O';
input_th2 = 'Q_CO2';
input_th3 = 'Q_heater';
input_th4 = 'Q_HTM';
input_th5 = 'Q_TREMP1';
input_th6 = 'Q_TREMP2';
input_th7 = 'Q_TREMP3';
% System general INPUT
T_SOEC = 850;
p_SOEC = 1;
T_HTM = 450;
p_HTM = 1;
T_LTM = 200;
p_LTM = 1;
% Material OUTPUT
output='SNG';
```

The code above shown refers to a specific configuration of the P2G system, in which the operating values are conventional.

3.2.2 - The co-electrolyzer semi-empirical sub-model

The SOEC off-design sub-model is presented in Fig. 3.8; the model is based on experimental data and allows to determine the electrochemical operating point of the electrolyzer as the electrical input varies. The model shows as main output the outlet temperature and the electrical efficiency of the SOEC in off-design conditions. The knowledge of these two output parameters is essential in order to predict the SOEC behavior within the overall thermodynamic model, and therefore to evaluate the performance of the whole P2G system operated in variable load conditions. Indeed, the SOEC electrical efficiency strongly affects the conversion efficiency of the overall P2G system, due to the high electrical energy consumption of this component, while the outlet temperature of the SOEC products affects the thermal distribution of the system and determines the operating point of the downstream sections (HTM, LTM and C. & Sep.) and of the heat recovery section (HRS).
The model inputs can be divided into two main categories:

- experimental data (related to a reference co-electrolyzer);
- actual operating conditions (related to the investigated P2G system).

In particular, the semi-empirical model requires, as experimental data, a limited number of information derived from an existing SOEC stack (representative of the technology), used as reference. The reference experimental data that have been used for the development of the model are:

- a set of polarization curves (i.e. voltage-current density of the experimental stack) at different operating conditions of temperature and pressure (T_{exp}, p_{exp});
- the stack surface (A_{SOEC});
- the stack inlet mass flow ($\dot{m}_{SOEC}$).

The used experimental data derive from an experimental work by Mehran et al. [49], in which a tubular SOEC co-electrolyzer has been tested at laboratory scale, under different temperature and pressure conditions. It must be highlighted that the scientific study taken as a reference, shows data in line with the current state-of-the-art of co-electrolysis technology, also shown by other studies [32], and provides a wide enough set of experimental points and test operating conditions, needed for a reliable extrapolation.

The actual operating conditions (T_{SOEC}, p_{SOEC}) of the SOEC in off-design are additional input of the model, which can be different from the operating conditions of the experimental tests (T_{exp}, p_{exp}).

Finally, an operating range that goes from – 50 % to + 50 % of the design energy input of the co-electrolyzer has been defined; therefore, the SOEC can operate within the range: 500 - 1500 kW.

The calculation procedure of the SOEC sub-model can be divided into three steps:

i. the calculation of generalized polarization curves;
ii. design condition definition;
iii. off-design performance evaluation.

Each step of the process will be described below.

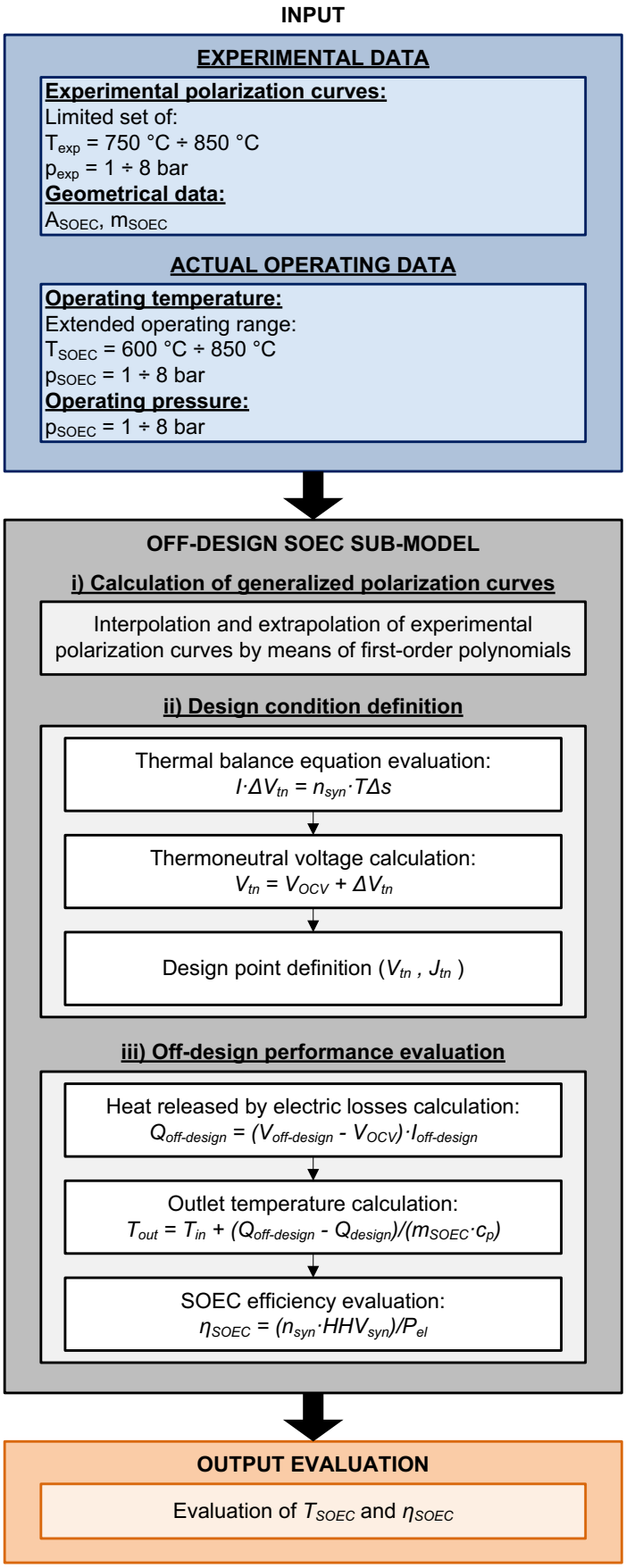

Fig. 3.8. Flow chart of the SOEC semi-empirical sub-model for the off-design conditions evaluation.

i. Calculation of generalized polarization curves

The first step of the sub-model calculation process consists in the calculation of generalized polarization curves, i.e. first-order polynomials that describe the evolution of the cell voltage as a function of the current density, at given operating pressure and temperature conditions of the SOEC.

Starting from a limited set of experimental polarization curves for the reference SOEC, the numerical model is able to obtain generalized polarization curves in a wider range of operating conditions (temperature and pressure), by means of the interpolation and extrapolation of the experimental data with first-order polynomials (Fig. 3.9 and Fig. 3.10).

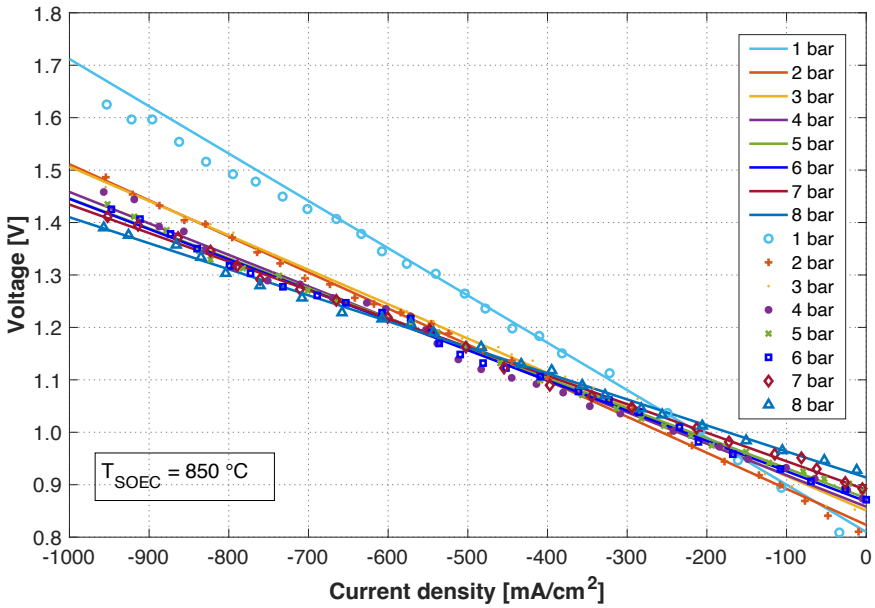

Fig. 3.9. Generalized (interpolated) polarization curves plotted for various operating pressure values, at T_{SOEC} = 850 °C (dots: experimental data points [49]; continuous lines: polynomial curves).

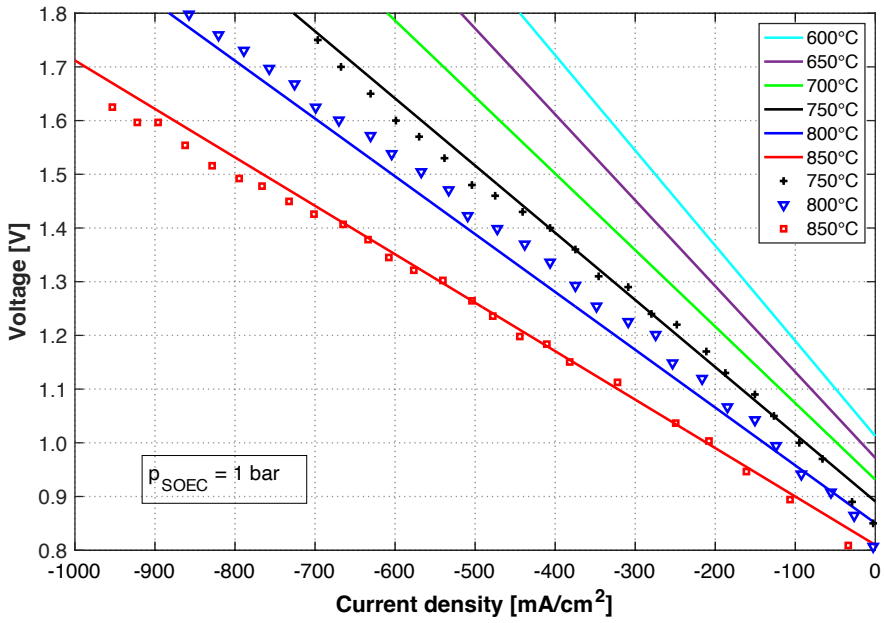

Fig. 3.10. Generalized (extrapolated) polarization curves plotted for various operating temperature values, at p_{SOEC} = 1 bar (dots: experimental data points [49]; continuous lines: polynomial curves).

The used experimental polarization curve points derive from an experimental study [49], in which the reference co-electrolyzer (representative of the SOEC technology) has been tested in a limited set of operating conditions (variable temperatures in the range 750 - 850 °C with increasing steps of 50 °C, while the pressure has been varied in the range 1 - 8 bar, with increasing steps of 1 bar). Regarding the operating temperature, the available experimental data have been extrapolated obtaining polarization curves in a wider range, between 600 °C and 850 °C, i.e. the extended operating range considered in this study (see Fig. 3.10), typical for a co-electrolyzer of SOEC technology [32]. Moreover, regarding the operating pressure, generalized polarization curves have been obtained for different pressure values in the range 1 - 8 bar, by interpolating the experimental available points (see Fig. 3.9).

ii. Design condition definition

In this step, the SOEC electrochemical design operating point (i.e. the cell voltage and related current density in design condition) has been identified on the corresponding polarization curve for the actual operating conditions, by referring to the generalized polarization curves. In particular, in this study, the SOEC design point has been assumed coinciding with the *thermoneutral* condition, where the thermoneutral voltage V_{tn} is defined as the potential at which the cell is thermally stable with respect to its equilibrium state V_{OCV} (Open Circuit Voltage) [50]. In thermoneutral condition, the heat released by the electrical losses in the cell is equal to the energy required by the co-electrolysis reactions. This operating condition is highly desirable for SOEC technology, in order to avoid any additional device to provide heat

or to extract it from the stack; in addition, this particular condition leads to have the same temperature value for the inlet reactants and the outlet products.
In off-design conditions instead, the heat released by the electric losses in the cell differs from the energy required by co-electrolysis reactions; generally, the electric energy demand due to the co-electrolysis reactions can be expressed as the variation of the Gibbs free energy Δg:

Eq. 3.10. $\Delta g = \Delta h - T \cdot \Delta s$

where, Δh [kJ/kmol] is the enthalpy variation of the co-electrolysis reactions, T [K] is the SOEC operating temperature equal to the reactants inlet temperature and Δs [kJ/kmolK] is the entropy variation of the reactions; it must be highlighted that the enthalpy variation and the entropy variation are influenced by the operating temperature and pressure of the SOEC.
If the cell voltage $V_{cell} < V_{tn}$ (endothermic mode), the electric energy Δg is lower than the enthalpy variation Δh and then additional heat is required to maintain the operating temperature. If instead $V_{cell} > V_{tn}$, the cell operates in the exothermic mode and this corresponds to an increase in the cell temperature, because the electric energy supply Δg exceeds the enthalpy variation. Thus, in order to evaluate the thermoneutral voltage, the following thermal balance equation has to be solved:

Eq. 3.11. $I \cdot \Delta V_{tn} = \dot{n}_{syn} \cdot T\Delta s$

where, I [A] is the electric current of the SOEC ($I = J \cdot A_{SOEC}$), ΔV_{tn} [V] is the voltage related to the losses in the thermoneutral condition and $\dot{n}_{syn}$ [kmol/s] is the molar flow of produced syngas.
According to the Faraday's Law (Eq. 3.12), in the electrochemical reactions $\dot{n}_{syn}$ can be expressed as:

Eq. 3.12. $\dot{n}_{syn} = \frac{I}{ZF}$

where, Z is the valency number of ions of the substance and F [C/kmol] is the Faraday constant.
Then, Eq. 3.11 can be reformulated as:

Eq. 3.13. $\Delta V_{tn} = \frac{T\Delta s}{ZF}$

Finally, V_{tn} can be calculated by:

Eq. 3.14. $$V_{tn} = V_{OCV} + \Delta V_{tn}$$

By means of the calculated V_{tn} value at given pressure and temperature, the corresponding design current density (J_{tn}) can be obtained directly from the specific generalized polarization curve (see Fig. 3.11). The obtained point of coordinates (J_{tn}, V_{tn}) represents the design point for a specific temperature and pressure.

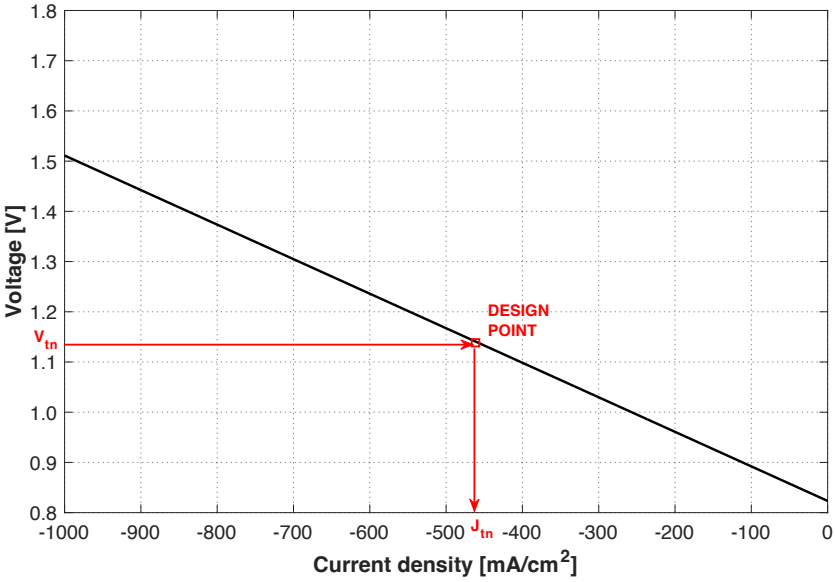

Fig. 3.11. Design point definition on the generalized polarization curve for a specific temperature and pressure.

iii. Off-design performance evaluation

Once the design (thermoneutral) point is identified on the generalized polarization curve, it is possible to identify the off-design point, i.e. when the input electric power value ($P_{el,off-design}$ [W]) and the related current ($I_{off-design}$ [A]) and voltage ($V_{off-design}$ [V]) values differ from the design values; then, the new SOEC performance and, in particular, the updated SOEC outlet temperature (T_{out} [K]) can be calculated in off-design operations. This temperature value coincides with the value of the inlet temperature (T_{SOEC} [K]) only in design conditions. The off-design T_{out} estimation can be performed using the heat released by electric losses in off-design conditions ($\dot{Q}_{off-design}$ [W]) expressed according to Eq. 3.15:

Eq. 3.15. $$\dot{Q}_{off-design} = \left(V_{off-design} - V_{OCV}\right) \cdot I_{off-design}$$

In this equation, in order to quantify the heat released by electric losses, the heat flux has been expressed as the product of the electric current in off-design conditions and the difference between the voltage and the open circuit voltage (i.e. the voltage given by the electric current flow in the circuit). Once calculated the heat released by electric losses in thermoneutral condition, the outlet temperature (T_{out}) in off-design conditions can be estimated by means of the heat released by the electric losses in thermoneutral condition ($\dot{Q}_{design}$ [W]):

Eq. 3.16. $$T_{out} = T_{SOEC} + \frac{\dot{Q}_{off-design} - \dot{Q}_{design}}{\dot{m}_{SOEC} \cdot c_p}$$

where $\dot{m}_{SOEC}$ is the actual SOEC inlet reactants mass flow [kg/s] and c_p [J/kgK] is the related specific heat.
Finally, the SOEC electrical efficiency [13] can be calculated according to:

Eq. 3.17. $$\eta_{SOEC} = \frac{\dot{n}_{syn} \cdot HHV_{syn}}{P_{el}}$$

where, HHV_{syn} [kJ/kmol] is the higher heating value of the produced syngas and P_{el} [kW] is the electrical power input of the SOEC, related to the electrical current consumption of the cell ($P_{el} = V \cdot I$). According to Eq. 3.12, the SOEC efficiency is proportional to a constant factor per applied voltage:

Eq. 3.18. $$\eta_{SOEC} = \frac{HHV_{syn}}{ZF} \cdot \frac{1}{V} \propto \frac{constant}{V}$$

Then, the SOEC efficiency in off-design conditions can be calculated through the evaluation of the off-design voltage value.

SOEC co-electrolyzer performance with a variable operating point

In this section, the SOEC generalized operating curves, which describe its behavior in design/off-design conditions, are presented. In particular, these curves represent the component performance as the electrical load varies, in the whole considered operating range of the co-electrolyzer. These dimensionless curves have been obtained by means of the electrochemical sub-model of the SOEC, normalizing the several calculated quantities with respect to the values in the design condition.
In particular, in Fig. 3.12a, the normalized polarization curves for several operating temperatures are shown. Since both quantities (current density and voltage) shown on the axes are normalized with respect to the related values in the design point, the latter

corresponds to point (1;1) in the graph. Considering at first the operating scenario in which the current density is lower than the current density at the design point ($0.5 \leq J_{normalized} < 1$), the results show that, with the same current density, with the increase in the temperature a lower voltage is required; on the other hand, for higher current densities ($1 < J_{normalized} \leq 1.5$), the situation is the opposite. Furthermore, the pressurized SOEC behavior has been also evaluated (Fig. 3.12b), considering an operating range between 1 bar and 8 bar (operating range of the reference experimental SOEC), with a step equal to 1 bar. The pressurization of the SOEC appears to be penalized due to the higher voltage required for current densities lower than the design point current density ($0.5 \leq J_{normalized} < 1$); for current densities higher than this point ($1 < J_{normalized} \leq 1.5$), the situation is the opposite.

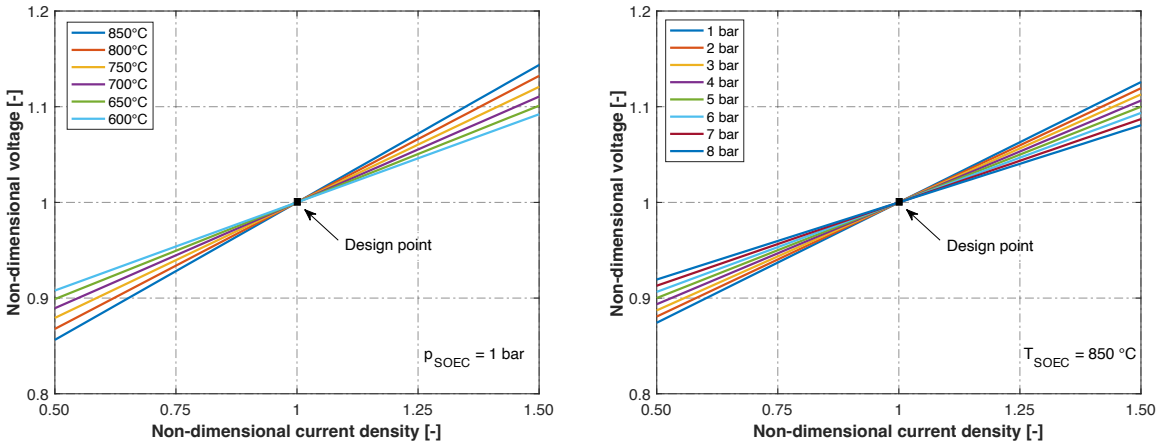

Fig. 3.12. Effect of a) T_{SOEC} and b) p_{SOEC} on the normalized polarization curve for a) p_{SOEC} = 1 bar and b) T_{SOEC} = 850 °C.

Fig. 3.13a shows the temperature trend at the output of the SOEC as a function of the electrical load for different operating temperatures. The outlet temperature varies from a minimum of about – 15 % (for an electrical load equal to the 50 % of the design point) to a maximum of about + 13 % (for an electrical load equal to the 150 % of the design point), considering an operating temperature of 850 °C. For lower operating temperatures the slope of the curve is lower. Indeed, for electrical loads lower than the design point, the voltage value for a set current density is higher for lower operating temperatures (see Fig. 3.12a) and, then, the output temperature is higher, according to the equations Eq. 3.15 and Eq. 3.16; for electrical loads higher than the design point, the situation is the opposite: this leads to a slope of the curve lesser degree. Fig. 3.13b shows the effect of the operating pressure on the temperature at the outlet of the SOEC, as a function of the electrical load. The outlet temperature varies from a minimum of approximately – 11 % (for an electrical load equal to the 50 % with respect to the design point) to a maximum of approximately + 10 % (for an electrical load equal to the 150 % with respect to the design point), considering an operating pressure of 8 bar. In this

case, for lower operating pressures the slope of the curve is higher. This behavior can be explained through the evaluation of the voltage (see Fig. 3.12b) for different operating pressures, according to equations Eq. 3.15 and Eq. 3.16.

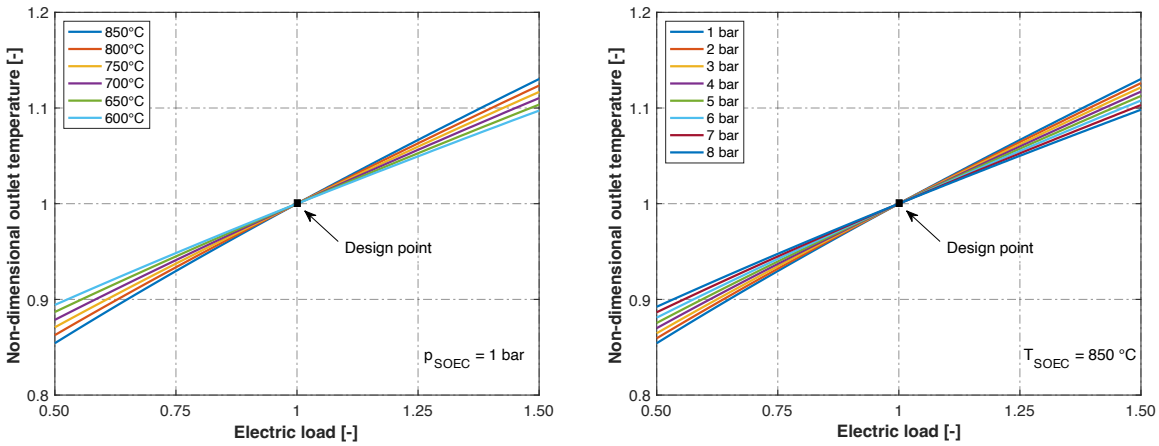

Fig. 3.13. Normalized outlet temperature as a function of the electric load for several a) operating temperatures (p_{SOEC} = 1 bar) and b) operating pressures (T_{SOEC} = 850 °C).

Fig. 3.14a shows the SOEC efficiency gain as a function of the electrical load for several operating temperatures. In this figure, the design point is represented by the point (1; 0), with a null efficiency gain in correspondence of the design electric load. The efficiency gain varies from a maximum of about + 14 % (for an electrical load equal to 50 % of the design point) to a minimum of about – 10 % (for an electrical load equal to 150 % of the design point), considering an operating temperature of 850 °C. Even in this case, for lower operating temperatures the slope of the curve is lower. Finally, Fig. 3.14b shows the SOEC efficiency gain as a function of the electrical load for several operating pressures. The efficiency gain varies from a maximum of about + 10 % (corresponding to an electrical load halved compared to the electrical design load) to a minimum of about – 7 % (for a load equal to 150 % of the design load), considering an operating pressure of 1 bar. For higher operating pressures the slope of the curve is higher.

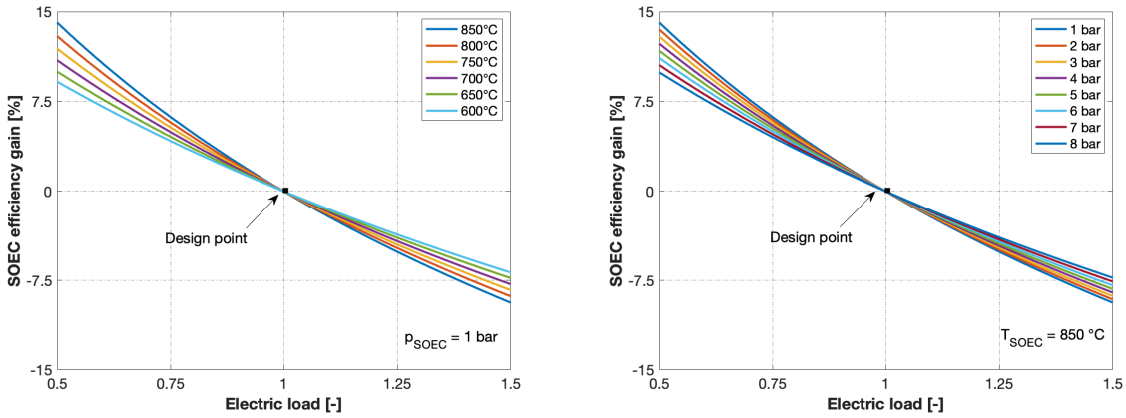

Fig. 3.14. SOEC efficiency gain as a function of the electric load for several a) operating temperatures (p_{SOEC} = 1 bar) and b) operating pressures (T_{SOEC} = 850 °C).

3.2.3 – Thermodynamic model modification

As shown previously, in order to predict the behavior in off-design conditions of the SOEC co-electrolyzer - a fundamental component of the P2G system and with the highest electrical energy consumption – a detailed electrochemical sub-model has been implemented, by referring to a set of experimental data. This sub-model has to be integrated with the other components of the P2G system, which are led to operate in off-design conditions; therefore, the overall thermodynamic model has been properly adapted. In order to simulate the off-design behavior of the other sub-sections, a simpler approach has been used, but always based on a lumped-parameters method, and by means of:

1) off-design maps and parameter correction, derived from manufacturers and/or from physical correlations;
2) simplifying hypotheses, with the assumption of constant values for different operating parameters (for a variable load).

In particular, specific modifications have been implemented for the off-design conditions on the thermodynamic model in the Aspen HYSYS™ environment, both in the HRS section, in the methanation sections, and in the compression section, as detailed below.

HRS and methanation sections

Regarding the HRS, whose purpose is to pre-heat the water stream at the inlet of the P2G system, here the available heat in the downstream sections of the P2G system is exploited. In more detail, the heat is recovered from the streams at the outlet of the cathode and of the anode of the SOEC and from all the cooling sections of the methanation reactors.

When the system operates in off-design conditions, the values of the temperatures and of the flow rates of the several streams involved in the HRS differ from the values in design

conditions, mainly due to the different electrical input of the SOEC; this situation determines a change in the flow and temperature values of the SOEC products (quantifiable with the SOEC sub-model previously illustrated).

In order to simulate the off-design behavior of the HRS, first of all, the (UA) values (where U [W/m²K] is the global heat transfer coefficient and A [m²] is the heat exchange surface) of each heat exchanger of this section have been calculated in design conditions (these values have been obtained through the simulation of the P2G model in the Aspen HYSYS™ environment). Once the UA values have been obtained for the several heat exchangers in design conditions, they have been modified under variable load conditions according to the flow rate of the hot fluid stream, by means of a simplified correction law of the *thermal resistance scaling* type:

Eq. 3.19. $$UA_{off-design} = UA_{Design}\left(\frac{\dot{m}_{Design}}{\dot{m}_{off-design}}\right)^{x}$$

where, the values of UA and the flow rate $\dot{m}$ of the hot fluid in design and the flow rate value in off-design are known for each heat exchanger and the correction coefficient of the flow rate x can be assumed to be equal to 0.8. This relationship, based on dimensional analysis, is commonly used for heat exchangers [51] and it considers the geometric exchange area fixed and assumes that the thermo-hydraulic properties of the flows do not change significantly as the load varies. The modification of the UA values in off-design conditions is determined by means of an external routine integrated with the thermodynamic model of the system, according to Fig. 3.7 and determines a re-adjustment of the temperature levels of the fluid streams leaving each heat exchanger of the HRS section. Due to this modification, the overall thermodynamic model in the Aspen HYSYS™ environment determines the new conditions of external thermal power in input to the HE_{H2O} and HE_{CO2} heaters (see Fig. 3.5 and Fig. 3.6) on which the system performance depends.

Regarding the off-design behaviour of the methanation sections (HTM and LTM), it has been assumed that the related chemical reactors in the lumped-parameter thermodynamic model keep working at the temperature set by the design boundary conditions (see Tab. 3.2). The structure of the chemical reactions model set in Aspen HYSYS™ for the design point (see 3.1 - Design modelling) is able to follow the change in the value of the input flow even under variable load conditions. Following the simulation of the system with the solution of the thermochemical balances of the reactors in off-design conditions, the thermal conditions of the streams leaving the methanation reactors will be modified.

SNG processing section

Regarding the compression section (and water separation), when the overall P2G system works in off-design conditions, the installed devices are forced to operate in conditions

different from the design point. In particular, as the electrical load input to the electrolyser varies, the flow rates of the SOEC reactants vary proportionally and, as a consequence, the flows of the produced synthesis gas vary too; the several compressors of the system therefore work in off-design conditions, determined by the different flow rate to be processed; for a given compressor, the corresponding operating point moves on the performance map of the specific machine, which can be experimentally derived, for the general form of which reference is made to Cohen et al. [52]. The magnitude of the variations in load and performance that can be achieved depends on the type of compressor, the model and the specific application of the compressor.

For example, large centrifugal compressors installed in natural gas compression stations can operate with very variable loads – see, for example, the head-flow diagram of Fig. 3.15 reported by Kurtz et al. [53] - with several operating points in off-design conditions characterized by a flow rate decrease to values below the 50 % of the value in design condition; as a consequence, there are significant variations in the performance of the machines, to be considered in order to correctly evaluate the energy balance of the compression section. The calculation of the compression energy consumption in off-design conditions can then be carried-out by means of the performance maps for the compressors as the load varies.

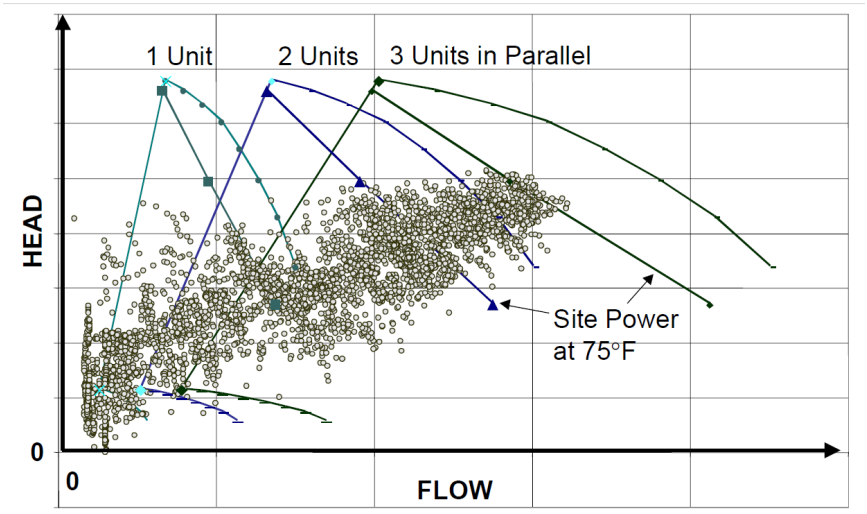

Fig. 3.15. Operating points of a typical compression station on the head-flow diagram (data reported in [53] and referring to 6 months operation of a natural gas compression station).

To this regard, in Fig. 3.16, the normalized operating maps for a typical centrifugal compressor [54] is shown; this map can be used for the application of this study.

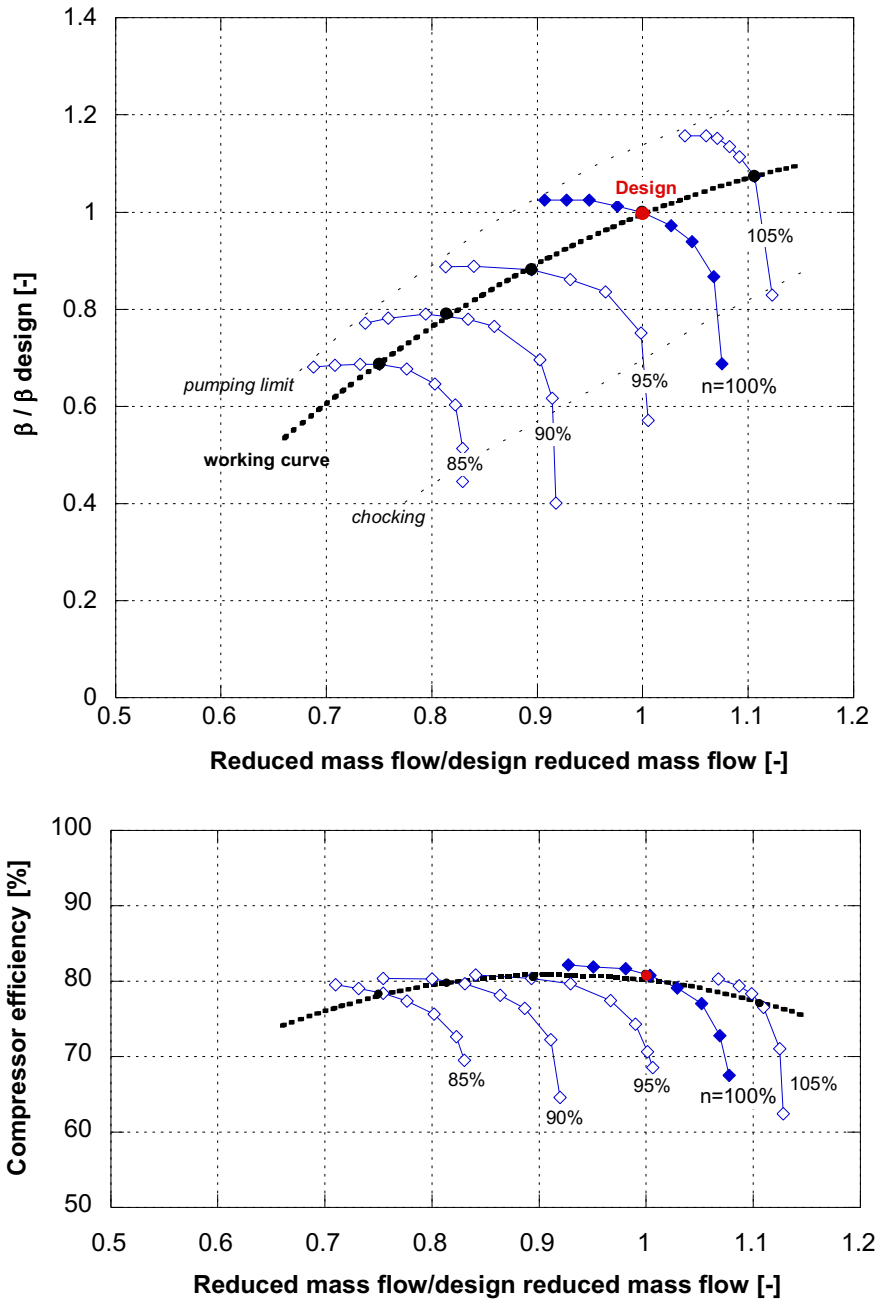

Fig. 3.16. Operating map of a centrifugal compressor for the off-design performance evaluation, reworked from [54]; design point definition.

In more detail, Fig. 3.16 provides the trends of the compression ratio (β), normalized with respect to the design value, as a function of the normalized reduced flow rate, for different values of the reduced speed. In Fig. 3.16, the compression efficiency as a function of the flow rate and of the speed is also shown; a possible working curve and the related performance curve is presented in the figure.

These curves have been used in the study to describe the performance of the system compressors in design and off-design conditions. The operating curve has been supposed in an intermediate position between the pumping limit and the sonic block condition of the

machine, interpolating different operating points on the curves at constant speeds; these points ensure high efficiency and allow to operate in a wide range of flow rate values. In this case, it is observed that moving on the working curve, the normalized flow rate can assume values between less than the 70 % and more than the 110 % of the design value, affecting the compression ratio. The corresponding isentropic compression efficiency is kept around the design value, that is set at 80 % in this study.

Referring to the above-mentioned maps, a modification has therefore been introduced in the Aspen HYSYS™ model, which allows to evaluate the operating point in off-design conditions and the corresponding variation of compressor energy consumption, due to the different gas flow rate processed.

Due to the intermittency of the renewable production, the SOEC electric energy input is variable during the considered time frame and, as a consequence, the flow rate processed by the compressors is variable too; then, in this work, a multi-unit compression group has been considered, made up of several parallel compressors, able to operate in succession as the flow rate to be processed increases. This multi-unit architecture is frequently used in real installations (see, for example, the study presented by Kurtz et al. [53] on the state-of-the-art of natural gas compression stations) and offers a great flexibility during the operations.

The optimal sizing of a multi-unit pumping/compression system depends on several factors, including the magnitude of the load variations and the partial load regulation capacity for the single unit, as highlighted in a previous work by Beevers et al. [55]. Considering these sizing criteria, the compression unit has been designed consisting of 4 centrifugal compressors, according to the layout of Fig. 3.17. In particular, the following assumptions have been made:

- in the P2G system design condition, only three parallel compressors are operational;
- the compressors in the multi-unit architecture have the same capacity, equal to 1/3 of the design capacity of the system at full load; therefore, each of these compressors works at full load at the design point of Fig. 3.16.
- in off-design conditions, when the SNG flow rate is lower with respect to the design point (electrical input of the P2G system between the 50 % and the 100 % of the design point), the three parallel compressors work at partial load, processing the same flow rate;
- the fourth compressor, which is inactive when the P2G system is in design condition or in off-design conditions with partial loads, works only if the processed flow rate increases with respect to the design point (electrical input of the P2G system between the 100 % and the 150 % of the design point);
- for the sake of simplicity, it has been assumed that the fourth compressor is of the same size as the other three;
- therefore, in order to meet the maximum demand, that is higher with respect to the design point of the four compressors (i.e. when the electrical input of the P2G system is between the 133 % and the 150 % of the design point), it has been considered that the four

compressors work in off-design conditions, with an over-compression power consumption with respect to the design point.

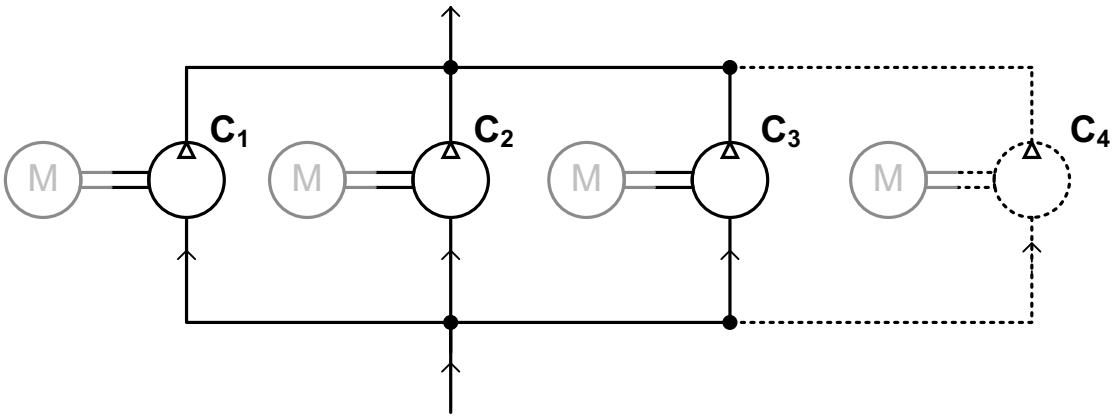

Fig. 3.17. Layout of the compression block.

Fig. 3.18 shows the load diagram for the four compressors of the multi-unit compression group, which allows to meet the increasing demand of gas flow rate to be processed as the electrical input of the P2G system varies; instead, Fig. 3.19 shows the trend of the normalized compression ratio as a function of the P2G system electric load, while, in Fig. 3.20, the trend of the isentropic efficiency for the multi-unit compression group as a function of the P2G system electric load is presented.

With the considered architecture of the compression section, consisting of 3 + 1 parallel compressors, the compression ratio varies on the basis of the load, limited between about the 60 % and the 110 % of the design value.

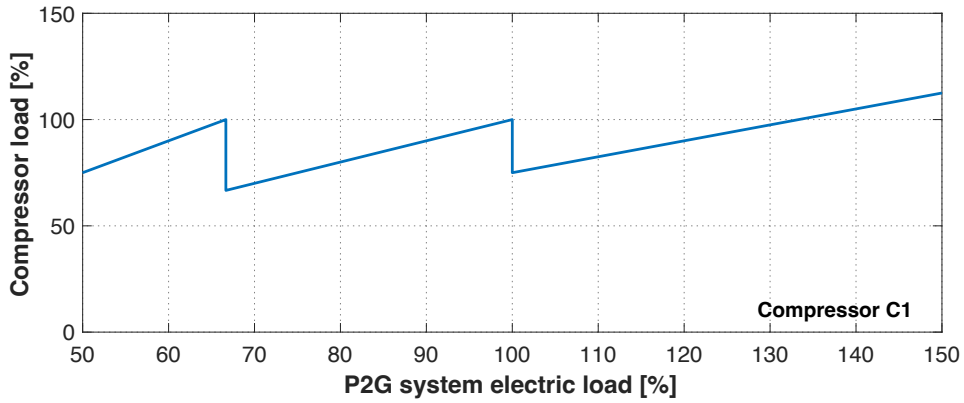

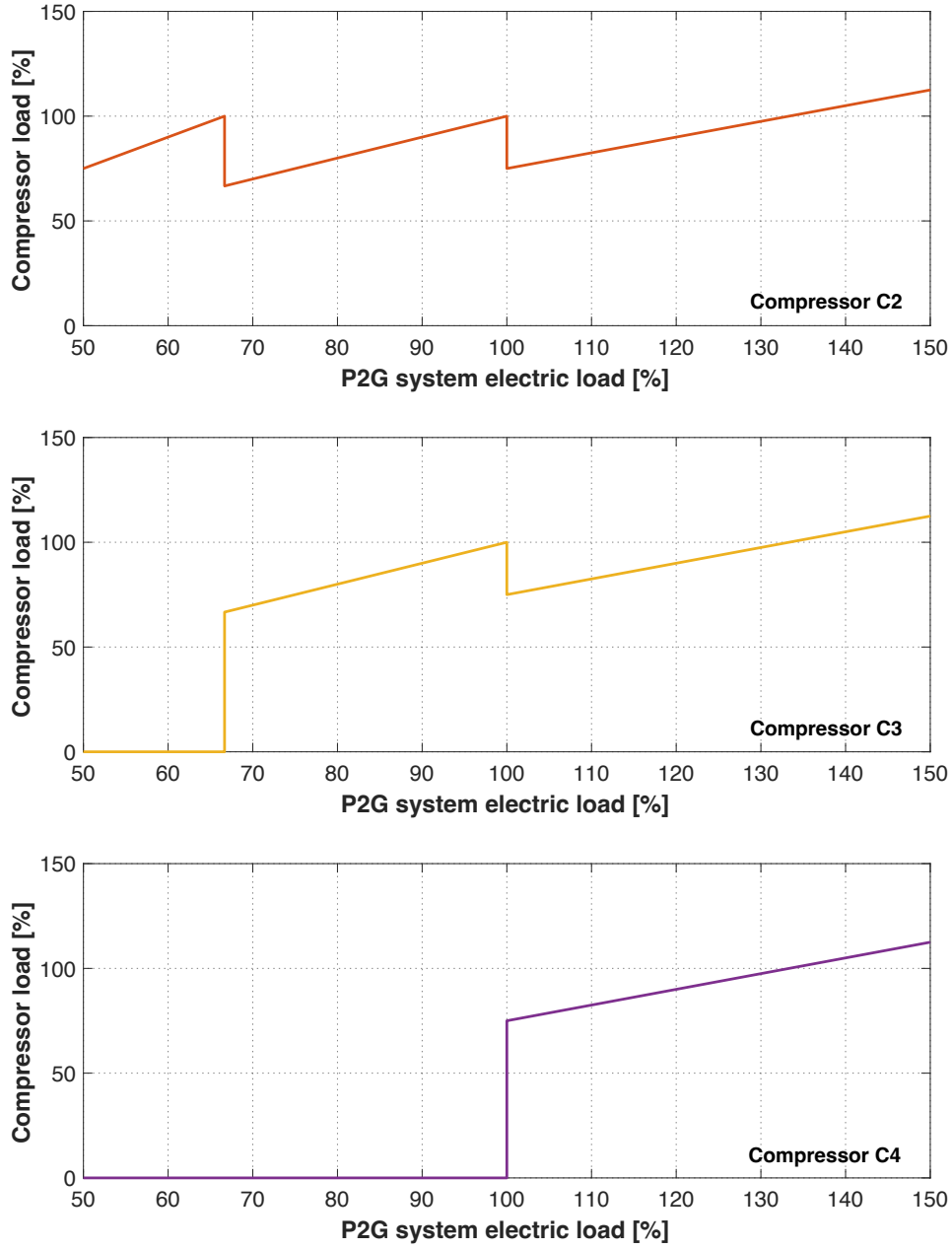

Fig. 3.18. Load diagram for compressors C1, C2, C3 and C4 as a function of the P2G system electric load.

In case that a lower variation of this parameter is required, it is necessary to further divide the compression layout, using a larger number of compressors, each of a smaller size. The number of machines that can be installed also depends on the actual total capacity required, which depends on the size of the P2G system (here considered equal to 1 MW, as a reference value). More complex strategies are also possible (not considered in this study) for the management of the compression section, for example by providing also the series connection and/or the switch between series-parallel connection of some machines of the compression section [56].

Finally, it is highlighted that, with the used architecture and management strategy, the compression efficiency is quite constant near the design value, as the electric load of the P2G system varies.

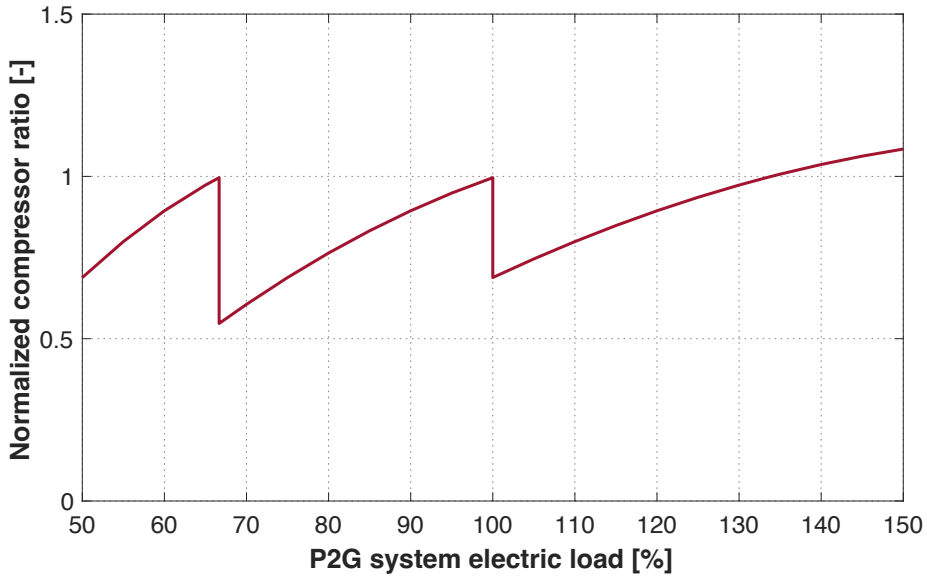

Fig. 3.19. Normalized compression ratio of the compression section, as a function of the P2G system electric load.

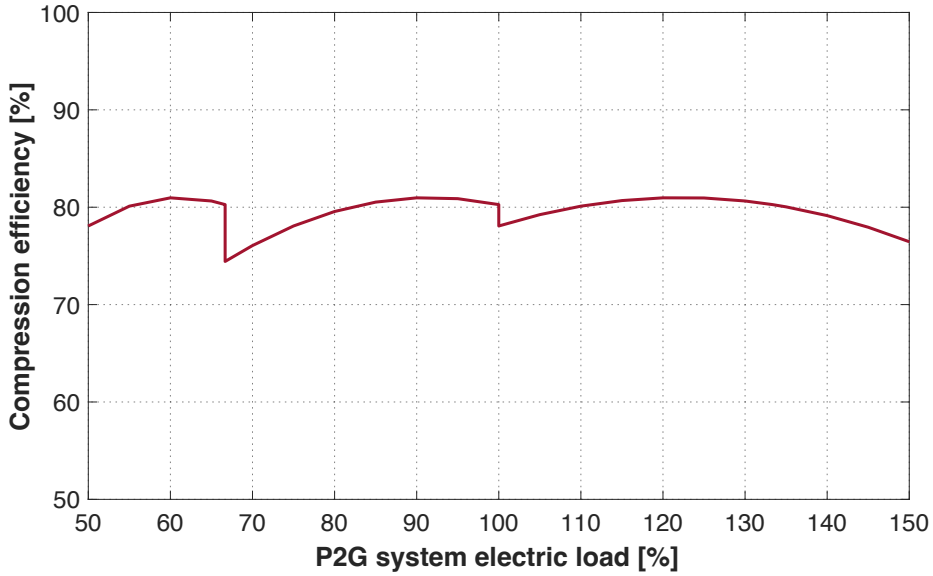

Fig. 3.20. Compression section efficiency as a function of the P2G system electric load.

Chapter 4 – Synthetic natural gas application: design analysis

In this chapter, parametric analyses on the behaviour of the P2G system have been carried out, starting from a reference case. In a first approach, the operating temperatures of the two key components (SOEC and HTM) have been varied: it has been assumed to reduce the maximum operating temperature of the co-electrolyser and to increase the operating temperature of the methanation section. In this analysis, any issue (thermal, composition, performance, …) related to the modification of the operating point of the several components has been evaluated. The main aim of this first step is to evaluate a possible unique operating temperature, considering the co-electrolysis section and the HTM reactor as a single process, in order to achieve the thermal integration between these sections.
Then, in a second step, an additional thermodynamic analysis has been carried out, varying the operating pressure of the co-electrolyser and of the methanation sections. The aim of this phase is to identify an optimal operating pressure level for the several components of the system.

4.1 – Analysis of the operating temperature effect on the system's components

Regarding the plant layout, specific improvements have been implemented to the reference layout, described in the previous chapter. In particular, the implementation of a heat recovery has been examined, as shown in Fig. 4.1. The scheme in the figure shows a simplified representation of the system with the heat recovery section (*HRS* in the figure) placed upstream of the co-electrolyser (*SOEC* in the figure). As already described in the previous chapter, with the implementation of this section it is possible to partially re-use the heat flows coming from the SOEC, the HTM and the LTM, for the pre-heating of the process reactants, as it will be examined in detail below.

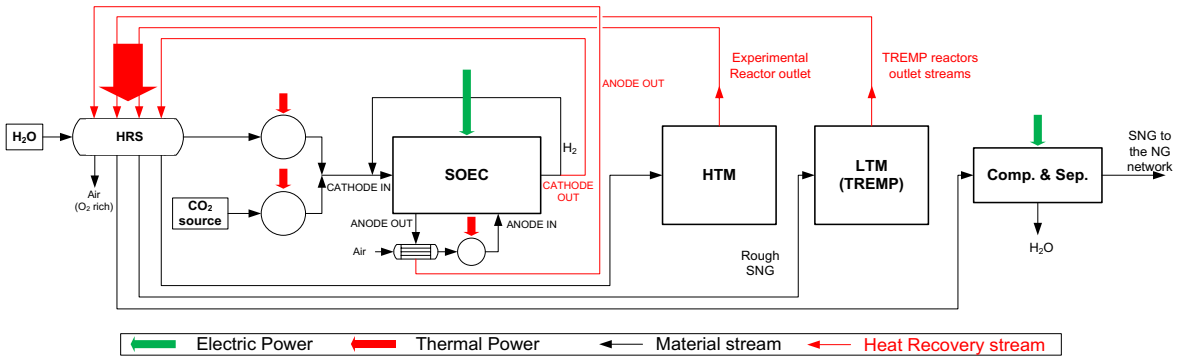

Fig. 4.1. Simplified scheme of the P2G system, in which the potential heat recoveries are highlighted in red.

In Fig. 4.2, instead, the actual scheme of the heat recovery section, whose architecture depends on the temperature levels of the recovered heat flows, has been presented. This scheme represents the starting point for all the reported analyses; from here on out, this system configuration will be referred as the "Base Case".

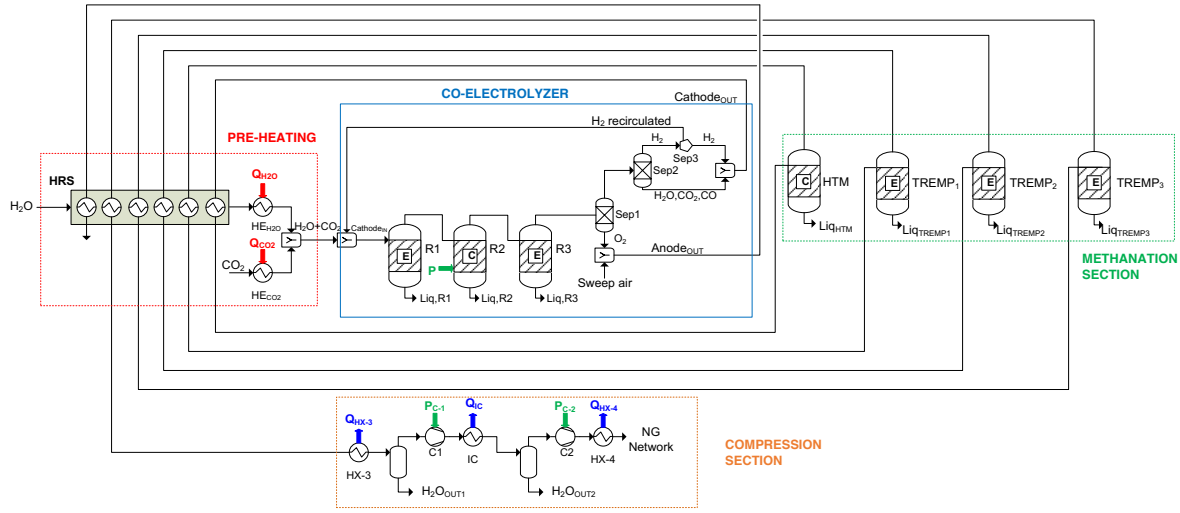

Fig. 4.2. The reference model with heat recovery (HRS section): scheme related to the "Base Case".

In this layout, it has been decided to pre-heat only the SOEC feed water stream by means of internal heat recoveries. In general, in this case, it has been considered to recover six different heat flows coming from the downstream processes. As it can be seen in the figure, the water, before entering into the co-electrolyzer with the carbon dioxide, passes through the HRS preheating section, in which the recovery of thermal power from the following streams takes place:

i. the sweep air stream at the outlet of the SOEC anode side;
ii. the syngas stream at the outlet of the SOEC cathode side;

iii. the cooling stream from the HTM reactor;
iv. three cooling streams from the reactors of the LTM section.

The choice of the available streams at high temperature levels, usable in the preheating line, and the arrangement of the heat exchangers have been made on the basis of the temperature levels of the several streams. However, the recovered thermal power is not sufficient to reach the operating temperature of the co-electrolyser. Therefore, an external supply of heat is necessary and additional thermal inputs for the H_2O and CO_2 streams are provided in the model. These external heat exchangers, indicated in the figure as HE_{H2O} for the water stream and HE_{CO2} for the carbon dioxide stream, are necessary in order to ensure that the operating temperature of the SOEC is achieved.
In Fig. 4.3 the layout of the Base Case developed on the Aspen HYSYS™ environment is shown.

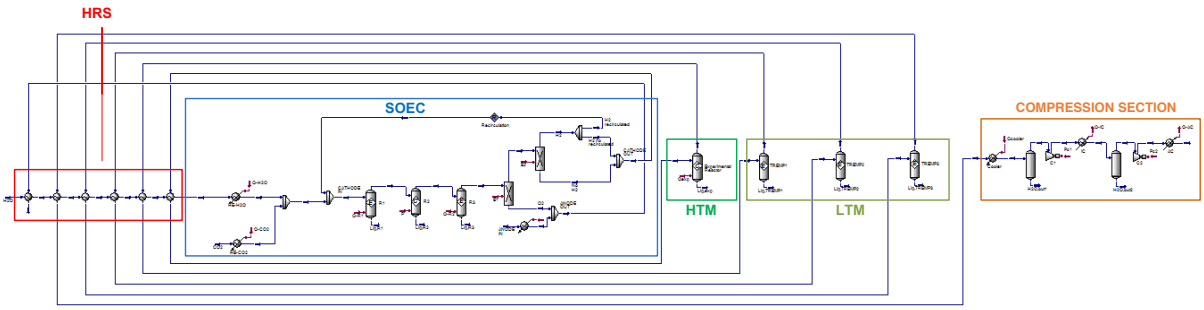

Fig. 4.3. Base Case layout in the Aspen HYSYS™ environment.

The main set point parameters (introduced in the previous chapter), representing the inputs of the model for the Base Case, are presented in Tab. 4.1.
The operating temperatures related to the Base Case have been varied, in order to evaluate - as already mentioned - how the temperature affects the system performance and to identify a possible unique temperature value for the SOEC and the experimental methanator (HTM). The other operating parameters, on the other hand, have been kept constant.

Tab. 4.1. Main set point parameters for the P2G system Base Case.

Parameter	Value	Units
SOEC operating temperature	850	[°C]
HTM operating temperature	450	[°C]
LTM operating temperature	200	[°C]
H_2O inlet temperature	25	[°C]
CO_2 inlet temperature	25	[°C]
Sweep air inlet temperature	25	[°C]
Electrolysis reactions conversion rate	80	[%]
SOEC inlet H_2O fraction	80	[%]
SOEC inlet CO_2 fraction	20	[%]
SOEC input electric power	1	[MW]
SOEC operating pressure	1	[bar]
Methanation section operating pressure	1	[bar]
$x_{O2,anode,out}$	0.5	[-]
Inter-cooling temperature	25	[°C]
NG distribution network pressure	60	[bar]
Inter-cooling pressure	7.75	[bar]
After-cooling temperature	25	[°C]

In more detail, in this first phase of analyses:

1. the operating temperature of the SOEC has been gradually reduced starting from 850 °C (which corresponds to the Base Case and represents a technology standard that guarantees high efficiency) up to 600 °C (value that has been considered as the lower limit for the SOEC study – see the previous chapter);
2. the operating temperature of the methanation section has been increased (starting from the value equal to 450 °C, optimal for the HTM according to the previous experimental investigations, up to 600 °C, which allows, based on the available experimental data, a still sufficient conversion to methane).

At first, only the temperature of the SOEC has been varied (keeping constant the operating temperature of the methanation section) and, subsequently, the operating temperature of the

HTM reactor has been varied. In Tab. 4.2 the cases analysed in this first phase of work are presented. In the carried-out simulations, the operating temperature of the LTM, instead, has been kept constant and equal to 200 °C; the only exception is Case 10 (see Tab. 4.2), in which a LTM section operating at 600 °C has been considered. Indeed, the TREMP™ technology represents, in the study, an auxiliary of the integrated SOEC-HTM system to be used in its optimum conditions. The LTM section has been introduced mainly due to the need to increase the methane yield (maximum yield at 200 °C). The last examined case, however, with the three macro-components operating at the same temperature, allows a still acceptable operation of the LTM system, but with lower efficiencies.

Tab. 4.2. Analysed cases in the operating temperature analysis.

Case	T_{SOEC} [°C]	T_{HTM}[°C]	T_{LTM} [°C]	Case name
1*	850	450	200	850/450/200
2	800	450	200	800/450/200
3	750	450	200	750/450/200
4	700	450	200	700/450/200
5	650	450	200	650/450/200
6	600	450	200	600/450/200
7	600	500	200	600/500/200
8	600	550	200	600/550/200
9	600	600	200	600/600/200
10	600	600	600	600/600/600

** Case 1 represents the Base Case*

*** The cases in which the SOEC temperature has been varied are highlighted in orange; the cases in which the HTM temperature has been varied are highlighted in green; the case in which the LTM temperature has been varied is highlighted in blue.*

4.1.1 – HRS section architectures

Regarding the HRS recovery section used to preheat the water stream at the inlet of the P2G system, the several cases presented in Tab. 4.2 show relevant differences in the architecture of the heat exchangers' arrangement. In particular, according to the operating temperature level of the SOEC, HTM and LTM components, three different arrangements of the heat exchangers have been developed in the HRS section, respectively shown in Fig. 4.4, Fig. 4.5 and Fig. 4.6. In Tab. 4.3, instead, these architectures have been divided according to the thermal levels of the three macro-components.

In the arrangement developing, a general criterion has been adopted in the stream order of use: first the streams characterized by a lower thermal level, and then the streams available at a gradually higher thermal level. In this way, as commonly known, the heat exchange is optimized, reducing the irreversibility of the heat exchange between the two considered fluids.

In the Base Case, the HRS section consists of 6 heat exchangers, according to Fig. 4.4: in order, the anodic stream, the stream at the outlet of the *TREMP3* reactor, the stream at the outlet of the *TREMP2* reactor, the stream at the outlet of the *TREMP1* reactor, the stream at the outlet of the HTM reactor and the cathodic stream are recovered. This architecture has also been applied to the cases in which the outlet temperature of the streams from the HTM and LTM sections is lower than the operating temperature of the SOEC.

Tab. 4.3. HRS section architectures on the basis of the operative temperatures.

# **HRS architecture**	**HRS heat exchangers**	**Case** ($T_{SOEC}/T_{HTM}/T_{LTM}$) **[°C]**
HRS #1	6	1) 850/450/200 2) 800/450/200 3) 750/450/200 4) 700/450/200 5) 650/450/200 6) 600/450/200 7) 600/500/200 8) 600/550/200
HRS #2	5	9) 600/600/200
HRS #3	2	10) 600/600/600

Instead, in Case 600/600/200, the configuration of the HRS section includes only 5 heat exchangers (see Fig. 4.5). In this case, indeed, the co-electrolyser and the experimental methanation reactor are at the same temperature (600 °C) and, then, the products of the co-electrolysis at the inlet of the downstream HTM section do not require cooling; the cooling of the co-electrolysis products has been implemented in the other cases (Fig. 4.4) by means of the last heat exchanger (next to the external thermal input, *HE-H_2O*) in the preheating line.

Finally, for Case 600/600/600 the configuration of the HRS line has been reduced to 2 heat exchangers (Fig. 4.6), since also the three reactors of the LTM section (TREMP™ reactors) work at the same temperature (600 °C) of the SOEC and of the HTM section; as a consequence, the streams at the outlet of the first two reactors of the LTM section cannot be used for preheating

purposes. In more detail, it is possible to exploit only the thermal content of the anodic stream at the outlet of the SOEC and of the stream at the outlet of the last methanation reactor of the LTM section, upstream of the compression section of the SNG.

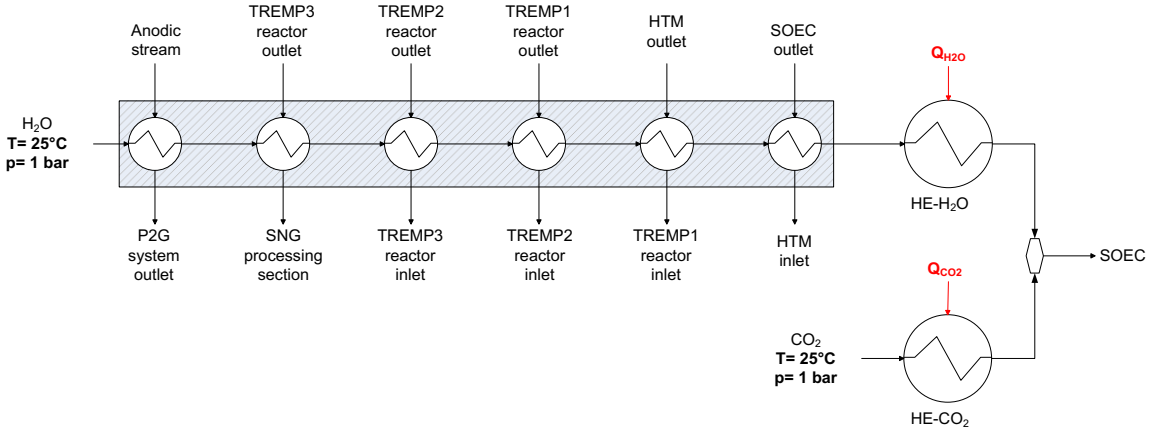

Fig. 4.4. HRS section configuration with 6 heat exchangers (Base Case and variants with $T_{SOEC} > T_{HTM}$ and $T_{SOEC} > T_{LTM}$).

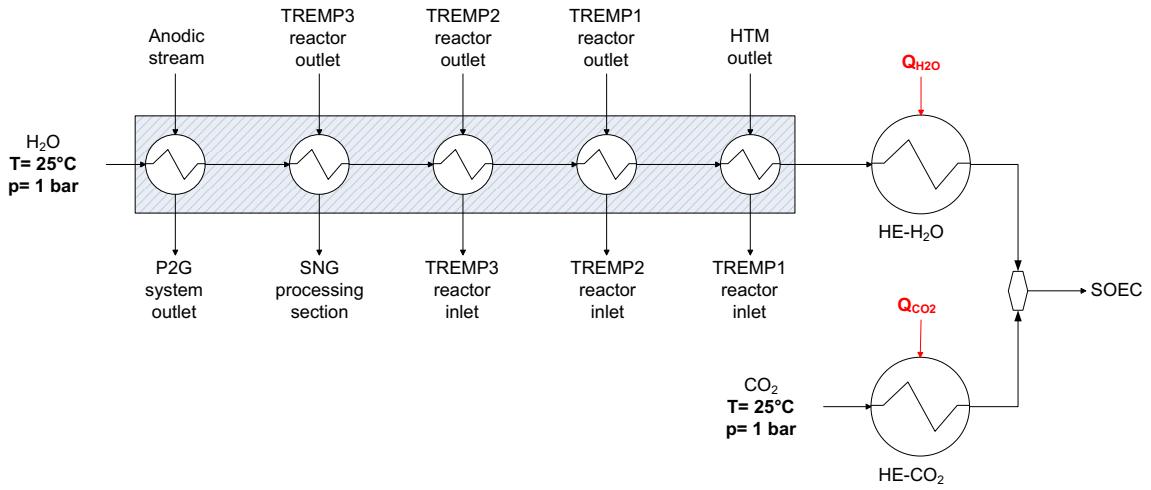

Fig. 4.5. HRS section configuration with 5 heat exchangers (Case 600/600/200).

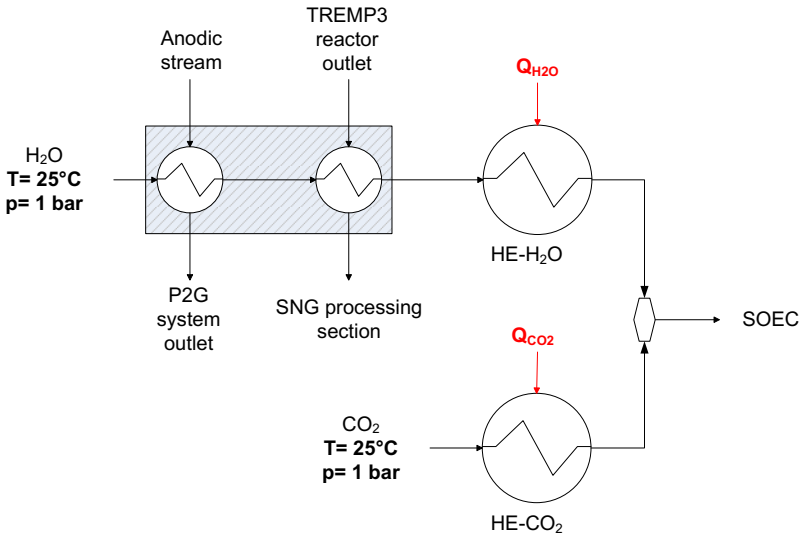

Fig. 4.6. HRS section configuration with 2 heat exchangers (Case 600/600/600).

4.1.2 – Results

The results of the thermodynamic simulations carried out for the cases of Tab. 4.2 have been examined in order to compare the several variants of the system and to identify the most promising configurations of the P2G storage system. The performances have been assessed by means of specific parameters in order to evaluate:

i. the energy conversion efficiency of the P2G system, with a focus to the first law efficiency, the second law efficiency and the different types of energy consumptions of the system;
ii. the quality of the produced SNG. In particular, the most important system performance parameters have been calculated, the definition of which is presented in Appendix A.

Fig. 4.7a shows the calculated values of the first law efficiency (η_I) and the second law efficiency (η_{II}), for the analysed cases in terms of operating temperatures; the figure shows also the values of the thermal power required by the overall process ($Q_{requested}$), of the thermal powers supplied from external thermal inputs ($Q_{IN,TOT}$) and of the recovered thermal power ($Q_{recovered}$).

The first law efficiency shows a trend as a function of the operating temperatures not constant (even if with limited variations) for the several analysed cases. This type of efficiency presents an average value around 75 % for $\eta_{I(LHV)}$ and around 83 % for $\eta_{I(HHV)}$; the average values of η_{II} are around 77 %, with a trend similar to the first law efficiency. The peak value for the efficiency is observed for the case 600/600/200 (Case 9), with $\eta_{I(HHV)}$ = 85.2 %, with respect to a value for the Base Case equal to 83 %; instead, a minimum value of efficiency is observed in the case 600/600/600 ($\eta_{I(HHV)}$ = 82.5 %). The maximum value of η_{II} is in correspondence of

the case 600/600/200 and is equal to 79 %, with respect to a value equal to 77.2 % for the Base Case.

The differences in the values of the two considered efficiencies are essentially due to the different thermal power supplied from an external source, in relation to the overall demand of the P2G process. In Fig. 4.7b it is highlighted that the thermal demand of the process $Q_{requested}$ (to preheat the reactants at the inlet of the SOEC) decreases from Case 1 to Case 6 (as the operating temperature of the SOEC decreases); then, the thermal demand is constant for the cases in which T_{SOEC} = 600 °C (from Case 6 to Case 10). The thermal power supplied from an external source, $Q_{IN,TOT}$, instead, does not follow a monotonous behaviour and it varies for the several analysed cases on the basis of the different temperature levels of the single sections. In particular, $Q_{IN,TOT}$ is minimum for the case 600/600/200 and it is maximum in the case 600/600/600, in which the heat recovered is lower.

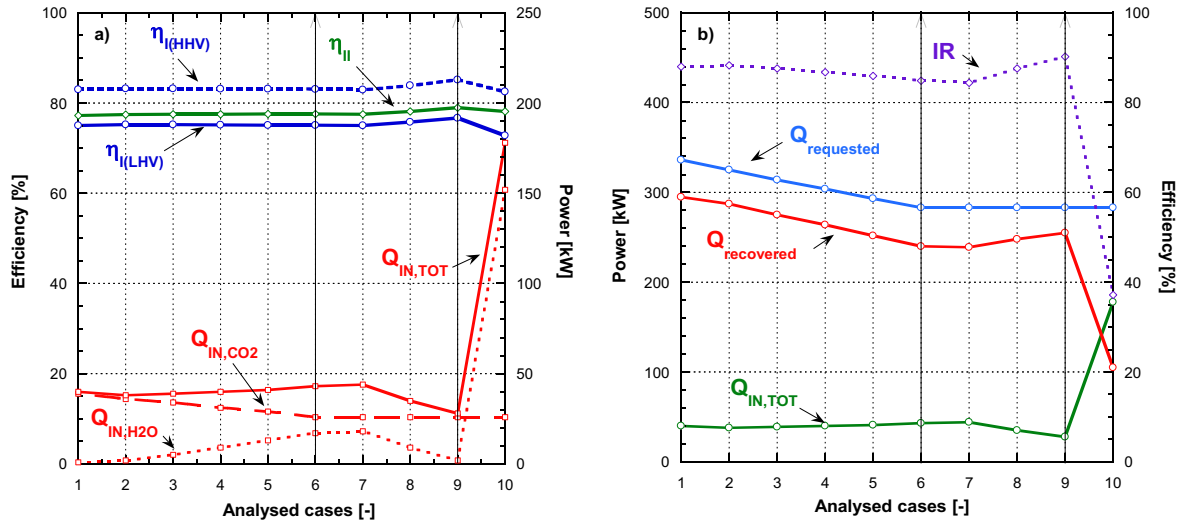

Fig. 4.7. a) First law efficiency, second law efficiency and supplied thermal power; b) heat recovered, heat requested and index of recovery.

Fig. 4.8 shows the "electric-to-fuel" conversion index, η_{E2F}, that is the ratio between the energy content of the produced SNG and the electric energy input to the P2G system (see the formulas in Appendix A). The values of this parameter are shown in Fig. 4.8a, referring to both the lower heating value (LHV) of the produced SNG and to its higher heating value (HHV), for the considered cases. From the results, it is shown that the calculated values of η_{E2F} for the greater part of the analysed cases are around 78 %, on LHV-basis, and around 86 % on HHV-basis. Only in Case 10 (case of temperatures 600/600/600) the value of this parameter is greater, mainly due to the higher content of hydrogen in the stream at the outlet of the P2G system, which - as it will be seen later - affects the chemical energy of the SNG stream at the outlet of the P2G system. The electrical power consumption of the system, instead, is quite

constant for the greater part of the cases (Fig. 4.8b) and only in the case of 600/600/600 there is an increase in the electrical power consumption for compression, due to the higher flow rate at the outlet of the P2G system. However, the increase in the electrical power consumption is balanced by the higher chemical power of the SNG stream. As shown in Appendix A, the definition of η_{E2F} does not include the thermal power consumption of the P2G system and, then, the results shown in Fig. 4.7 (first and second law efficiency) are considered more relevant.

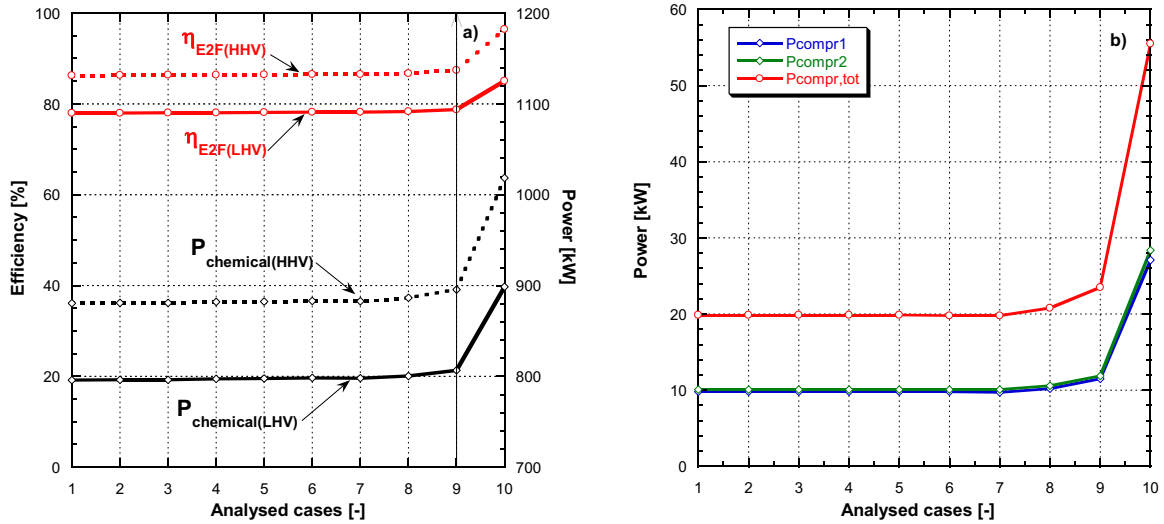

Fig. 4.8. a) Electric-to-fuel conversion index and chemical power of the system outlet stream; b) total electric power consumption for compression and for the single compressors.

Finally, Fig. 4.9 shows the results regarding the composition and values of the HHV and of the Wobbe index for the SNG stream at the outlet of the whole system, for the several analysed cases. In the cases in which only the operating temperature of the co-electrolyser has been varied (cases from 1 to 6), the composition of the SNG stream is quite constant (in particular the methane content, with a molar fraction value equal to $x_{CH4} = 0.79$ - Fig. 4.9a); this result can be explained since the methanation sections work at a set temperature, with the boundary conditions of the reference case. By increasing, instead, the operating temperature of the experimental methanation reactor (cases from 7 to 9) starting from the optimum value equal to 450 °C, a decrease in the molar fraction of methane in the stream is pointed out (up to $x_{CH4} = 0.64$ for the case 600/600/200). Finally, by increasing the operating temperature of the LTM reactors from 200 °C to 600 °C, there is a severe decrease in the molar fraction of methane ($x_{CH4} = 0.13$), since the equilibrium reactions of the methanation tend towards the reactants (and as a consequence more hydrogen is produced).

In a similar way, the HHV of the SNG stream at the outlet of the overall system shows a rather constant trend in cases 1 to 6 (Fig. 4.9b), with a value around approximately 31500 kJ/Sm^3. By

increasing the temperature of the HTM section, the HHV tends to decrease due to the decrease of the methane molar fraction in the SNG stream up to a value equal to about 27000 kJ/Sm^3 for case 9. Finally, for case 10, the HHV shows a decrease up to about 14000 kJ/Sm^3. The Wobbe index shows a trend very similar to that assumed by the HHV, going from a maximum of about 44000 kJ/Sm^3 (cases from 1 to 6) to a minimum of about 23000 kJ/Sm^3 (case 10).

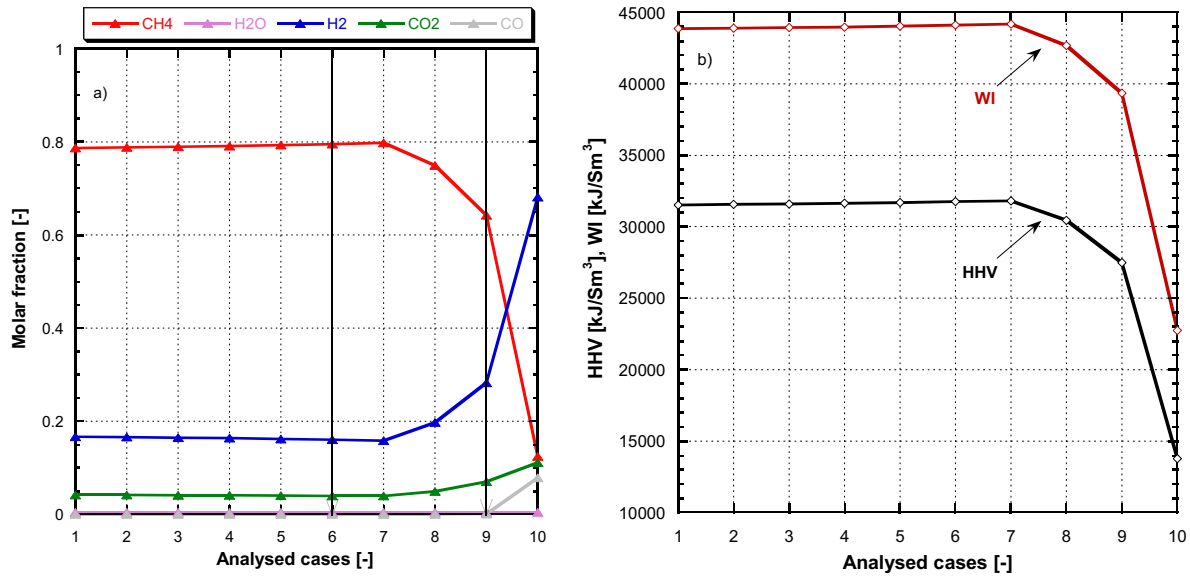

Fig. 4.9. a) SNG composition for the analysed cases; b) HHV and Wobbe index (WI).

From this first sensitivity analysis of the system performance, varying the operating temperature of the single sections and by means of the model developed on Aspen HYSYS™, it can be concluded that:

- in a system in which heat exchangers, for heat recovery and to preheat the reactants at the inlet of the SOEC, are provided, when the SOEC operating temperature decreases (from 850 °C to 600 °C) the conversion efficiencies in terms of η_I do not vary considerably, since both the thermal power demand and the amount of heat recovered decrease;
- moreover, if the operating temperature of the HTM increases up to 600 °C, a slight increase in the 1st law and 2nd law efficiencies is observed; for both parameters, the advantage with respect to the starting Base Case is equal to an increase of about 2 - 3 percentage points;
- the temperature increase in the LTM reactors up to 600 °C is not beneficial in terms of first and second law efficiency. This effect can be considered positive only from the point of view of the less significant "electric-to-fuel" conversion index. However, this variant shows a decrease in the methane content and an increase in the concentration of hydrogen in the produced SNG.

4.2 – Analysis of the operating pressure effect on the system's components

In this phase, a further thermodynamic analysis has been carried out, in which the operating pressure of the co-electrolyser and of the methanation sections has been varied. Both the effects of the operating pressure on the main subsystems and the electrical energy consumption of the main compression and pumping machines, that represent the auxiliaries of the plant to be placed upstream and/or downstream of each subsystem, have been considered in the energy and exergy balance. In particular, the thermodynamic model has been modified, evaluating and comparing different configurations of the system layout, in which the pressurization section has been placed differently.

The aim of this investigation phase is to identify an optimal operating pressure condition for the different components of the system; in particular, it is known that, in general, the electrolysis chemical reactions are negatively affected by high pressure values, while the methanation chemical reactions are favoured by high pressure values [57]. For example, if the operating pressure of the LTM increases with respect to what it has been presented so far (in the analyses carried out in 4.1 – Analysis of the operating temperature effect on the system's components, it has been considered that the process takes place at ambient pressure), the production of methane should increase, compared to the case with non-pressurized methanation.

In order to investigate the effect of the operating pressure on the overall performance of the P2G system, by means of the developed numerical model, several modifications to the original layout of the P2G system have been implemented.

It should be highlighted that the considered P2G system provides for the introduction into the NG network of the produced SNG; in the carried-out survey, it has been assumed that the network storage pressure is always equal to 60 bar in all the considered configurations. Therefore, in order to achieve this final storage pressure level, a pressurization subsystem is always required, but it is possible to place this compression section in different points of the P2G system. In particular, the carried-out parametric analysis takes into account the following three main configurations:

a) pressurization placed downstream of the LTM section (cases shown and discussed in the previous paragraph);
b) pressurization of the LTM section;
c) pressurization of the SOEC.

Fig. 4.10 schematically shows a block diagram of the three pressurized configuration.

In the following paragraphs, each variant of the pressurized system will be introduced and presented in detail, describing the layout characteristics and the inputs used in the simulation,

and then the results will be analysed, for a comparison of the different configurations taken into account.

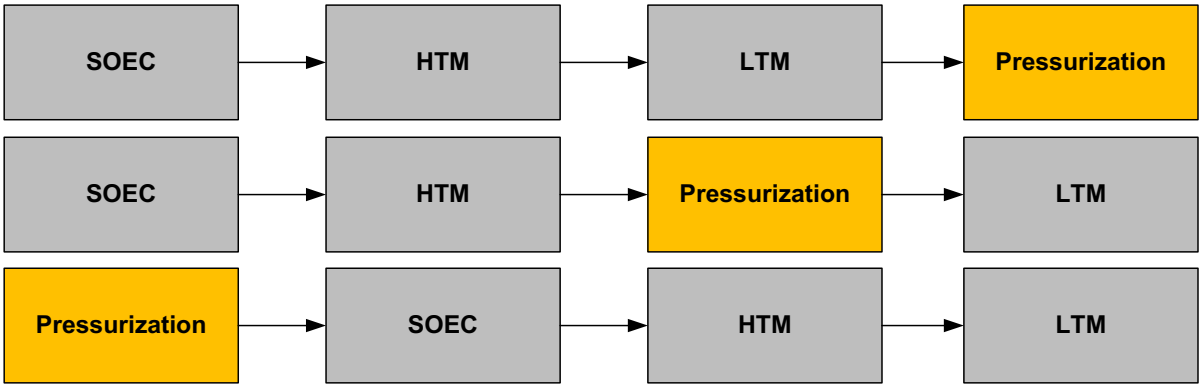

Fig. 4.10. Analysed pressurized configurations.

4.2.1 – Analysed variants

Tab. 4.4 summarizes the examined configurations in this further investigation on the effect of the pressure. The acronym "P-TAIL" is related to the layout cases in which the pressurization of the SNG takes place downstream of the last methanation stage (downstream of the LTM); "P-LTM" is related to the layouts in which the pressurization occurs upstream of the LTM section; finally, "P-SOEC" is related to the cases in which the electrolyser is pressurized (and then the related flows at the inlet/outlet are pressurized, as well as the components downstream of the SOEC).

In Tab. 4.4 it is shown that for each pressure variant, different operating temperatures of the three key plant sections (SOEC, HTM and LTM) have been considered; different system schemes correspond to each of these thermal level conditions, regarding the HRS section, as detailed below and presented in the table.

Tab. 4.4. Analysed cases in the operating pressure analysis.

Pressurization	Case name	Operating temperature	HRS heat exchangers	Sweep air pre-heating
Downstream LTM	**P-TAIL**	1) 850/450/200	6	Yes/No
		2) 800/450/200		
		3) 750/450/200		
		4) 700/450/200		
		5) 650/450/200		
		6) 600/450/200		
		7) 600/500/200		
		8) 600/550/200		
		9) 600/600/200	5	Yes/No
		10) 600/600/600	2	Yes/No
Upstream LTM	**P-LTM**	1) 850/450/200	6	Yes/No
		2) 800/450/200		
		3) 750/450/200		
		4) 700/450/200		
		5) 650/450/200		
		6) 600/450/200		
		7) 600/500/200		
		8) 600/550/200		
		9) 600/600/200	5	Yes/No
		10) 600/600/600	2	Yes/No
Upstream SOEC	**P-SOEC**	1) 850/450/200	7	Yes
		2) 800/450/200		
		3) 750/450/200		
		4) 700/450/200		
		5) 650/450/200		
		6) 600/450/200		
		7) 600/500/200		
		8) 600/550/200		
		9) 600/600/200	6	Yes
		10) 600/600/600	2	Yes

4.2.2 – P-TAIL cases (with and without sweep air pre-heating)

These cases are characterized by the pressurization of the produced SNG by means of the compression system placed downstream of the LTM section. In this case, a modification to the Base Case layout has been implemented: an additional heat exchanger to preheat the sweep air, at the inlet of the SOEC, by means of the stream at the outlet of the anodic side. This

solution - even if an additional heat exchanger is required - has been considered due to the energy savings, reducing the thermal power consumption from an external source to preheat the sweep air (see Fig. 4.11).

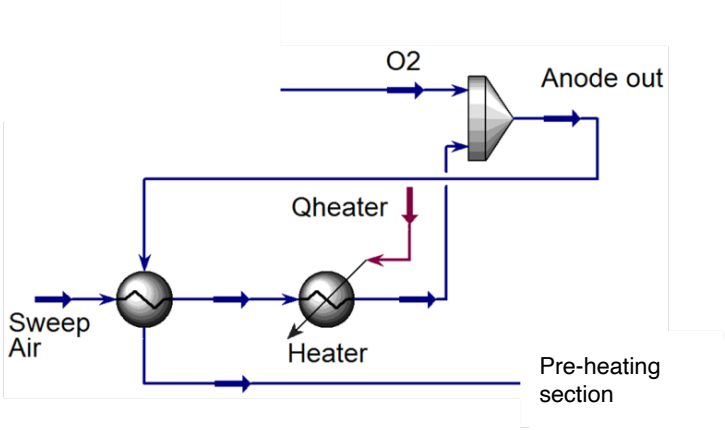

Fig. 4.11. Configuration with sweep air pre-heating.

In this way, it is possible to recover most of the thermal power necessary to heat-up the sweep air. In particular, the net thermal consumption (Q_{heater} in the figure) is almost constant for the analysed cases and it is equal to about 0.6 kW.

The layout of the P-TAIL pressurization case has been applied to different thermal levels of the main components (SOEC, HTM and LTM), designing in a proper way the preheating section. In particular, as highlighted in Tab. 4.4, 10 cases have been analysed, corresponding to the thermal configurations already considered in the analysis of the previous paragraph. For each case of temperature, different preheating configurations have been developed:

a) configuration with 6 heat exchangers in the HRS section, for cases: 850/450/200, 800/450/200, 750/450/200, 700/450/200, 650/450/200, 600/450/200, 600/500/200 and 600/550/200;
b) configuration with 5 heat exchangers in the HRS section, for the case: 600/600/200;
c) configuration with 2 heat exchangers in the HRS section, for the case: 600/600/600.

Fig. 4.12 shows the layout of the P-TAIL case with the HRS section consisting of 6 heat exchangers and with preheated sweep air.

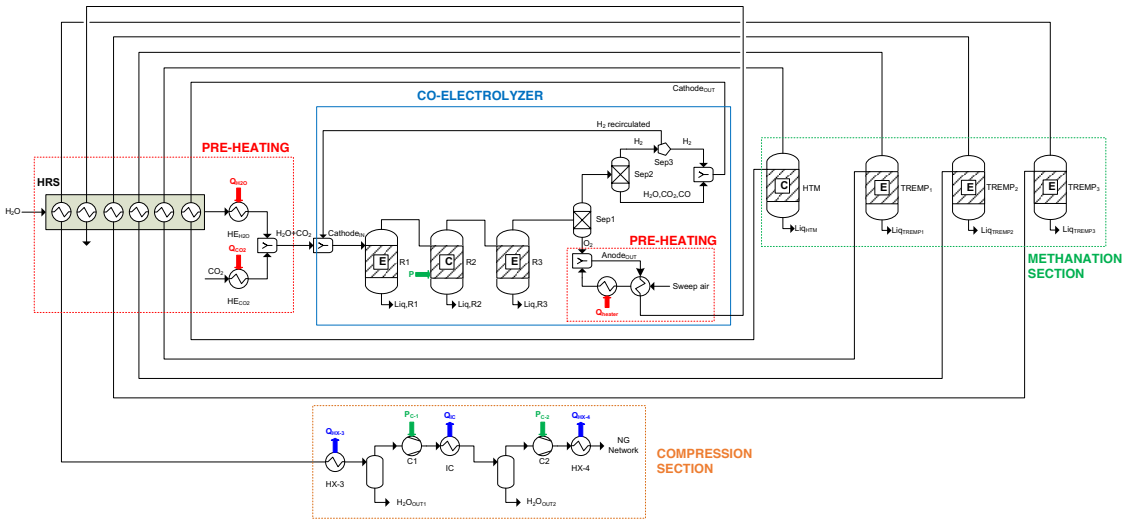

Fig. 4.12. P-TAIL layout with the HRS section consisting of 6 heat exchangers (and with pre-heated sweep air).

As it can be seen in the figure, the compression section is placed downstream of the whole process, while the co-electrolyzer and the methanation section work at ambient pressure. In addition, as a result of the sweep air preheating, a modification to the configuration of the heat exchangers in the HRS section has been made, in order to partially recover the thermal power for the sweep air preheating.

4.2.3 – P-LTM case (without sweep air pre-heating)

In this variant, the pressurization of the LTM section has been analysed, as shown in Fig. 4.13.

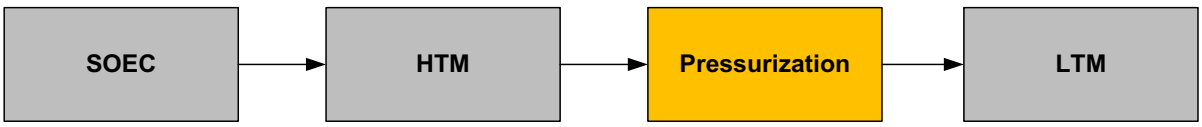

Fig. 4.13. Block diagram of the P-LTM configuration.

As illustrated in the literature [57], the operation of the methanation reactors at higher pressures should allow to achieve higher efficiencies, leading to an increase in the methane production with respect to the Base Case (whose methanation section is at ambient pressure). In this case, the operating conditions of the experimental methanation reactor (working at ambient pressure) have been kept constant; only the effect of the pressurization on the LTM section, characterized by the commercial TREMP™ technology, has been evaluated.
Regarding the several configurations of the HRS section, the following solutions, with a different arrangement of the heat exchangers in the preheating line, have been considered:

a) configuration with 6 heat exchangers in the HRS section, for cases: 850/450/200, 800/450/200, 750/450/200, 700/450/200, 650/450/200, 600/450 200, 600/500/200 and 600/550/200;
b) configuration with 5 heat exchangers in the HRS section, for the case: 600/600/200;
c) configuration with 2 heat exchangers in the HRS section, for the case: 600/600/600.

Fig. 4.14 shows the layout of the P-LTM case with the HRS section consisting of 6 heat exchangers. In this configuration, the water preheating section at the inlet of the overall P2G system is the same of the Base Case. Moreover, the compression section is placed upstream of the LTM section and, then, at the outlet of the HTM section. In particular, the stream at the outlet of the experimental reactor, after transferring part of the heat content to the water preheating section, is then cooled down to 25 °C (in the preheating section, the full exploitation of the available heat content is not possible and, then, an additional cooler is required, *HX-3* in the figure) and sent to the compression section, where it is compressed up to 60 bar by means of an inter-refrigerated compression and separated from the residual water. The configuration of the compression section is the same of the P-TAIL case; as a consequence, the gas stream is processed in the LTM section in order to complete the methanation process.

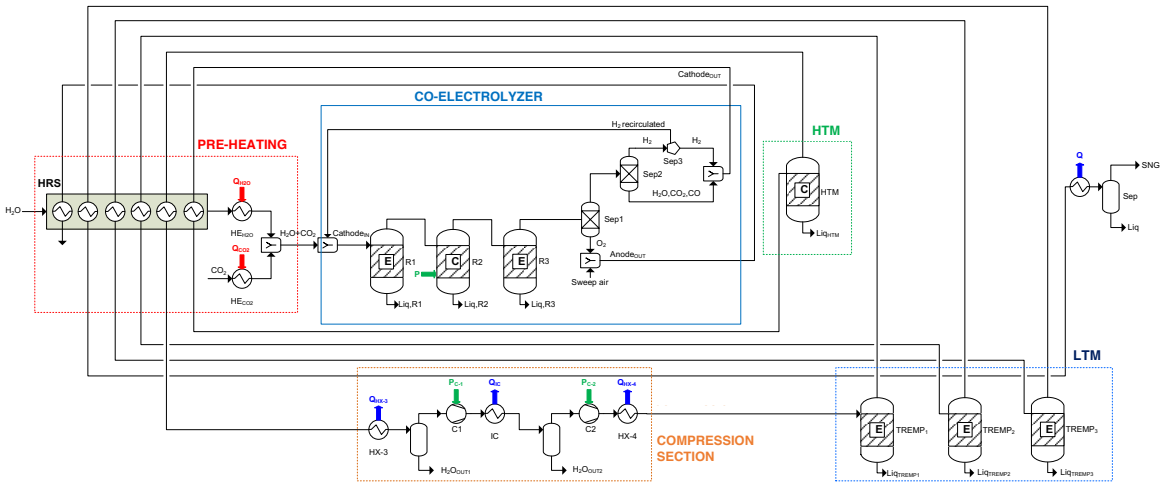

Fig. 4.14. P-LTM layout with the HRS section consisting of 6 heat exchangers.

4.2.4 – P-LTM cases (with sweep air pre-heating)

In this case, the air at the inlet of the co-electrolyser is preheated with a heat exchanger, with a configuration similar to the P-TAIL case. Also in this case, regarding the configurations of the HRS section, the following solutions, with different heat exchanger arrangements, have been considered:

a) configuration with 6 heat exchangers in the HRS section, for cases: 850/450/200, 800/450/200, 750/450/200, 700/450/200, 650/450/200, 600/450/200, 600/500/200 and 600/550/200;
b) configuration with 5 heat exchangers in the HRS section, for the case: 600/600/200;
c) configuration with 2 heat exchangers in the HRS section, for the case: 600/600/600.

Fig. 4.15 shows the layout of the P-LTM case with the HRS section consisting of 6 heat exchangers and with preheated sweep air. The layout of this solution is similar to the layout of the solution of Fig. 4.14, with the difference concerning the preheating of the sweep air and the resulting modification in the arrangement of the heat exchangers in the HRS section (as in the case of Fig. 4.12).

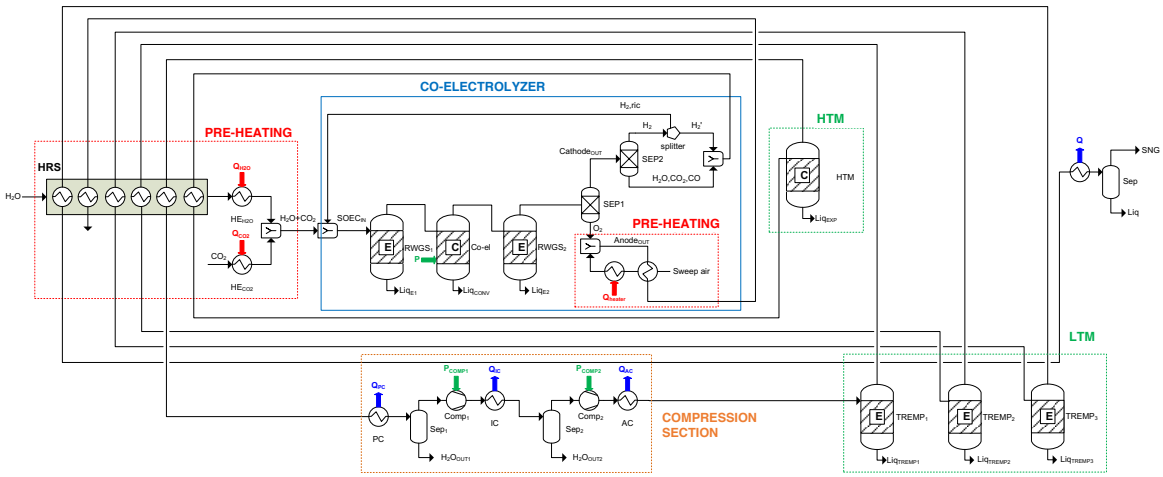

Fig. 4.15. P-LTM layout with the HRS section consisting of 6 heat exchangers and with pre-heated sweep air.

4.2.5 – P-SOEC cases

In this variant of the P2G system layout, the pressurization of the whole process has been provided, starting from the SOEC, according to the scheme in Fig. 4.16.

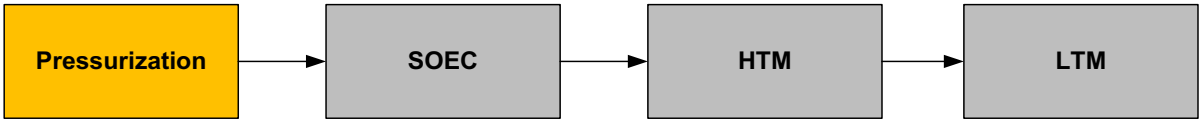

Fig. 4.16. Block diagram of the P-SOEC configuration.

In this case, due to the operation of the co-electrolysis process at operating pressures higher than the ambient pressure, the production of methane in the reactions occurs [37]. The chemical model of the co-electrolyser implemented in Aspen HYSYS™ has therefore been

modified in order to take into account this phenomenon, adding the following methanation reaction in the second equilibrium reactor of the model (reactor *R3* of Fig. 3.1):

Eq. 4.1. $CO + 3H_2 \rightarrow CH_4 + H_2O$

Regarding the configurations of the HRS section, in this case, the following solutions have been implemented, on the basis of the temperature levels of the components:

a) configuration with 7 heat exchangers in the HRS section, for cases: 850/450/200, 800/450/200, 750/450/200, 700/450/200, 650/450/200, 600/450/200, 600/500/200, 600/550/200;
b) configuration with 6 heat exchangers in the HRS section, for the case: 600/600/200;
c) configuration with 2 heat exchangers in the HRS section, for the case: 600/600/600.

The system solution with 7 heat exchangers in the HRS section is shown in Fig. 4.17. In this case, the pressurization of the water occurs in the liquid state (a pump is required, while the compression of CO_2 is carried out with a compressor before the heating from an external source); moreover, an additional heat exchanger has been included with respect to the previous configurations, in order to recover the residual heat of the air stream at the outlet anode side in an optimal way.
The system solution with 6 heat exchangers in the HRS section, related to the thermal configuration 600/600/200, is shown in Fig. 4.18, while the system solution with 2 heat exchangers in the HRS, related to the thermal configuration 600/600/600, is shown in Fig. 4.19.

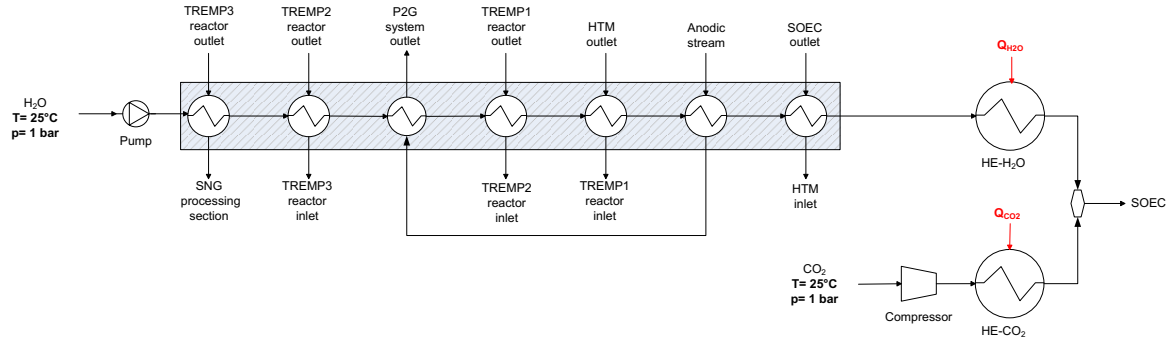

Fig. 4.17. P-SOEC case with the HRS section consisting of 7 heat exchangers.

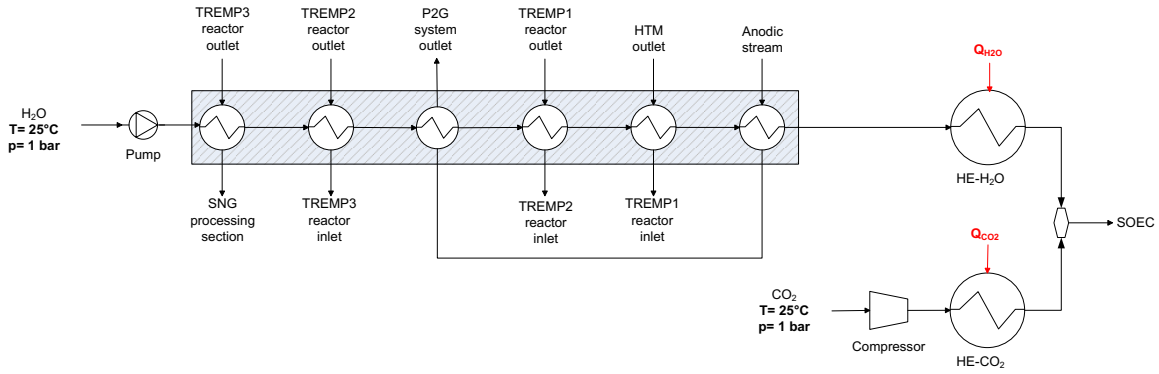

Fig. 4.18. P-SOEC case with the HRS section consisting of 6 heat exchangers.

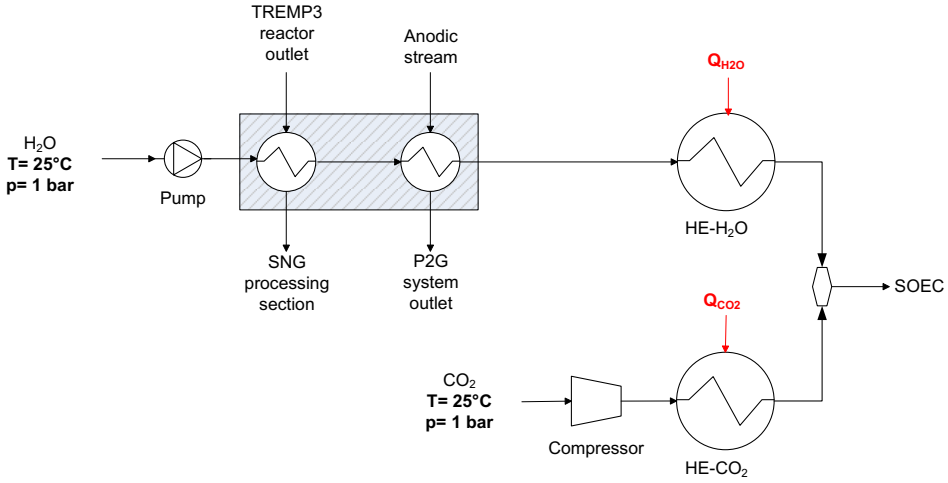

Fig. 4.19. P-SOEC case with the HRS section consisting of 2 heat exchangers.

Finally, Fig. 4.20 shows the layout of the P-SOEC case with the HRS section consisting of 7 heat exchangers and with preheated sweep air. In this case, the pressurization implementation and the preheating of the sweep air with an heat exchanger have been taken into account in the model (see *Sweep Air line* in the figure). An inter-refrigerated compression (with inter-refrigeration at 25 °C) has been considered and it has been assumed that the SOEC works at the operating pressure of the whole P2G system (60 bar), equal to the pressure of the natural gas distribution network. This boundary condition represents an upper limit for the SOEC and it is not technologically feasible at present, representing, however, a prospect interest. Anyway, currently it is possible to conceive intermediate solutions, with a pressurized electrolyser operated at limited pressure levels and with an additional compression stage.

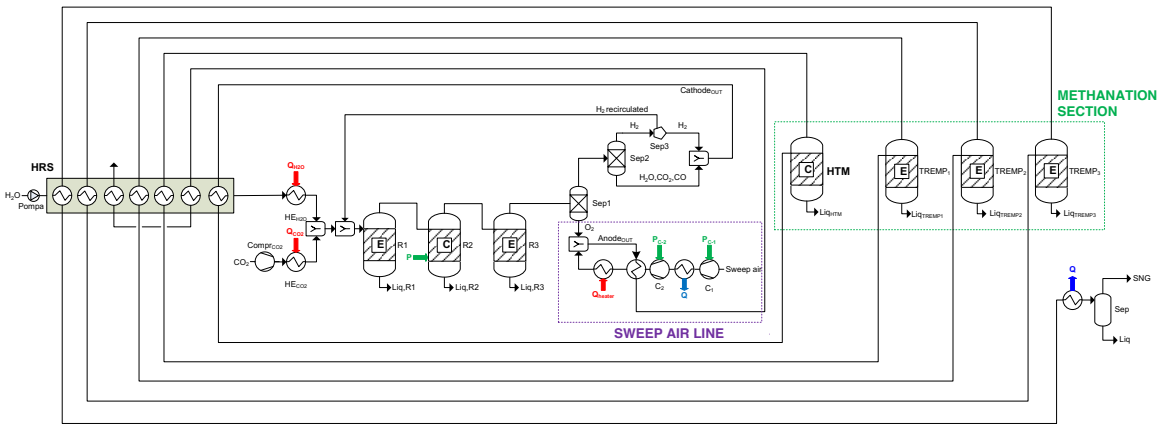

Fig. 4.20. Layout of the P-SOEC case with the HRS section consisting of 7 heat exchangers.

4.2.6 – Results

The results of the carried-out thermodynamic analysis on the pressure effect, for the several plant configurations, are presented in this section, based on the assumptions illustrated above. Fig. 4.21 and Fig. 4.22 show the calculated values of the system efficiency parameters and of the different thermal power consumptions, for the cases:

- P-TAIL with air preheating (from this point referred as the P-TAIL case);
- P-LTM with and without air preheating;
- P-SOEC.

Each figure presents the performance for the 10 analysed cases of temperature levels, related to the three key components (SOEC, HTM and LTM). In particular, in Fig. 4.21 the comparison among the four presented solutions in terms of first law efficiency, second law efficiency and "electric-to-fuel" conversion index is shown.

For the first three solutions, Case 9 with operating temperatures (600/600/200) provides the maximum value of η_I, while with the P-SOEC configuration the maximum value of η_I occurs in Case 10 (600/600/600). The P-TAIL solution generally provides higher performance values, with a maximum value of $\eta_I = 85\ \%$ and $\eta_{II} = 79\ \%$.

It is also interesting to compare the first solution (P-TAIL) with the solution of the Base Case previously analysed (P-TAIL case without air preheating, see previous paragraph). Comparing Fig. 4.21a, for the P-TAIL Case, with Fig. 4.7 and Fig. 4.8 for the Base Case, an increase in the efficiency values of the 1st and 2nd law on average of 5 - 7 percentage points is observed. The P-LTM set-up with air preheating is also more efficient than the P-LTM system without preheating, with the same operating temperatures (see the comparison between Fig. 4.21b and Fig. 4.21c). However, the pressurization of the LTM section does not show relevant advantages, in terms of efficiencies, compared to the P-TAIL set-up, with the same operating temperatures of the components. Finally, the pressurization of the SOEC leads

to efficiency values of the overall system compared to the P-TAIL system on average 8 - 12 percentage points lower. On the other hand, in the case of the P-SOEC arrangement, the reduction of the SOEC operating temperature is always favourable in terms of efficiency of the first and second laws.

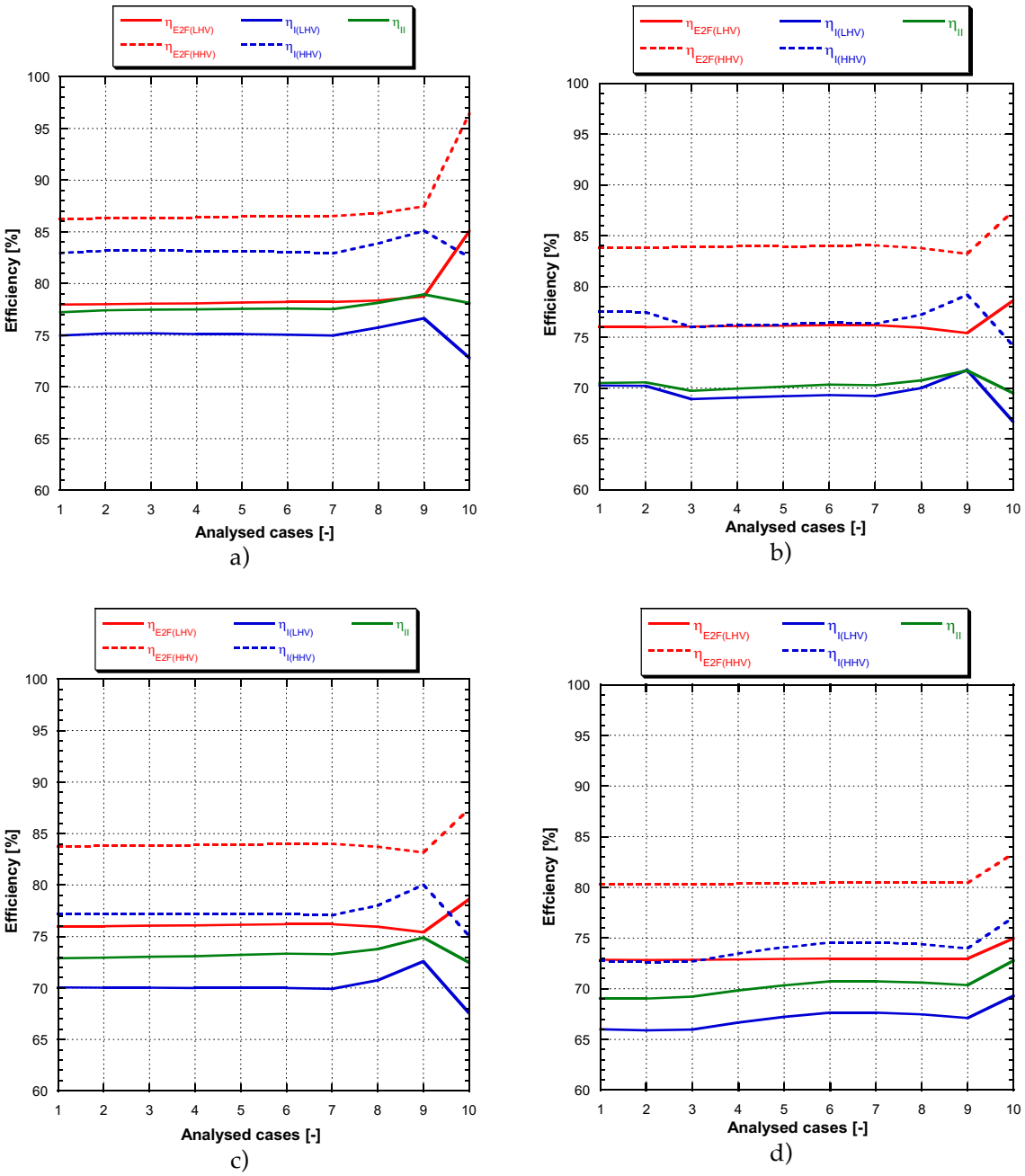

Fig. 4.21. First law efficiency, second law efficiency and electric-to-fuel conversion index, for the 10 cases of different thermal levels among the components: a) case P-TAIL; b) case P-LTM without sweep air pre-heating; c) case P-LTM with sweep air pre-heating; d) case P-SOEC.

The above-described system efficiency results are strongly influenced by the thermal input of the P2G system and by the heat recovery capacity of the HRS section placed upstream of the co-electrolyser. In particular, in Fig. 4.22 it is shown that the thermal power required to heat

up the co-electrolysis reactants ($Q_{requested}$) is partially balanced by the thermal power recovered in the HRS section ($Q_{recovered}$), especially in the case of the P-TAIL system (Fig. 4.22a) and in the case of the P-LTM system with air preheating (Fig. 4.22c). These solutions show the highest values of the index of recovery (IR), with values close to 100 % for the P-TAIL 600/600/200 case and values over 90 % in the other type of pressurization layout (Case P-LTM). The advantage of the air preheating is also highlighted, by comparing Fig. 4.22b with Fig. 4.22c. In the P-SOEC case (Fig. 4.22d), the IR shows values on average around 70 %, but with a lower heat demand ($Q_{requested}$) with respect to the other cases.

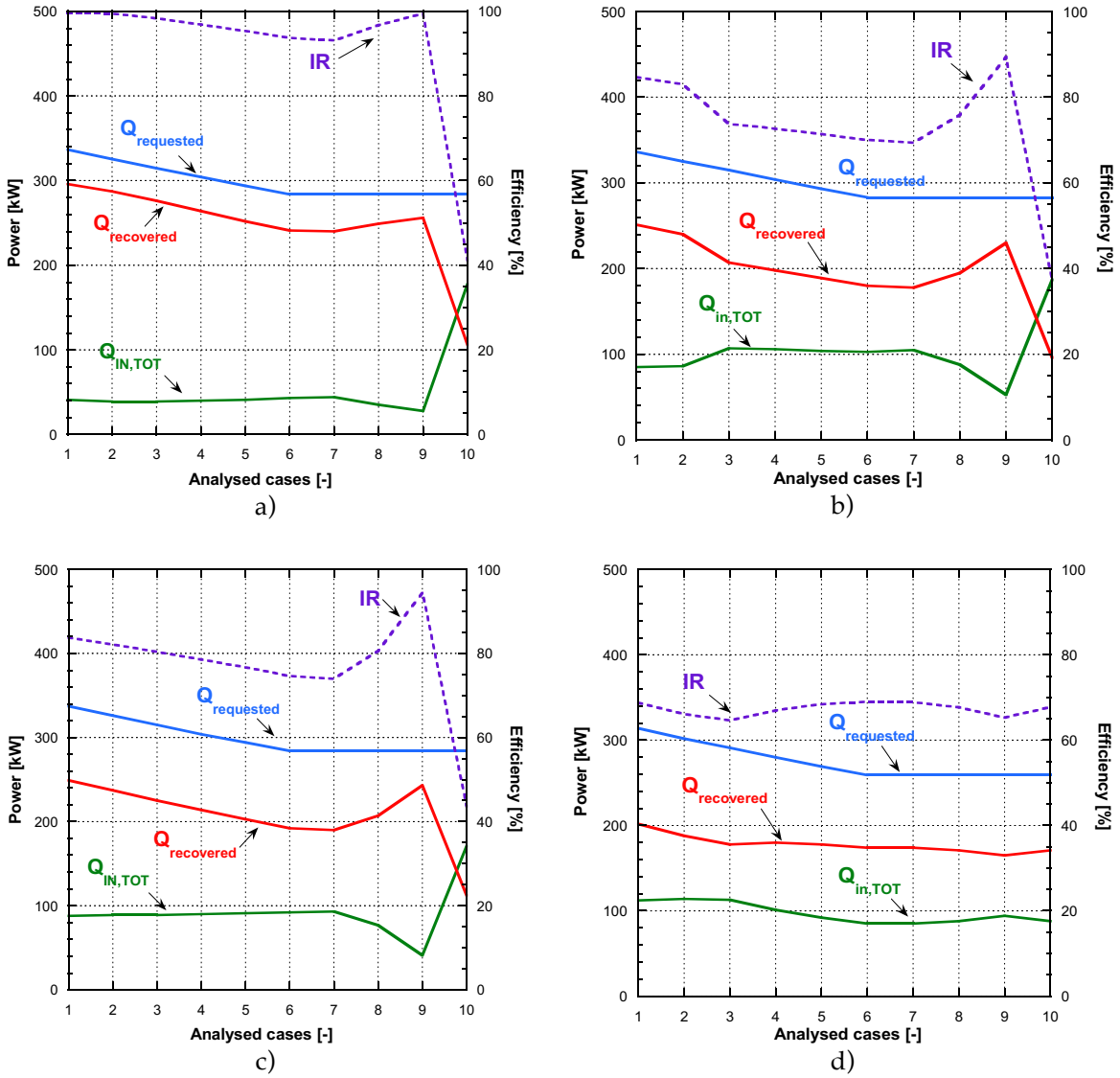

Fig. 4.22. Requested thermal power, recovered thermal power and IR, for the 10 cases of different thermal levels among the components: a) case P-TAIL; b) case P-LTM without sweep air pre-heating; c) case P-LTM with sweep air pre-heating; d) case P-SOEC.

For the pressurized settings, the "electric-to-fuel" conversion index shows (Fig. 4.21) an almost constant trend for many cases as the thermal configuration varies. Only in the latter case

(600/600/600), an increase in this index is noted; this result, as already observed in the case of Fig. 4.8, also in these solutions can be explained by the different composition of the produced SNG.

Then, it has been analysed how the concentration of the SNG elements is affected by the pressure set-up.

Regarding the P-TAIL case, the values of the SNG composition for the case with air preheating are the same of the case without preheating (already described in the temperature analysis, see Fig. 4.9 for the numerical values obtained).

In Fig. 4.23 the results regarding the SNG composition and the values of HHV and WI of the stream at the outlet of the whole process for the two cases P-LTM (with air preheating) and P-SOEC are shown. In both cases, a similar behaviour is observed when the operating temperatures of the components vary; moreover, the CH_4 molar fraction results higher than 98 % if the operating temperature of the LTM section is equal to 200 °C. In the P-LTM case, the molar fraction of methane is much higher than in the P-TAIL configuration (on average $x_{CH4} = 0.985$ compared to the value of 0.780, related to the case of Fig. 4.9); in addition, as the operating temperature of the experimental methanation reactor increases, there is a slight decrease in the molar fraction of methane (up to $x_{CH4} = 0.960$). Finally, the 600/600/600 case shows a decrease in this parameter ($x_{CH4} = 0.489$) since, by increasing the operating temperature, the equilibrium methanation reactions tend to move towards the reactants and then to produce more hydrogen. The concentration of the other elements (CO, H_2O and CO_2) increases, but still below 5 %.

The concentration values of the P-LTM case with air preheating are the same of the P-LTM case without air preheating; as a consequence, only one composition figure related to the P-LTM case is shown (Fig. 4.23a). In the case of the P-SOEC setup (Fig. 4.23b), the molar fraction of methane at the system outlet is higher with respect to the previous configurations (on average $x_{CH4} = 0.995$); a similar trend to the other cases is observed, showing optimum values of methane concentration also for cases with the HTM operated at higher temperatures (cases from 7 to 9). Finally, the 600/600/600 case shows a lower concentration of methane (0.581), since the methanation reactions within the LTM system are disadvantaged by high temperatures.

Finally, regarding the values assumed by the HHV and the Wobbe index, the trend is similar to the trend of the methane content. In particular, for the P-LTM configuration (Fig. 4.23c) the HHV achieves a maximum value of about 35000 kJ/Sm^3 (cases from 1 to 6) and then decreases to about 18000 kJ/Sm^3 (case 10), while the Wobbe index ranges from a maximum of about 48000 kJ/Sm^3 to a minimum of about 33000 kJ/Sm^3. For the P-SOEC configuration (Fig. 4.23d), the HHV shows a value equal to about 37000 kJ/Sm^3 constant in cases from 1 to 9 (similar to the trend of the methane molar fraction, Fig. 4.23b), and then decrease in case 10 to a value of about 26000 kJ/Sm^3. Finally, the Wobbe index, for this specific configuration, show a constant

value (equal to about 50000 kJ/Sm^3) up to case 9, and then decreases to a value of about 38000 kJ/Sm^3 in case 10.

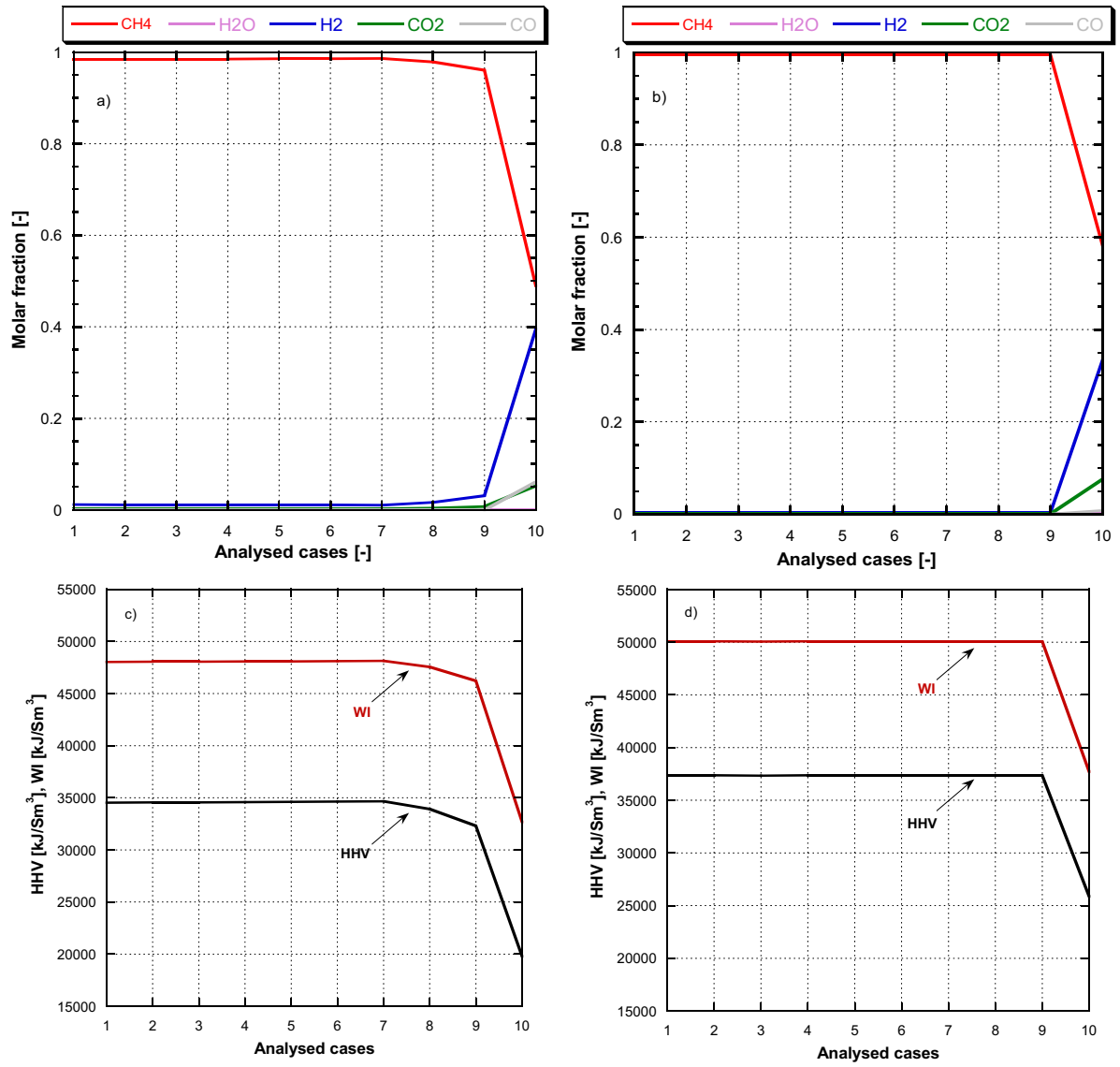

Fig. 4.23. SNG composition: a) case P-LTM; b) case P-SOEC. HHV and Wobbe index: c) case P-LTM; d) case P-SOEC.

4.3 – Considerations

A summary of the most relevant results of the thermodynamic design analyses carried-out in this chapter is shown in Fig. 4.24, where a comparison between some solutions previously analysed is presented. The selected solutions are:

- P-TAIL 850/450/200 case: configuration with SOEC, HTM and LTM operating at ambient pressure, with the SNG pressurization downstream of the last methanation reactor, with reactants and sweep air preheating, with different operating temperatures for the key components (the SOEC operating at 850 °C, the experimental methanator at 450 °C and

the commercial methanation section at 200 °C); this configuration has first law efficiency values η_I equal to about 78 % and a methane content in the SNG equal to about 80 %;

- P-TAIL 600/600/200 case: configuration that differs from the previous since the SOEC and the experimental methanator are operated at the same temperature (both at 600 °C); compared to the previous one, this configuration shows higher values from the point of view of the efficiency parameters η_{E2F}, η_I and η_{II} (the first law efficiency is slightly higher and close to 79 %), but presents a lower methane molar fraction in the produced SNG;
- P-SOEC 850/450/200 case: pressurized configuration, with the SOEC operating at 850 °C, the experimental methanator at 450 °C and the commercial methanation section at 200 °C; this configuration shows the highest values in terms of x_{CH4}, but the lowest efficiency values;
- P-SOEC 600/600/200 case: configuration that differs from the previous since the SOEC and the experimental methanator are operated at the same temperature (both at 600 °C); the performance parameters vary with respect to the previous case in the same direction as in the P-TAIL 600/600/200 case with respect to the P-TAIL 850/450/200, but with a greater variation;
- P-LTM 600/600/200 case: intermediate pressure configuration, with the pressurization starting from the low temperature methanation section and the SOEC and the experimental methanator operating at ambient pressure; SOEC and HTM work at 600 °C, while the low temperature methanation section operates at 200 °C; this configuration represents a trade-off solution between the goal of maximizing the efficiency and the goal of maximizing the quality of the produced SNG. In addition, this case is in line with one of the aims of the study to identify a single operating temperature for the co-electrolyser and for the experimental methanator (also in this case equal to 600 °C).

Tab. 4.5 shows the numerical values of the performance parameters calculated in design conditions for the above-mentioned cases.

In conclusion, the first law efficiency achieves values up to about 78 – 79 % in the best case (P-TAIL 600/600/200), while the cases with the whole system pressurized show a higher quality in the SNG stream (best case P-SOEC 850/450/200), with the SNG stream composed mainly by methane.

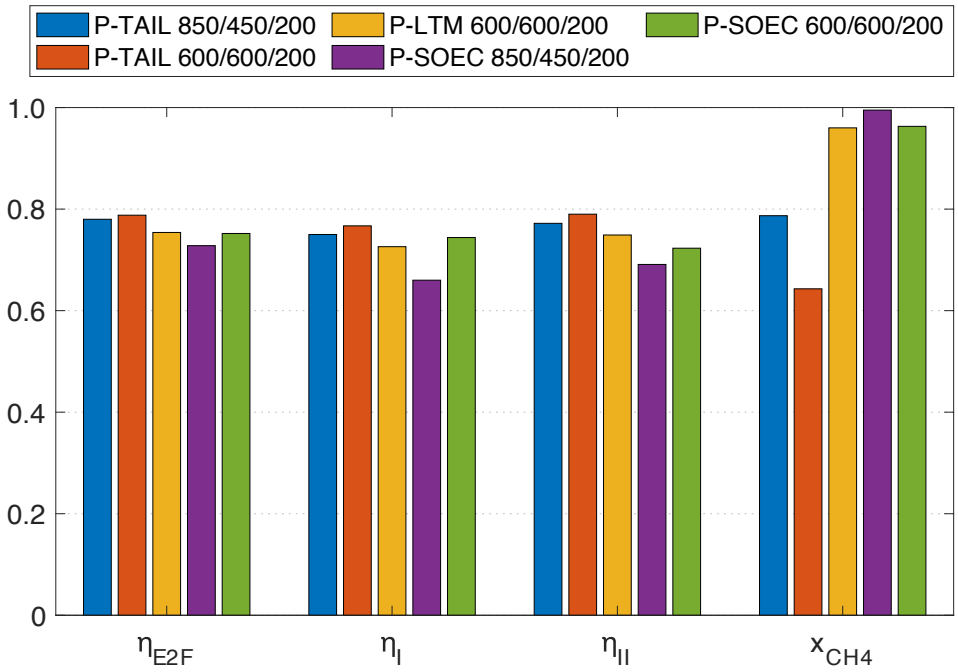

Fig. 4.24. Comparison of the optimal solutions from the carried-out thermodynamic analysis.

Tab. 4.5. Numerical values of the performance parameters for the optimal solutions.

	η_{E2F} [-]	η_{I} [-]	η_{II} [-]	x_{CH4} [-]
P-TAIL 850/450/200	0.780	0.750	0.772	0.787
P-TAIL 600/600/200	0.788	0.767	0.790	0.643
P-LTM 600/600/200	0.754	0.726	0.749	0.960
P-SOEC 850/450/200	0.728	0.660	0.691	0.995
P-SOEC 600/600/200	0.752	0.744	0.723	0.963

4.3.1 – Selection of reference scenarios for the off-design analysis

In this parametric study in design condition, several cases have been considered, differentiated by the layout, the operating pressures (varied in a range between 1 and 60 bar) and the operating temperatures (in the whole possible range of variation for each key component). In the analysis related to the behaviour of the P2G system in off-design conditions (next chapter), on the other hand, only some system configurations have been considered, corresponding to scenarios characterized by different thermodynamic set-points of the main system components, selected on the basis of the performance.

In particular, on the basis of the operating parameters of the SOEC co-electrolyser, four configurations have been considered. The key analysed parameters are the operating pressure

and the operating temperature of the several sub-sections of the P2G system; in particular, the pressurization of the P2G system has been investigated since it can significantly increase the SOEC power density, improve the produced SNG quality and reduce the size of the auxiliary components; furthermore, different temperature settings have been evaluated, in order to explore possible thermal synergies among the sub-sections. The choice of the SOEC (and then of the downstream sub-sections) pressure level has generated two different layouts of the P2G system. The first one (Fig. 4.25) is a P2G system with the SOEC and the methanation sections (HTM and LTM) at ambient pressure and with a tail end pressurization, before the introduction into the NG network. The final SNG storage pressure has been set equal to 60 bar, consistent with a high-pressure NG pipeline.
The second one (Fig. 4.26) is a P2G system with a pressurized SOEC. Thus, in this system, the HTM and the LTM sections operate at the same pressure of the SOEC; also in this case, at the end of the process the produced SNG is pressurized up to the same final storage pressure (60 bar). As shown in Fig. 4.26, the pressurized layout requires at the inlet a pump for the inlet water stream and a compressor for the inlet carbon dioxide stream. Moreover, the pressurization of the sweep air stream has also been considered.
Regarding the pressurized layout, for the SOEC (and then for the downstream sub-sections) an operating pressure equal to 8 bar has been chosen; this value is in line with the current state-of-the-art of pressurized SOEC technology (even if higher values are also expected in the future – see the HELMETH project [13]) and it corresponds to the experimental data provided in the study by Mehran et al. [49] on a prototypal co-electrolyzer SOEC.
Then, for both layouts, two different temperature settings have been considered. Indeed, the studied configurations can be summed up in:

- Ambient 1: P2G system at ambient pressure, with the SOEC at 850 °C, the HTM at 450 °C and the LTM at 200 °C;
- Ambient 2: P2G system at ambient pressure, with the SOEC at 600 °C, the HTM at 600 °C and the LTM at 200 °C;
- Pressurized 1: pressurized P2G system, with the SOEC at 850 °C, the HTM at 450 °C and the LTM at 200 °C;
- Pressurized 2: pressurized P2G system, with the SOEC at 600 °C, the HTM at 600 °C and the LTM at 200 °C.

In the configurations Ambient 1 and Pressurized 1, the SOEC operating temperature has been set equal to 850 °C, in line with high performance SOEC operating conditions, in accordance with the available studies on high temperature SOEC [44]. The HTM operating temperature has been set equal to 450 °C, in order to exploit the HTM highest conversion rate value, according to [58]. The LTM operating temperature has been set after a parametric study of its effect, considering the typical temperature range of operation of this technology [33]. On the

other hand, in configurations Ambient 2 and Pressurized 2, in order to explore possible thermal synergies among the sub-sections, different temperature levels have been investigated in a previous study [43]; in particular, the thermal synergy can be achieved operating both the co-electrolyzer and the methanation section within relatively high temperature ranges (the co-electrolysis operation at intermediate temperature has been demonstrated in a work by Lo Faro et al. [29]).

For the sake of simplicity, in the P-SOEC configurations the double heat exchanger configuration for the anodic stream (see Fig. 4.17) has been graphically considered as one.

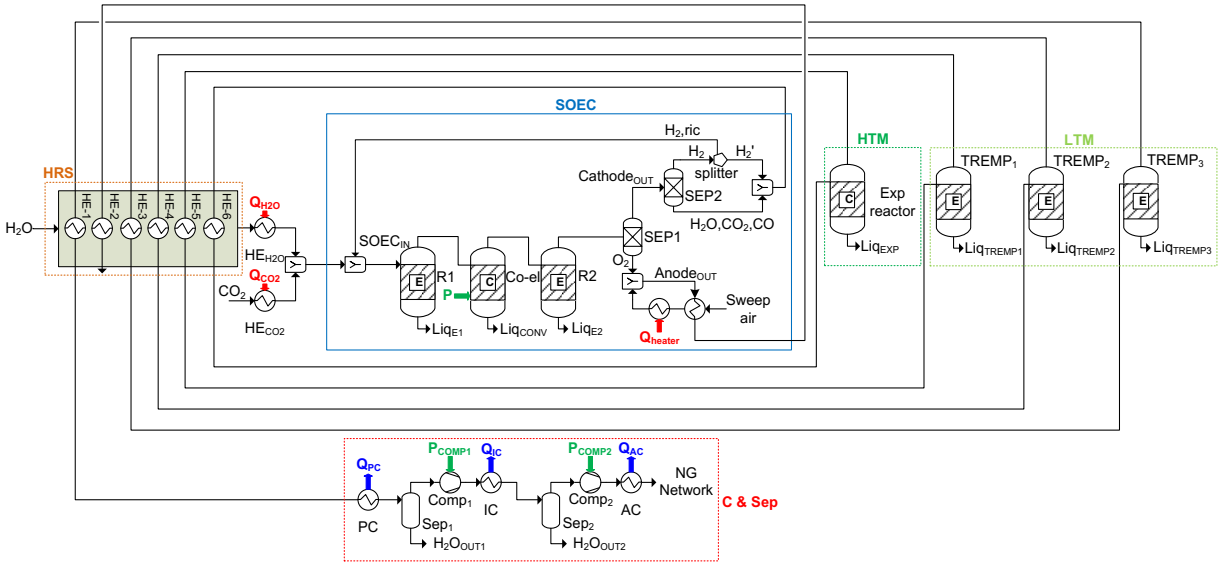

Fig. 4.25. Layout of the P2G system in the scenario with the SOEC at ambient pressure.

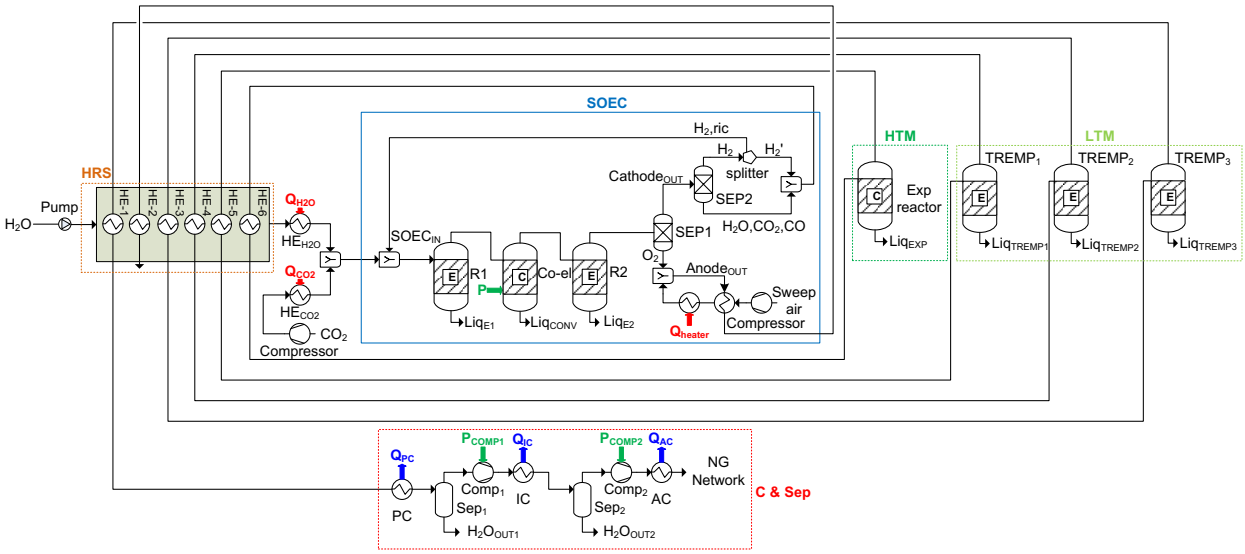

Fig. 4.26. Layout of the P2G system in the scenario with the pressurized SOEC.

The applied boundary conditions in the design and off-design analyses, for the four considered reference scenarios, are summarized in Tab. 4.6; the performance parameters and the main energy and mass flows of the P2G system in the design point (electrical power input equal to 1 MW) are shown in Tab. 4.7.

Tab. 4.6. Applied boundary conditions in the design and off-design analyses, for the four considered reference scenarios.

Parameter	Units	Ambient 1 (850/450/200)	Ambient 2 (600/600/200)	Pressurized 1 (850/450/200)	Pressurized 2 (600/600/200)
SOEC operating temperature	°C	850	600	850	600
SOEC operating pressure	bar	1	1	8	8
HTM operating temperature	°C	450	600	450	600
HTM operating pressure	bar	1	1	8	8
LTM operating temperature	°C	200	200	200	200
LTM operating pressure	bar	1	1	8	8
Reactants inlet temperature	°C	25	25	25	25
Reactants inlet pressure	bar	1	1	1	1
SOEC inlet H_2O fraction	$\%_{vol}$	80	80	80	80
SOEC inlet CO_2 fraction	$\%_{vol}$	20	20	20	20
H_2O electrolysis reaction Conversion Rate	%	80	80	80	80
CO_2 electrolysis reaction Conversion Rate	%	80	80	80	80
O_2 molar fraction in the anode stream	-	0.5	0.5	0.5	0.5
SOEC input electric power (design)	MW	1	1	1	1
NG distribution network pressure	bar	60	60	60	60

Tab. 4.7. Performance parameters and main energy and mass flows for the P2G system in the design point, for the four considered reference scenarios.

Parameter	Units	Ambient 1 (850/450/200)	Ambient 2 (600/600/200)	Pressurized 1 (850/450/200)	Pressurized 2 (600/600/200)
First law efficiency	%	74.97	76.65	72.78	74.37
Second law efficiency	%	77.23	78.95	74.48	72.30
Electric-to-fuel conversion index	%	77.98	78.76	74.96	75.15
H_2O inlet mass flow	kg/h	254.6	255.4	254.2	254.2
H_2O outlet mass flow	kg/h	120.4	120.7	125.3	126.0
CO_2 inlet mass flow	kg/h	155.5	156.0	155.3	155.3
Air inlet mass flow	kg/h	351.5	351.5	351.1	351.4
Air outlet mass flow	kg/h	575.5	579.3	576.9	577.2
SNG mass flow	kg/h	63.4	69.8	58.4	57.7
CH_4 fraction in the SNG	-	0.787	0.782	0.937	0.963
LHV_{SNG}	kJ/kg	45200	45070	48582	49116
HHV_{SNG}	kJ/kg	50012	49874	53605	54173
P2G system input electric power	kW	1020	1023	1052	1052
SOEC input electric power	kW	1000	1000	1000	1000
Auxiliaries electric consumption	kW	20	23	52	52
P2G system input thermal power	kW	41	42	32	41

Chapter 5 – Synthetic natural gas application: off-design analysis

By means of the developed calculation model for the simulation of the system in off-design conditions, a starting analysis on the behaviour of the whole P2G system in variable load conditions has been carried out, considering the coupling with a non-programmable renewable source system. In more detail, the numerical model introduced in a previous chapter (Chapter 3 – The Power-to-Gas model) has been implemented, evaluating and comparing different P2G system configurations in variable load conditions. In this first step, a specific NP-RES generation scenario has been selected, characterized by a set renewable source and by an assigned size in terms of power size.
In a second step, several operating scenarios have been analysed, by means of a parametric evaluation, in order to expand the obtained results and make them applicable to a wider range of situations. Indeed, due to the intermittency and the non-programmability of the main renewable sources, the storage system will work in unusual operating points (off-design conditions) for large periods of the year and in different load conditions from case to case, on the basis of the type and the size of the NP-RES system.

5.1 – First scenario

This paragraph, regarding the first scenario of analysis, is organised as described:

- description of the NP-RES characteristics for the considered scenario;
- introduction of the developed energy flow management;
- discussion of the results related to the comparative analysis between the different variants of the P2G system in the reference scenario during one year of operation.

5.1.1 – NP-RES characteristics

In the first analysed scenario, energy from wind generation has been considered as the electrical input to the storage system. A long-term yearly evaluation has been carried-out and the data used in the analysis are related to the Italian wind generation (Terna [59] - [60], data referring to year 2019). In particular, the normalized wind production profile (with respect to the yearly peak value) has been considered (see Fig. 5.1). It should be noticed that this is the average production profile on a wide region, used for the sake of generality of the carried-out study, aimed at investigating a large-scale storage solution.

In particular, in this scenario, a set ratio between the SOEC size and the renewable peak has been considered (aim of the next parametric analysis); the starting value of the power ratio has been set at 1 MW_{SOEC} / 1.7 $MW_{NP\text{-}RES}$ [2].

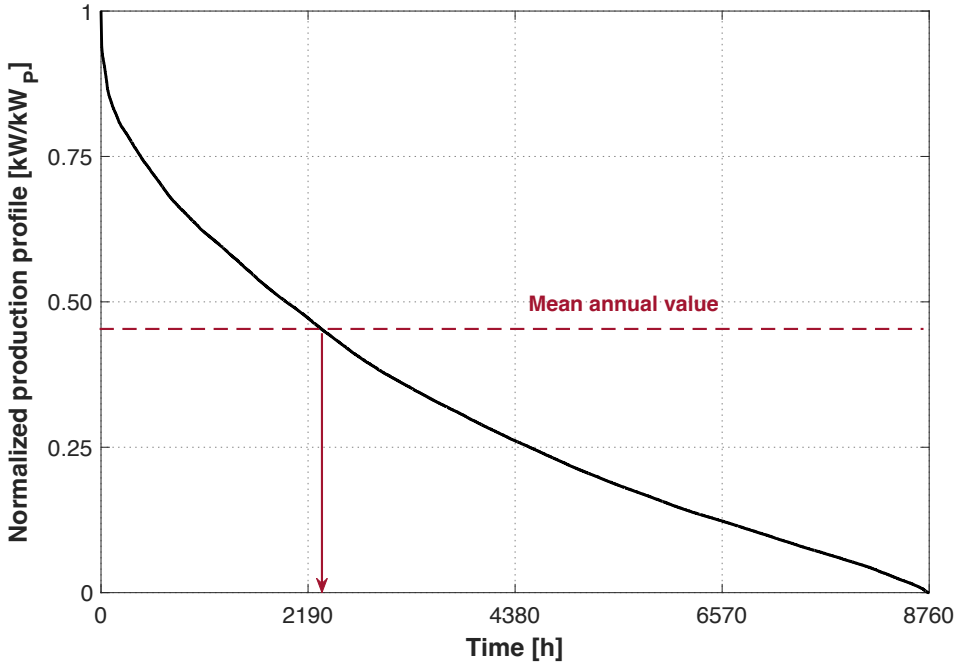

Fig. 5.1. The monotonic duration curve of the wind production normalized with respect to the annual peak production value, data based on the whole national scenario (TERNA [59]).

5.1.2 – Energy flow management with a variable NP-RES

Starting from the SOEC design electric power input (reference size equal to 1 MW) and accounting also for the compression and auxiliaries' consumption, the P2G off-design operating range has been assumed between – 50 % and + 50 % of the design inlet power.

The analysis has been carried out with a dedicated code, developed in MATLAB™ and integrated in the Aspen HYSYS™ environment. This code allows to evaluate the annual operating time of the P2G system, the surplus of electric energy not used by the system – and then introduced into the electric grid or eventually wasted – and the values of the performance parameters. In more detail, the code analyses each time step of the year:

[2] Considering the normalized profile of Fig. 5.1 and the reference power input of 1 MW for the SOEC, the generation from NP-RES coupled to the storage system shows then a peak annual production power value of 1.7 MW, with a mean annual power equal to 750 kW. Moreover, with a ratio between the peak production in the year and the installed size equal to 57 % (as in the case for the data from Terna), the nameplate power size is equal to 3 MW and the corresponding equivalent hours of operation are equal to 2200 hours/year. Actually, these data are highly site-specific, with values that can vary on the basis of the local wind from less than 1200 hours/year to over 3500 hours/year, but in this first analysis reference has been initially made to the average national scenario, for the sake of generality.

- if, in the given time step, the electric power produced by the wind plant is lower than the lower operating limit of the P2G system, then all the electric energy is introduced into the electric grid (or wasted);
- if, in the given time step, the electric power produced by the wind plant is within the operating range of the P2G plant, then all the electric energy is employed within the process;
- if, in the given time step, the electric power produced by the wind plant is greater than the upper operating limit of the P2G system, then the difference between the wind production and the maximum electric load of the P2G system is introduced into the electric grid (or wasted).

5.1.3 – Results of the comparative analysis

In this section, the results of the carried-out analysis are shown. In more detail, at first the results of the HRS and of the compression section sub-models are presented and, then, the results of the comparative analysis among the several P2G system configurations are discussed.

Heat recovery section off-design performance

In this section, the off-design performance of the HRS are presented. Fig. 5.2 shows the obtained results, in terms of thermal power exchanged by each heat exchanger in the HRS section, in design and off-design conditions (more specifically, in the operating points corresponding to the lower and upper limits of the system operating range), for the four analysed P2G configurations.

In all the considered configurations, the heat exchanger with the highest value of heat exchanged is HE-1, with a value between 105 kW and 109 kW in design condition. This situation is also confirmed in off-design conditions: HE-1 shows a value of the exchanged thermal power higher than 150 kW for all the analysed configurations at 150 % of the load and a value of about 50 kW at 50 % of the load. Comparing configurations with the same temperature setting, the results are similar: indeed, for Ambient 1 (Fig. 5.2a) and Pressurized 1 (Fig. 5.2c), the thermal power exchanged in the whole HRS in design condition is equal to about 295 kW for both the configurations; Ambient 2 (Fig. 5.2b) shows a value of the thermal power exchanged in design condition slightly higher with respect to the configuration Pressurized 2 (Fig. 5.2d), respectively 242 kW and 233 kW.

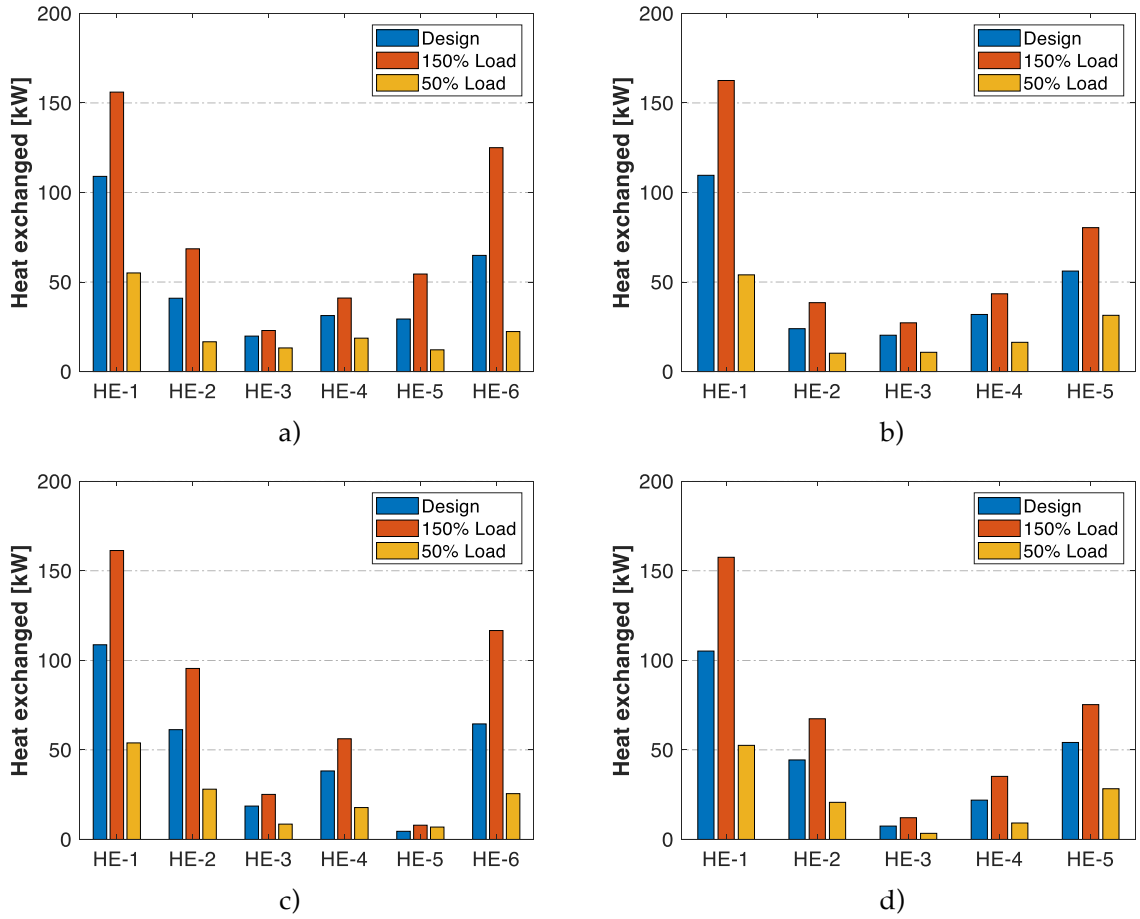

Fig. 5.2. Heat exchanged in each heat exchanger of the HRS, for the 4 analysed configurations, in design and off-design conditions (in the operating point related to the minimum and maximum points of the operating range): a) Ambient 1; b) Ambient 2; c) Pressurized 1; d) Pressurized 2.

Compression section off-design performance

An additional contribution to the energy balance of the system, which varies according to the operating conditions, is represented by the energy consumption of the mechanical auxiliaries, mainly for the SNG compression. In Fig. 5.3, the electrical power consumption for gas compression, as a function of the variable electrical input to the P2G system and for the four analysed configurations, is shown. In particular, the obtained results have been calculated considering the actual operating conditions of the machines, on the basis of the off-design performance maps presented in the previous chapter (Chapter 3 – The Power-to-Gas model). In the case of pressurized configurations (Pressurized 1 and Pressurized 2), the power consumption for the reactants' compression is included in the calculation.

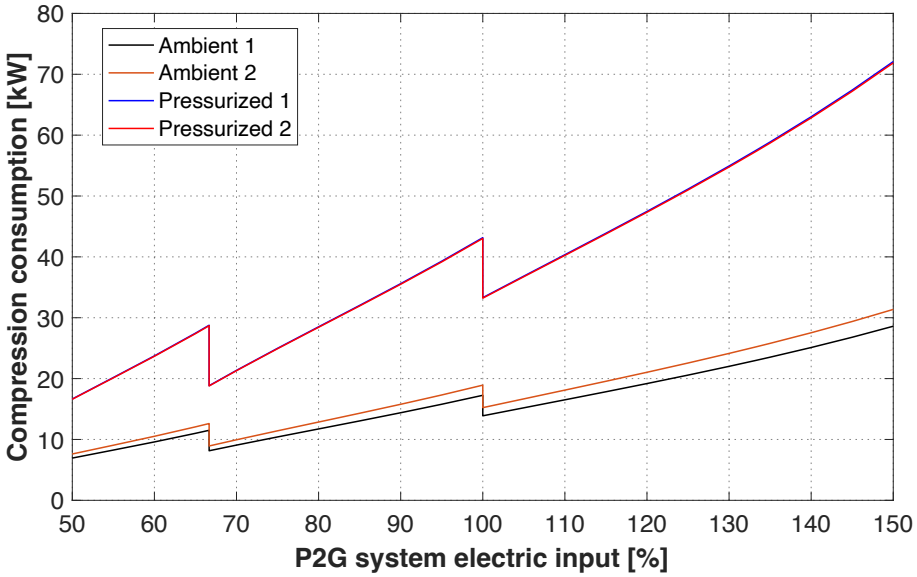

Fig. 5.3. Electric power consumption for gas compression, as the electrical load input to the P2G system varies and for the four thermodynamic scenarios considered.

In Fig. 5.4, instead, the electric power consumption, normalized with respect to the electrical power input of the SOEC, is presented. Even if the cost of the compression increases for higher loads, the auxiliaries' energy consumption does not represent an important cost item, being around a few percentage points of the SOEC electrical consumption.

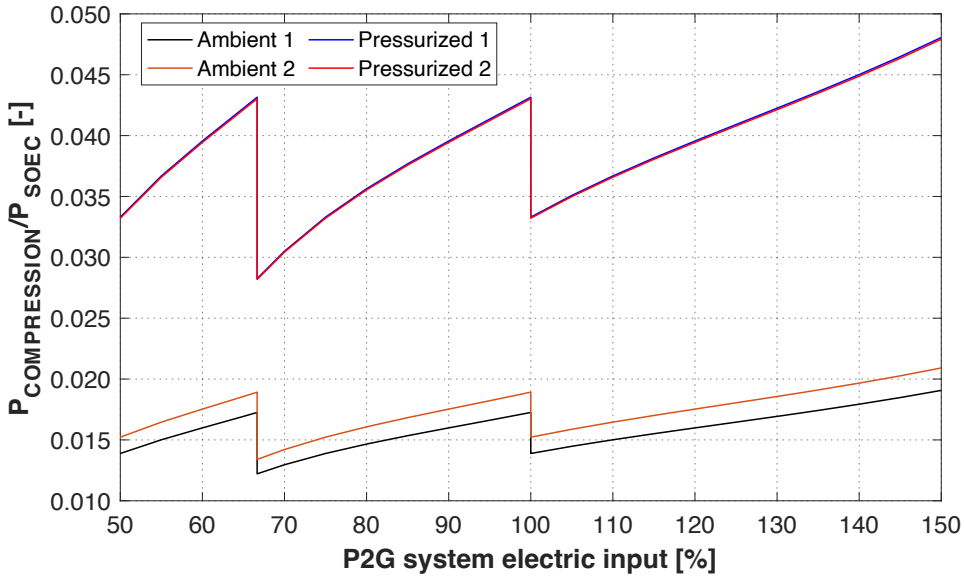

Fig. 5.4. Electric power consumption for gas compression, normalized with respect to the electrical power input of the SOEC, as the electrical load input of the P2G system varies and for the four thermodynamic scenarios considered.

Performance parameters of the overall P2G system

In order to compare the analysed cases and scenarios, several indices have been introduced for the evaluation of the P2G system performance, illustrated below.

- P2G plant utilization factor. It is possible to characterize an energy system in terms of plant operating time during the year of operation, in order to assess the operating time and the periods of inactivity. In particular, the first parameter considered in this comparative analysis is called the "P2G plant utilization factor", $f_{u\,P2G}$, related to the storage system coupled to the renewable generator and defined as the ratio between the annual operating hours, h_{P2G} (i.e. the time in which the P2G plant is operative during the year) and the total annual hours (h_{year} = 8760 h):

$$f_{u\,P2G} = \frac{h_{P2G}}{h_{year}}$$

- P2G equivalent hours. It is also possible to calculate the number of equivalent operating hours, or load factor of the P2G system, to assess whether the system is used in a proper way or underused. This parameter, $h_{eq\,P2G}$, can be expressed by the ratio of the electricity input to the P2G system during the year, $E_{in\,P2G}$ [MWh/year] and the design power size of the P2G system, $P_{P2G\,Design}$ [MW]:

$$h_{eq\,P2G} = \frac{E_{in\,P2G}}{P_{P2G\,Design}}$$

  In particular, the total input energy $E_{in\,P2G}$ has been calculated as the sum of the electrical power input contributions related to the different periods of the year in which the system is operative (with instantaneous electrical power input in the i-th period of the year $P_{P2G,i}$ [MW] different from zero):

$$E_{in\,P2G} = \sum_i h_i \cdot P_{P2G,i}$$

- SNG and methane production. Due to the aim of introducing the produced SNG into the natural gas distribution network, a few parameters concerning the productivity of the P2G system have been taken into account. The first considered parameter is the annual mass production of SNG by the different P2G system configurations. In addition, since - even if it is composed mainly by methane - other chemical elements (such as H_2, CO and CO_2) are also included in the produced SNG stream, it can be

useful to evaluate the annual mass production of methane and the annual mean molar fraction of methane in the produced SNG.
Finally, also the chemical energy related to the annual production of SNG, indicated as F_{SNG} [MWh/year], has been calculated as:

$$F_{SNG} = \sum_i h_i \cdot \dot{m}_{SNG,i} \cdot LHV_{SNG,i}$$

where $\dot{m}_{SNG,i}$ [kg/s] is the mass flow rate of the produced SNG in the i-th time step of the year and $LHV_{SNG,i}$ [MJ/kg] is the lower heating value of the produced SNG in the i-th time step of the year.

- Electricity utilization factor from NP-RES for P2G. Regarding the energy flows, the performance of the storage system have been estimated, at first, by evaluating the share of available renewable energy used by the P2G system and, then, the conversion of available electricity into SNG chemical energy.
  The data to be considered for this evaluation is the available energy input of the P2G system, that is equal to the electricity produced by the renewable source throughout the year (see the diagram in Fig. 5.5). Based on the size and the operating range of the P2G system, only a share of this energy feeds the storage system, while the residual share not used by the P2G system during the year cannot be stored by the system (it has been assumed that it is introduced into the electric grid or wasted). Then, it is possible to define a renewable energy usage factor or "electricity usage factor from NP-RES", $U_{E\ NP-RES}$:

$$U_{E\ NP-RES} = \frac{E_{in\ P2G}}{E_{NP-RES}}$$

where, $E_{in\ P2G}$ [MWh/year] is the energy used by the P2G system during the year and E_{NP-RES} [MWh/year] is the electricity produced by the renewable source, calculated as the sum of the instantaneous generation contributions over the whole year.

- Electric-to-fuel conversion index related to the P2G system. In order to describe the performance of the P2G system referring to the electrical input, an efficiency factor for the conversion of the electricity into fuel ($\eta_{E2F\ P2G}$) has been evaluated, defined as:

$$\eta_{E2F\ P2G} = \frac{F_{SNG}}{E_{in\ P2G}}$$

- First law efficiency of the P2G system. The previous parameter $\eta_{E2F\ P2G}$, however, does not take into account the energy consumption of thermal type. Therefore, the overall thermodynamic balance has been analysed, evaluating the thermal energy demand of the plant during the whole year and including the heat flows. With this purpose, the first law efficiency ($\eta_{I,P2G}$) has been introduced:

$$\eta_{I,P2G} = \frac{F_{SNG}}{E_{in\ P2G} + Q_{in\ P2G}}$$

where $Q_{in\ P2G}$ [MWh/year] is the annual thermal energy input of the plant evaluated as the sum of the required thermal flows $\dot{Q}_{in,i}$ [MW] in the i-th time step:

$$Q_{in\ P2G} = \sum_i h_i \cdot \dot{Q}_{in,i}$$

- Utilization factor and electric-to-fuel conversion of electricity from NP-RES. An additional parameter has been calculated, $U_{E2F\ NP-RES}$, defined as the ratio between the energy content of the produced SNG and the electrical energy available from the renewable source:

$$U_{E2F\ NP-RES} = \frac{F_{SNG}}{E_{NP-RES}}$$

This index is equal to the product of $U_{E\ NP-RES}$ and $\eta_{E2F\ P2G}$ and allows to calculate the share of available electricity (produced by the NP-RES) that is stored and converted into SNG.

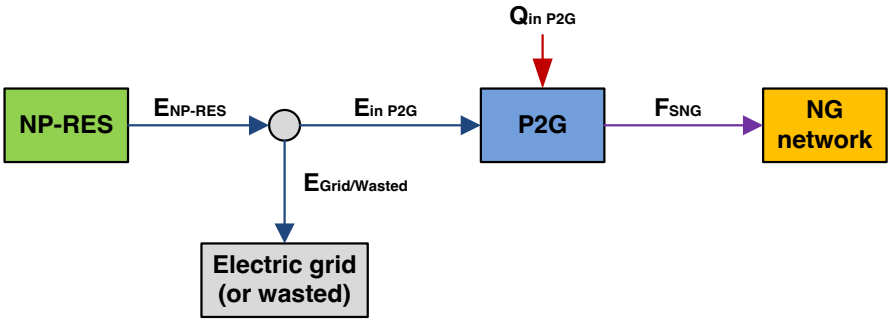

Fig. 5.5. Energy flow diagram for the definition of the performance parameters.

Results

In Tab. 5.1, the results of the comparative analysis among the different P2G system configurations are shown.

The P2G system operates with a plant utilization factor in the range of 43 – 44 %, with almost the same values for the four thermodynamic variants. The two configurations of the P2G system with the SOEC operating at ambient pressure show about the same number of operating hours and equivalent hours, slightly higher with respect to the values of the configurations with the pressurized SOEC (in the case of Ambient 2, h_{P2G} is equal to 3896 h/year and $h_{eq\ P2G}$ is equal to 3469 h/year). The difference in terms of operating hours is due to the lower electricity consumption for auxiliaries, allowing the P2G configurations at ambient pressure (Ambient 1 and Ambient 2) to operate in off-design conditions for larger periods: when the NP-RES production is at the minimum, close to the deactivation threshold of the P2G system (off-design at 50 % of the design load of the SOEC), the lower share of the auxiliaries' electrical consumption for the systems at ambient pressure allows to use the reduced electrical power from the NP-RES to operate the SOEC at minimum load and meet the demand of the auxiliaries.

The P2G systems with a pressurized SOEC (Pressurized 1 and Pressurized 2), operating for fewer hours during the year, show a higher amount of energy introduced into the electricity grid (1231 MWh/year for Pressurized 1 and 1224 MWh/year for Pressurized 2); as a consequence, the energy utilization factor is lower, equal to about 74 % for both the configurations; the value of $U_{E\ FRNP}$ for the systems at ambient pressure (Ambient 1 and Ambient 2) is slightly higher, equal to about 75 %.

Regarding the production of SNG, the systems at ambient pressure show higher values (216 tons/year for Ambient 2) with respect to the pressurized systems (188 tons/year for Pressurized 2). The production of methane follows the trend of the SNG production; indeed, even if the SNG quality is higher for pressurized systems (the mean fraction of methane in the final product is about 85 % in the case of systems at ambient pressure and equal to about 95 % - 97 % in the case of pressurized systems), the systems at ambient pressure, showing a higher number of operating hours during the year, are able to produce a greater amount of SNG, that leads to a slightly higher production of methane compared to the pressurized systems (184 tons/year for configuration Ambient 2). The average annual LHV value of the produced SNG varies between about 45 MJ/kg and 49 MJ/kg. The average annual electric-to-fuel conversion index of the P2G system is about 75 % - 79 %, with the highest value in the Ambient 2 case. This result can be explained through the evaluation of the SNG production, which results higher for this system.

From the point of view of the utilization factor and the electric-to-fuel conversion, variable values have been obtained in the range 55 % - 59 %, on the basis of the system configuration; Ambient 2 shows better performance, compared to the other thermodynamic solutions: indeed, the value of $U_{E2F\ NP-RES}$ is equal to 59 % with respect to 55% for pressurized cases. In addition, also from the point of view of the first law efficiency, Ambient 2 is the most performant, with a value of $\eta_{I,P2G}$ equal to about 75 %, despite the thermal energy

consumption is the highest among the analysed scenarios, with a value of about 175 MWh/year).

Tab. 5.1. Annual results of the comparative analysis carried-out in the considered scenario, for the thermodynamic configurations of the P2G system.

Parameter	Ambient 1	Ambient 2	Pressurized 1	Pressurized 2
P2G operating time - h_{P2G} [h/year]	3895	3896	3784	3797
P2G plant utilization factor - $f_{u\,P2G}$ [%]	44.4	44.5	43.2	43.3
P2G equivalent hours - $h_{eq\,P2G}$ [h]	3469	3469	3411	3417
NP-RES energy available - E_{NP-RES} [MWh/year]	4644	4644	4644	4644
P2G energy input - $E_{in\,P2G}$ [MWh/year]	3469	3470	3413	3420
Energy not used - $E_{Grid/Wasted}$ [MWh/year]	1175	1174	1231	1224
Electricity utilization factor - $U_{E\,NP-RES}$ [%]	74.7	74.7	73.5	73.6
SNG production [t/year]	215	216	189	188
Methane production [t/year]	183	184	181	183
Mean CH_4 molar fraction in the SNG [%]	85.1	85.2	95.8	97.3
Mean LHV [MJ/kg]	45.3	45.9	48.7	49.1
Electric-to-fuel conversion index - $\eta_{E2F\,P2G}$ [%]	78.0	79.0	75.0	75.1
Total thermal energy externally requested - $Q_{in\,P2G}$ [MWh/year]	160	175	117	154
First law efficiency - $\eta_{I,P2G}$ [%]	74.6	75.1	72.5	71.9
Utilization factor - $U_{E2F\,NP-RES}$ [%]	58.3	59.0	55.1	55.3

The four considered thermodynamic configurations are characterized by similar performance, but with some differences, already highlighted in the design analysis (see Chapter 4 – Synthetic natural gas application: design analysis), still clear also including the effect of off-design operations. With respect to the operations in design conditions (see Tab. 4.6), a limited variation in the average annual performance indices is observed. This result can be explained since, although in off-design conditions the energy demand contribution of the auxiliaries varies with respect to the operations in design conditions, some performance parameters of the components can worsen or even improve in off-design conditions. In more detail, the electrolyser in partial load conditions operates at higher efficiency points (see Fig. 3.14); instead, in overload conditions, in the periods in which the electrical input from the NP-RES

is higher than the design value, the trend is the opposite. As a consequence, periods with increased performance offsets periods with worsened performance.

In order to analyse the off-design performance of the studied variants, the instantaneous values of the key calculated quantities are presented in Fig. 5.6 - Fig. 5.9.
In particular, in Fig. 5.6, the instantaneous electrical power produced the NP-RES (and, then, the instantaneous electrical power input to the P2G system), related to Ambient 1, is shown; the areas under the two curves represent respectively the overall energy produced by the NP-RES, E_{NP-RES}, and the electricity used by the P2G system, $E_{in\ P2G}$. The difference between these areas represents the electricity introduced into the network (or wasted). In the figure, the monotonic curve of the instantaneous chemical power associated to the produced SNG and the monotonic curve of the instantaneous thermal power required by the P2G system (from an external source) are also presented. On the other hand, in Fig. 5.7 the monotonic curve of the instantaneous production of SNG during the year for the four thermodynamic configurations is shown and in Fig. 5.8 the corresponding monotonic curve of the instantaneous production of methane during the year is presented.
During the year, the instantaneous value of the SNG flow rate is variable (due to the variability of the electricity generation from NP-RES) and is nil out over a non-negligible number of hours in the year (when the power produced by NP-RES is below the minimum load limit - i.e. minimum electrical input - for the operation of the P2G system); indeed, in the considered NP-RES scenario, as already reported in Tab. 5.1, the operating hours of the P2G system are about 3900 h/year and, then, the hours in which the SNG is not produced are equal to almost 5000 h/year for the analysed cases. However, when the P2G system is operative, the SNG flow rate is always sufficiently high, with variations between 50 % and 150 % of the design value. The system Ambient 2 presents a production slightly higher than the system Ambient 1 in the times of the year with the highest wind power production (with a peak of about 0.028 kg/s), while when the wind production decreases the system Ambient 1 shows better performance from this point of view. The pressurized systems present nearly the same SNG production, lower with respect to the systems at ambient pressure. In Fig. 5.8, the instantaneous CH_4 production is shown. For all variants, the methane production is about the same, with the system Pressurized 2 showing a slightly higher production, due to the higher quality of the produced SNG. In Fig. 5.9 the instantaneous first law efficiency values are shown as a function of the wind production. The trend of the first law efficiency highlights that the lower is the electric load, the higher is the efficiency due to the trend of the SOEC efficiency (Fig. 3.14a and Fig. 3.14b). In particular, the system Ambient 1 shows a peak of about 82 %.

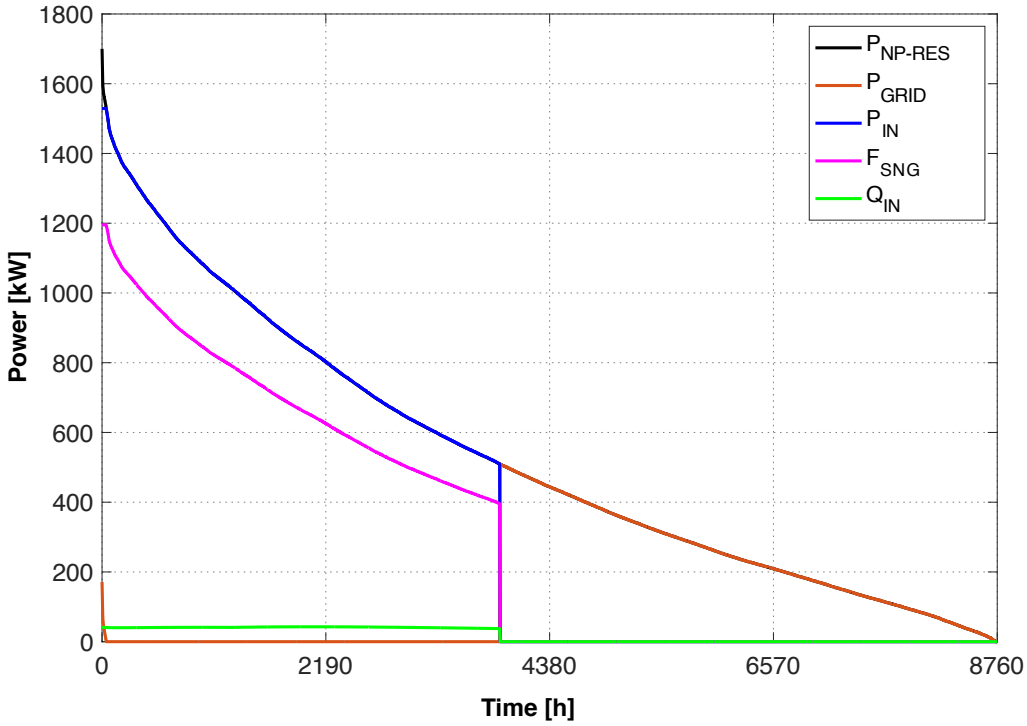

Fig. 5.6. Monotonic curves of the instantaneous electrical power from NP-RES, of the instantaneous electrical power input to the P2G system, of the instantaneous output power associated with the SNG produced and of the instantaneous thermal power required in input to the P2G system (Ambient 1).

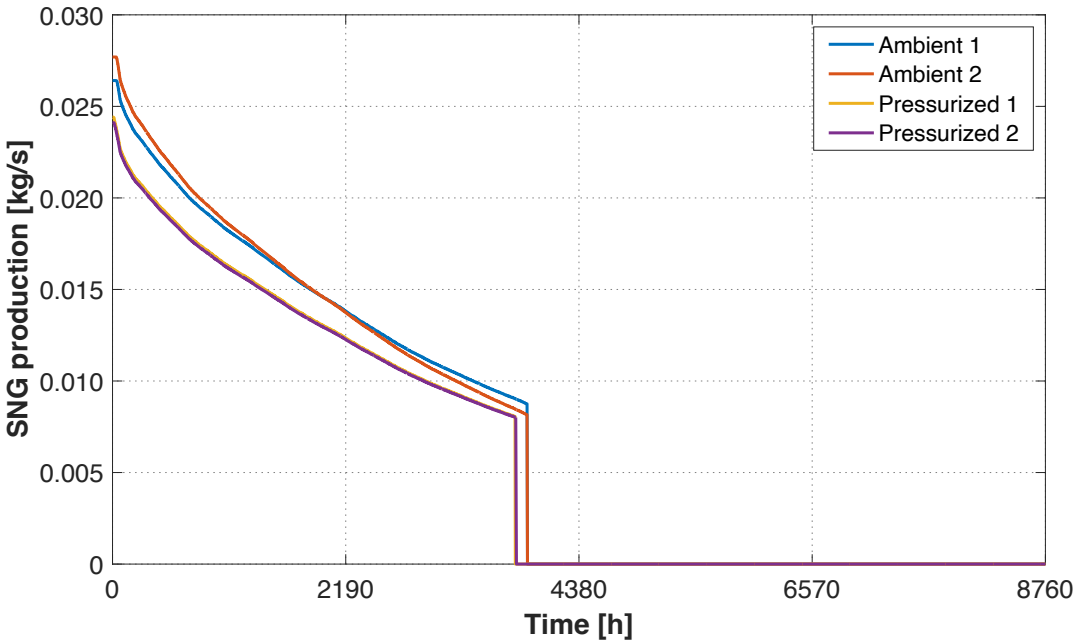

Fig. 5.7. Monotonic curve of the instantaneous production of SNG during the year, comparison between the four considered thermodynamic scenarios.

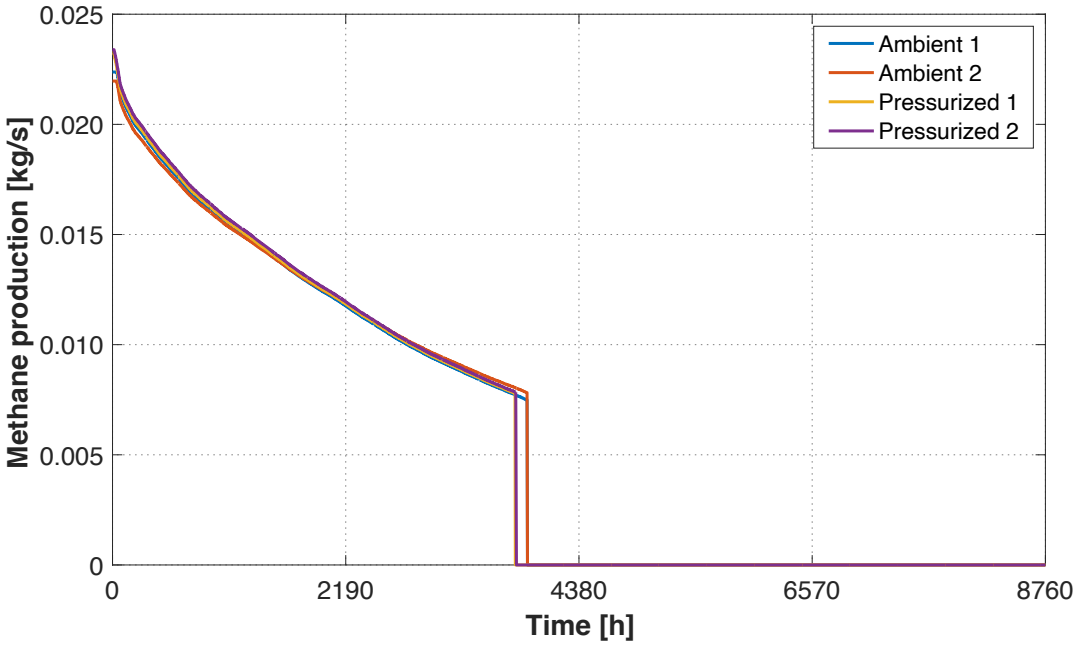

Fig. 5.8. Monotonic curve of the instantaneous methane production during the year, comparison between the four considered thermodynamic scenarios.

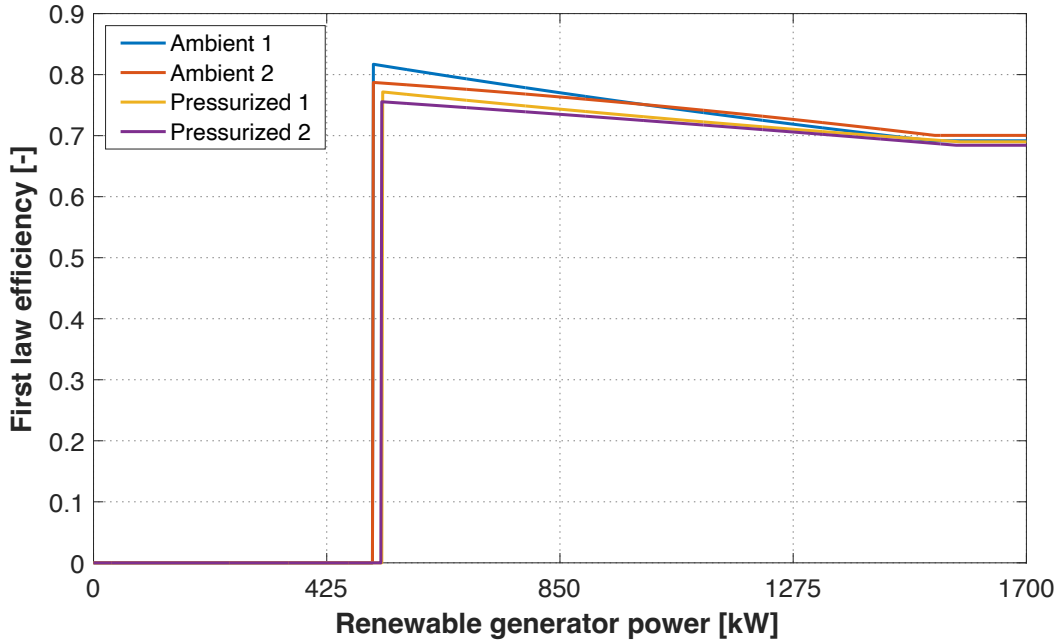

Fig. 5.9. Instantaneous first law efficiency as a function of the power produced by the renewable generator, comparison between the four considered thermodynamic scenarios (significant values only when the P2G system is on, above its minimum load).

Finally, in Fig. 5.10, the flow rate of O_2 potentially extractable from the air stream at the outlet of the anode side is presented; this parameter shows similar values for the four analysed thermodynamic scenarios.

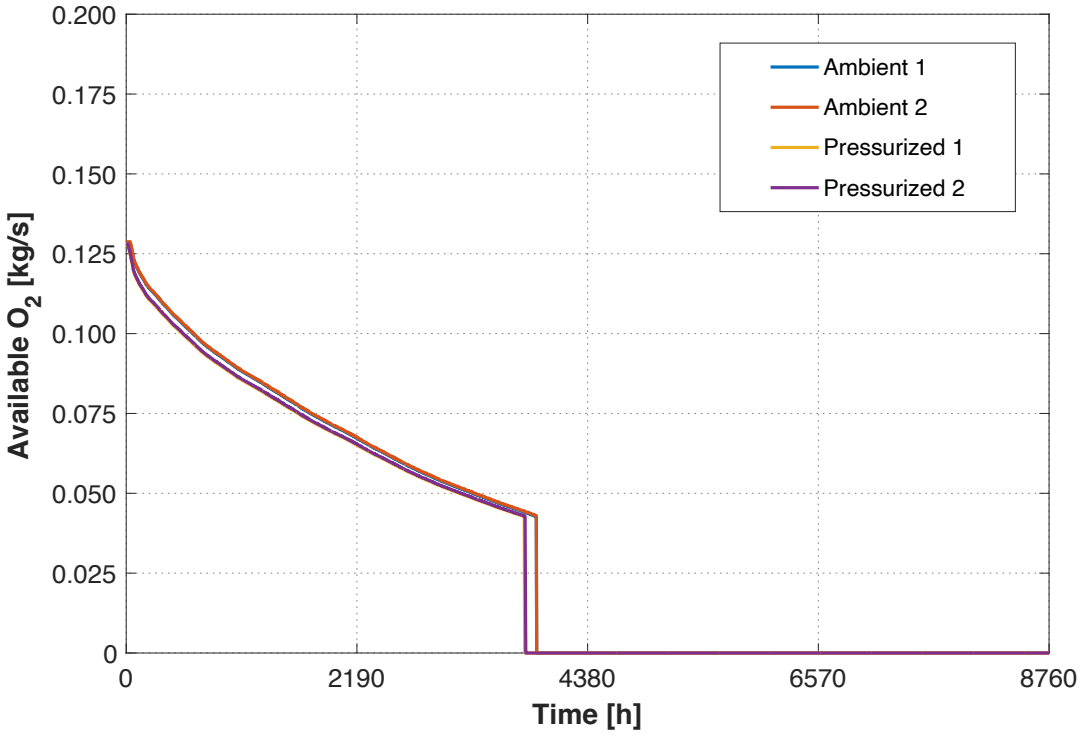

Fig. 5.10. Oxygen flow rate potentially available during the year, comparison between the four considered thermodynamic scenarios.

5.2 – Second scenario

In the previous paragraph, the results of a preliminary evaluation of the P2G system in a set operating scenario have been reported. For the sake of simplicity, in this starting scenario the following parameters have been set:

- the design power size of the P2G system;
- the ratio between the size of the P2G system and the size of the NP-RES generation;
- the electricity production profile of the NP-RES.

On the other hand, in this paragraph, the results of a broader parametric analysis on the behaviour of the considered P2G storage system, with different renewable energy inputs, have been presented. The main aim of this second analysis is to find the "optimum" coupling ratio between the NP-RES generator size and the P2G energy storage system size. In particular, the considered storage system can be considered optimally sized with respect to the NP-RES generator, if it allows to maximize the amount of the stored renewable energy (the storage is considered a priority in the study compared to the possibility of its direct use) and if the conversion into fuel takes place with maximum efficiency.

Different boundary conditions have been considered, referring to different scenarios in terms of renewable electricity generation profiles. In particular, two investigations have been carried out:

1. Large-scale dimensionless study: in this case, reference has been made to data related to the electricity generation from NP-RES on a large scale (national data of the whole territory), considering different types of non-programmable sources (wind and solar). In this first step of the analysis, the dimensionless ratio of electrical power sizes (R), between the renewable generator and the P2G storage system, has been investigated by means of a parametric study. In order to generalize the obtained results, the investigation was based on normalized curves related both to the NP-RES production and to the performance of the P2G storage system.
2. Small-scale dimensional study: in the second case, reference has been made to the annual electricity production of a specific site, by means of a set NP-RES wind power plant (with an installed electrical power equal to 2 MW); real electricity generation data have been used, representative of a potential installation scenario for the P2G system. The performance of the considered P2G system in a specific site have been evaluated; also in this case, the optimal sizing of the storage system has been identified.

5.2.1 – Boundary conditions and hypothesis: large-scale dimensionless study

In this first case study, reference has been made to data related to the Italian generation in recent years. After a description of the available data used in this study, the process to obtain the normalized production curves from NP-RES is presented and the normalized performance curves of the P2G storage system are summarized (as a function of the variable load). Finally, the management strategy implemented to find the optimal condition and the performance calculation are described.

NP-RES national generation data

In Tab. 5.2, the RES energy production in Italy during recent years, based on GSE [61] and Terna [59] data, is shown. During the years, the renewable electricity generation undergone to several variations linked both to the variability of the sources and to the availability of new plants. For example, in 2018 the production from renewable sources stood at 114.4 TWh, with an increase with respect to the previous year (+ 10.1 %), mainly due to the remarkable performance of the hydropower sector (+ 35 %). On the other hand, the data related to the wind (17.7 TWh) and to the geothermal sector (6.1 TWh) are in line with the previous year; the solar energy showed a significant drop (- 7%) on the national scene. The data in 2019 present an electricity production from renewables equal to about 116 TWh, slightly higher with respect to the previous year. The decrease in the hydropower production (- 2.5 TWh) is

offset by the increase in the wind (+ 2.5 TWh) and solar (+ 1.0 TWh) production; generation from geothermal sources and bioenergy, on the other hand, have been constant over the years.

Tab. 5.2. RES energy production in Italy [TWh] – GSE, Terna [61] - [59].

RES	**2012**	**2013**	**2014**	**2015**	**2016**	**2017**	**2018**	**2019**
Wind	13.4	14.9	15.2	14.8	17.7	17.7	17.7	20.2
Solar	18.9	21.6	22.3	22.9	22.1	24.4	22.7	23.7
Hydropower	41.9	52.8	58.5	45.5	42.4	36.2	48.8	46.3
Geothermal	5.6	5.7	5.9	6.2	6.3	6.2	6.1	6.1
Bioenergy[1]	12.5	17.1	18.7	19.4	19.5	19.4	19.2	19.6
Total RES	**92.2**	**112.0**	**120.7**	**108.9**	**108.0**	**103.9**	**114.4**	**115.9**

[1]*Bioenergy: solid biomasses, biogases and bioliquids.*

In this analysis, reference has been made to the whole year of operation of the system and to the production data available on a hourly basis (Terna – 2019, used as input for the developed model of the P2G system).

The electricity production profiles in the year 2019 (average hourly power) related to renewable energy sources (wind, solar, hydroelectric and geothermal) are shown in Fig. 5.11, Fig. 5.12, Fig. 5.13 and Fig. 5.14.

The wind-type production profile is more fluctuating and irregular, even if the data are related to a large territorial scale, on which the effects of local generation peaks and unavailability of the sources should partially offset each other. In addition, both the profiles of the wind and the solar production show high variations of seasonal and daily type, as well as hourly and "random" (non-programmable) types. These two sources represent the typical examples of NP-RES that can be coupled to a P2G energy storage system and the related production profiles have been used as a reference for this analysis. The production from hydroelectric source, on the other hand, is less interesting for the study: although there are seasonal variations and even over shorter periods, this source is only partially affected by non-programmable variations; part of the plants, instead, can be managed within 24 hours (this share of hydroelectric production is, indeed, of programmable type). Finally, the production from geothermal source - not considered in the study - is quite constant during the year, with limited variations, on average less than 10 % around an almost constant annual average value (between 0.6 and 0.7 GW).

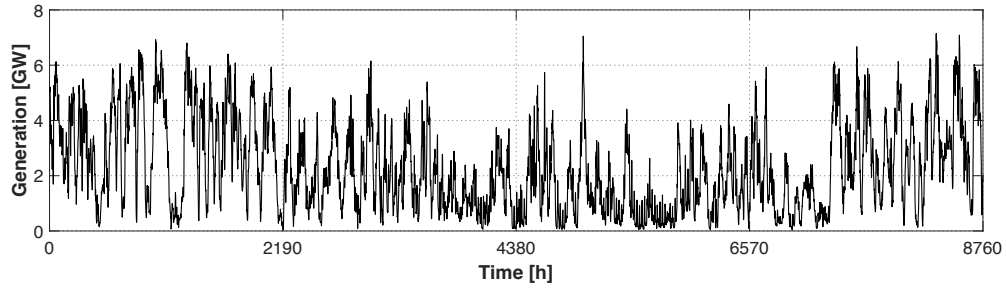

Fig. 5.11. Electric production from wind source in the year 2019.

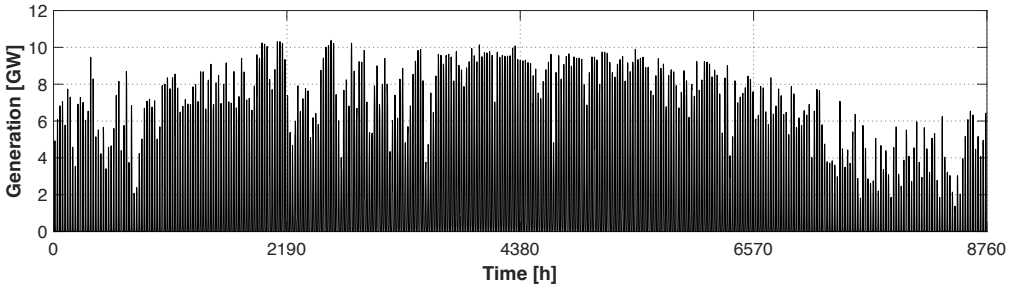

Fig. 5.12. Electric production from solar source in the year 2019.

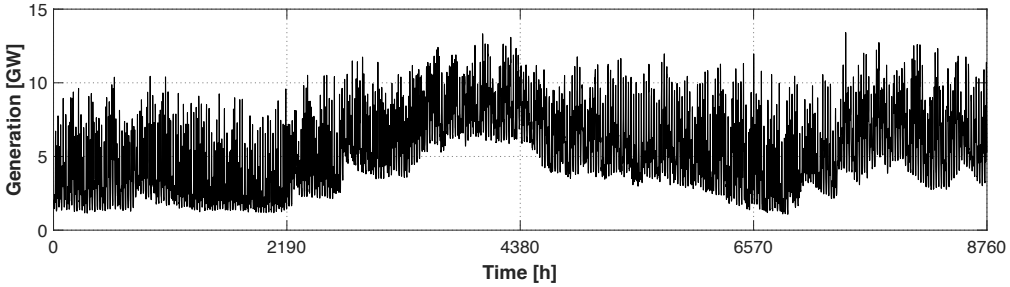

Fig. 5.13. Electric production from hydroelectric source in the year 2019.

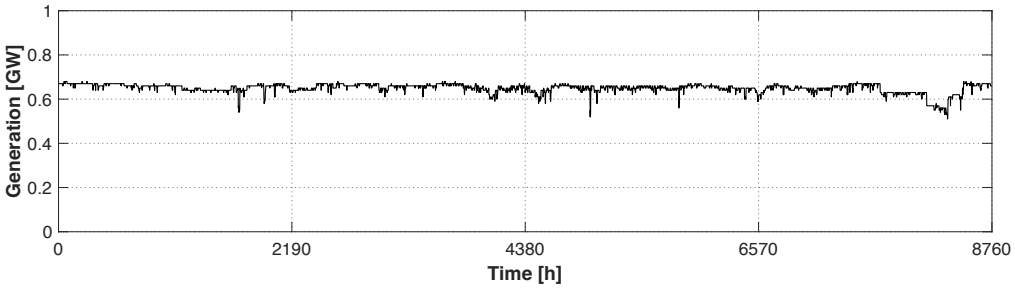

Fig. 5.14. Electric production from geothermal source in the year 2019.

NP-RES normalized profiles

On the basis of the previously introduced production profiles from NP-RES, the corresponding monotonic curves can be derived; these curves allow to highlight the

distribution of the electric power values available for the P2G system during the considered time horizon. In particular, the monotonic curves related to the year 2019 have been obtained for the considered sources, normalized with respect to the value of the total installed capacity of each source. In Tab. 5.3, the installed capacities for the several renewable sources in Italy [59], used to normalize the instantaneous production data, are presented.
The NP-RES (wind and solar) show a constant increase in the installed capacity during the last few years and a potential increase is foreseeable in the incoming years; regarding the hydroelectric and geothermal sources, instead, the installed capacity has been constant in the last years, mainly since full exploitation of the available sites has already been achieved.

Tab. 5.3. Installed capacity for the several renewable sources [GW] – Terna **[59]**.

RES	**2015**	**2016**	**2017**	**2018**	**2019**
Wind	9.1	9.4	9.7	10.2	10.7
Solar	18.9	19.3	19.7	20.1	20.9
Hydropower	22.2	22.3	22.4	22.5	22.5
Geothermal	0.8	0.8	0.8	0.8	0.8
Total	**51.0**	**51.8**	**52.6**	**53.6**	**54.9**

The normalized monotonic curves, for the two NP-RES considered in this analysis, are shown respectively in Fig. 5.15 (wind) and Fig. 5.16 (solar); in addition, the normalized monotonic curves of the hydroelectric production (Fig. 5.17) and of the geothermal production (Fig. 5.18) are presented too.
From the comparison between the different types of NP-RES, the curve related to the wind power over the whole national territory shows a decreasing profile with power values always different from zero, and a peak equal to about 70 % of the total installed power. The value of the annual equivalent hours of the whole national production is equal to 1876 h/year.
The shape of the duration curve related to solar power, instead, shows a period of inactivity (mainly at night) of the plants and a peak value equal to about 50 % of the total installed capacity; an equivalent number of hours can be deduced (equal to 903 h/year), lower with respect to the wind farms.

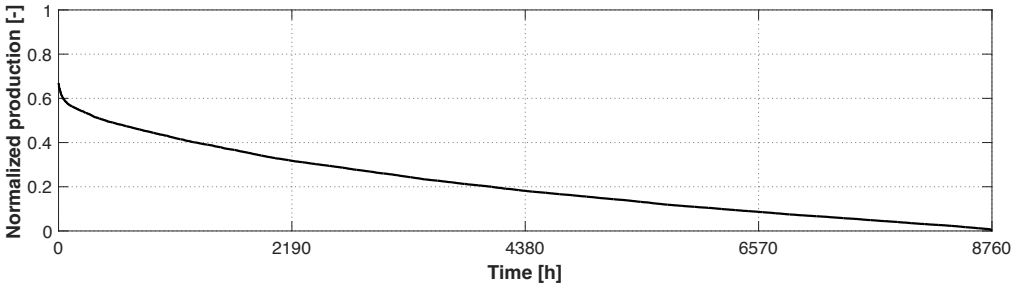

Fig. 5.15. Normalized monotonic curve of the national electrical production from wind source, in the year 2019.

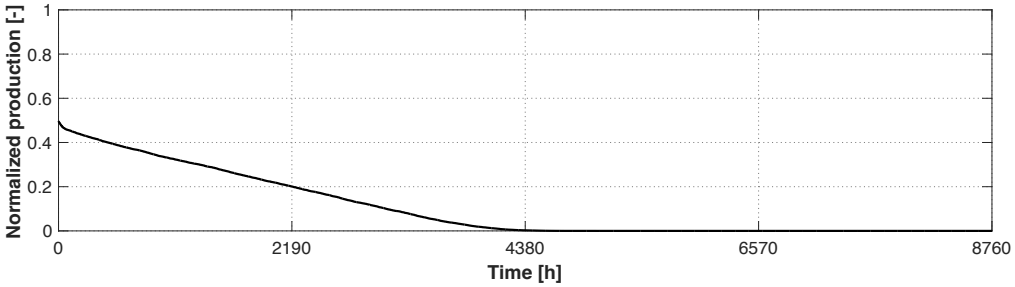

Fig. 5.16. Normalized monotonic curve of the national electrical production from solar source, in the year 2019.

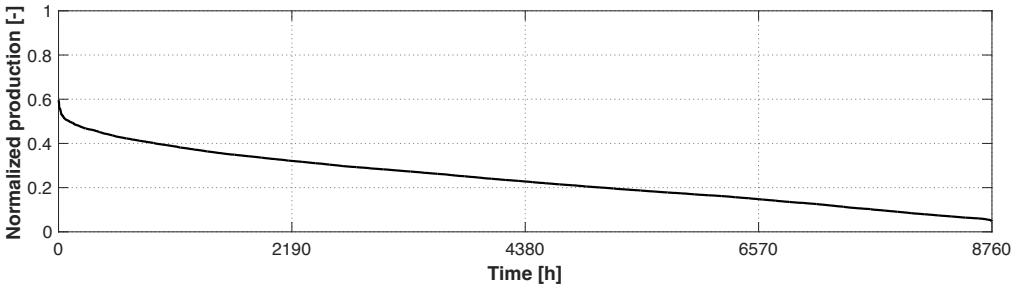

Fig. 5.17. Normalized monotonic curve of the national electrical production from hydroelectric source, in the year 2019.

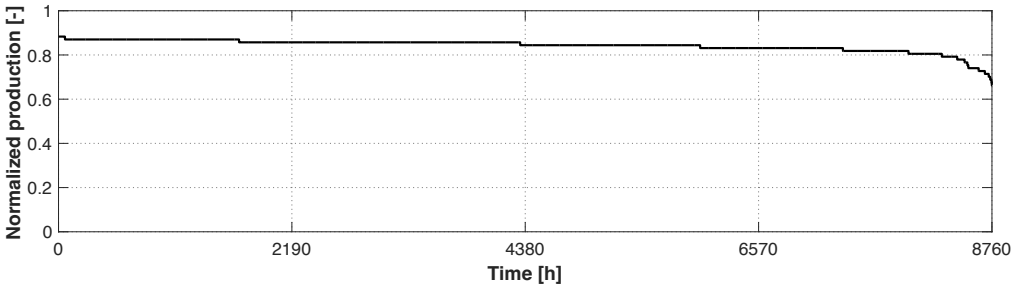

Fig. 5.18. Normalized monotonic production curve of the national electrical production from geothermal source, in the year 2019.

Normalized performance maps of the P2G system

As for the NP-RES production curves, also the behaviour of the P2G system as a function of the electrical input can be described by means of dimensionless performance maps. Through the results obtained with the thermodynamic model of the system (described in Chapter 3 – The Power-to-Gas model), the main performance as a function of the electrical input have been normalized with respect to the design value. In particular, the thermodynamic study of the P2G system with a variable load has been carried out considering a reference size for the SOEC system (set equal to 1 MW in the previous analysis).

In Fig. 5.19 - Fig. 5.24, the normalized values of the main quantities (efficiency and main inputs and outputs of the plant), considered to be the most representative of the system behaviour in design and off-design conditions, are presented. The displayed curves interpolate the single points obtained by means of the system simulation with the thermodynamic model in variable load conditions.

In the figures, the normalized performance maps refer to the most efficient P2G configuration from the point of view of the first law efficiency in design conditions; from the results of the previous analysis (see Chapter 4 – Synthetic natural gas application: design analysis), the configuration with the SOEC and the HTM section operating at ambient pressure and at the same operating temperature (case Ambient 2), turns out to be the most performant. The difference in the trend among the configurations is almost negligible, resulting in overlapping lines; thus, only configuration Ambient 2 has been considered in this section.

In Fig. 5.19, the values of the first law efficiency for the P2G system as a function of the normalized electrical input, are presented. The efficiency shows a decreasing trend with the increase in the electrical input, varying from a maximum of about + 4.5 % of the design value, related to the 50 % of the load, to a minimum of about – 6 % of the design value, in correspondence of 150 % of the electrical load. This trend is mainly affected by the trend of the SOEC component (see, in particular, the results related to the efficiency of the SOEC in off-design conditions in Fig. 3.14a and Fig. 3.14b).

In Fig. 5.20, the normalized SNG production as a function of the normalized electrical input is presented. The SNG production increases with the increase in the electrical load with a linear trend, pointing out a direct proportionality between the amount of energy introduced into the system (energy input) and the amount of produced SNG (material output). This result is in line with the consumption by the P2G system of water and carbon dioxide (material inputs, see Fig. 5.21 and Fig. 5.22): for both the reactants, the trend is linearly increasing.

In Fig. 5.23, the trend of the average LHV related to the produced SNG is shown; in this case, maximum variations of less than ± 4 % with respect to the design value are observed. This result can be explained by the operating temperatures of the methanation reactors, kept constant during the simulations.

Finally, in Fig. 5.24, the trend of the normalized thermal demand is presented. This trend, not monotonous, is affected by the different thermal re-arrangement at the partial loads of the several heat exchangers. In overload conditions, the required thermal power increases, due to the increased mass flows of the material streams; for electrical loads lower with respect to the design point, instead, even if the flow rates of the reactants decrease, the thermal recovery is not performant as in overload conditions (in some heat exchangers in the HRS section, the thermal recovery is limited).

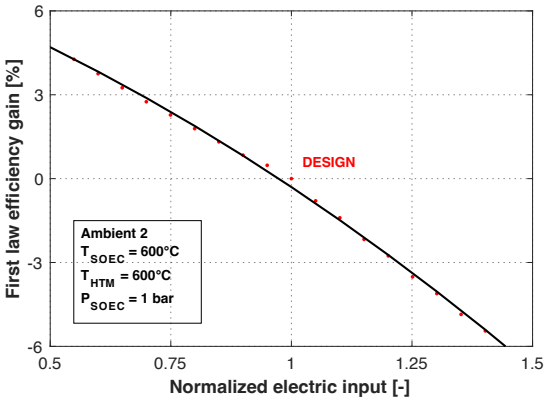

Fig. 5.19. First law efficiency of the P2G system (case Ambient 2), as a function of the normalized electrical input.

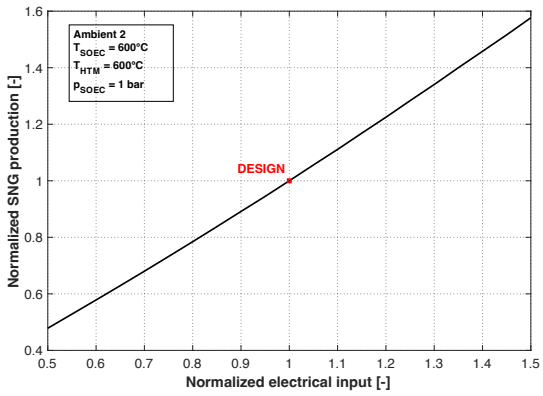

Fig. 5.20. Normalized SNG production of the P2G system (case Ambient 2), as a function of the normalized electrical input.

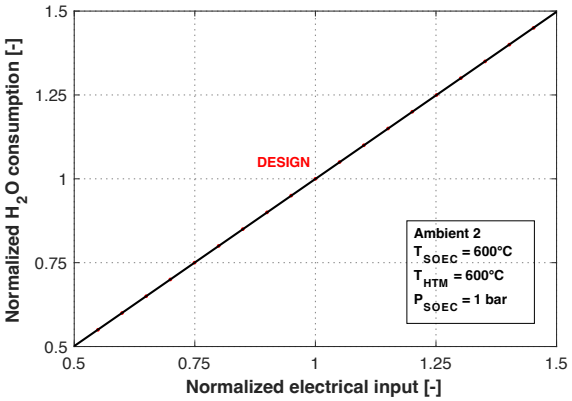

Fig. 5.21. Normalized H_2O consumption of the P2G system (case Ambient 2), as a function of the normalized electrical input.

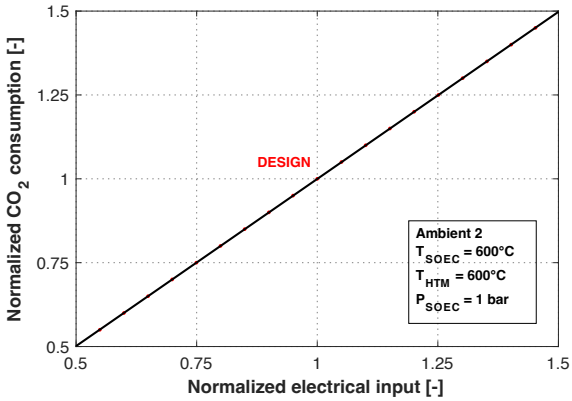

Fig. 5.22. Normalized CO_2 consumption of the P2G system (case Ambient 2), as a function of the normalized electrical input.

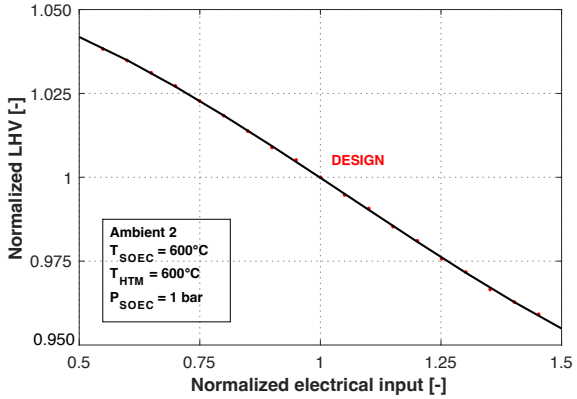

Fig. 5.23. Normalized SNG LHV of the P2G system (case Ambient 2), as a function of the normalized electrical input.

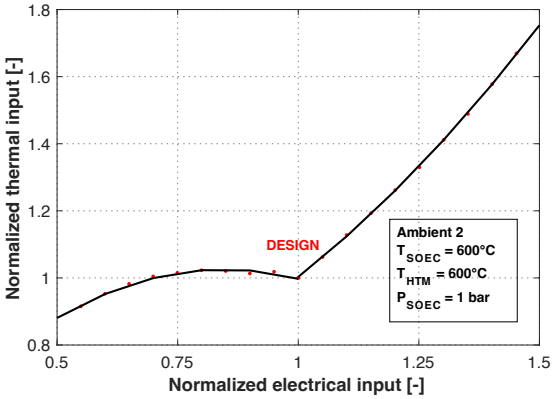

Fig. 5.24. Normalized thermal demand of the P2G system (case Ambient 2), as a function of the normalized electrical input.

Parametric analysis

On the basis on the dimensionless performance maps and the different normalized production profiles previously described, the size effect on the performance of the P2G system has been analysed, for a set size of the coupled renewable source. In more detail, in this analysis the value of the parameter R, defined as the ratio between the nameplate power of the NP-RES (P_{NP-RES}) and the power size of the P2G system (P_{P2G}), has been considered variable:

Eq. 5.1. $$R = \frac{P_{NP-RES}}{P_{P2G}}$$

The aim of the analysis is to identify the optimal size ratio, between the renewable generator and the P2G storage system, for variable sizes and types of renewable sources, in order to define a reference value that can be used as a starting point for a more detailed sizing of the storage system.

A wide range of values for the ratio R has been evaluated, ranging from 0.5 (corresponding to the maximum relative size of the P2G system, equal to double the size of the renewable generator) to 5 (minimum relative size of the P2G system). The two national generation profiles related to wind and solar (corresponding to the curves in Fig. 5.15 and Fig. 5.16) have been considered as scenarios of NP-RES.

During the year of operation, the P2G system can operate in off-design conditions by varying its electrical input load, in a range between 50 % and 150 % of the design electrical load. The operations of the P2G system have been analysed by means of an iterative calculation routine that, for each considered value of R, evaluates the load of the P2G system in each i-th time step of the year, considering a time step set equal to 1 hour (equal to the sampling time of the available production profile).

Since, in the study, the storage capacity of the gas distribution network has been considered boundless and any energy surplus not used by the P2G system can be introduced into the electrical network (or, alternatively, to be wasted), a management strategy has been implemented. The management of the P2G system has been developed according to the instantaneous value of the available power from the NP-RES; in Fig. 5.25, the block diagram of the P2G system management strategy is presented.
In more detail, the management strategy is based on the comparison, in each time step of the year, between the electric power produced by the renewable generator ($P_{NP-RES,i}$) and the operating limits of the P2G system ($P_{min,P2G}$ and $P_{max,P2G}$):

- if, in the given time step, the electric power produced by the renewable generator is lower than the lower operating limit of the P2G system, then all the electric energy is introduced into the electric grid (or wasted);
- if, in the given time step, the electric power produced by the renewable generator is within the operating range of the P2G plant, then all the electric energy is employed within the process;
- if, in the given time step, the electric power produced by the renewable generator is greater than the upper operating limit of the P2G system, then the difference between the wind production and the maximum electric load of the P2G system is introduced into the electric grid (or wasted).

As shown in Fig. 5.25, in order to calculate the instantaneous values of the P2G energy flows and performance, the normalized monotonic curves and the dimensionless performance maps of the P2G system have been resized, by means of the parameter R, which represents an input of the iterative routine (with iterative index n, for each value of the ratio R in the considered range 0.5 - 5).

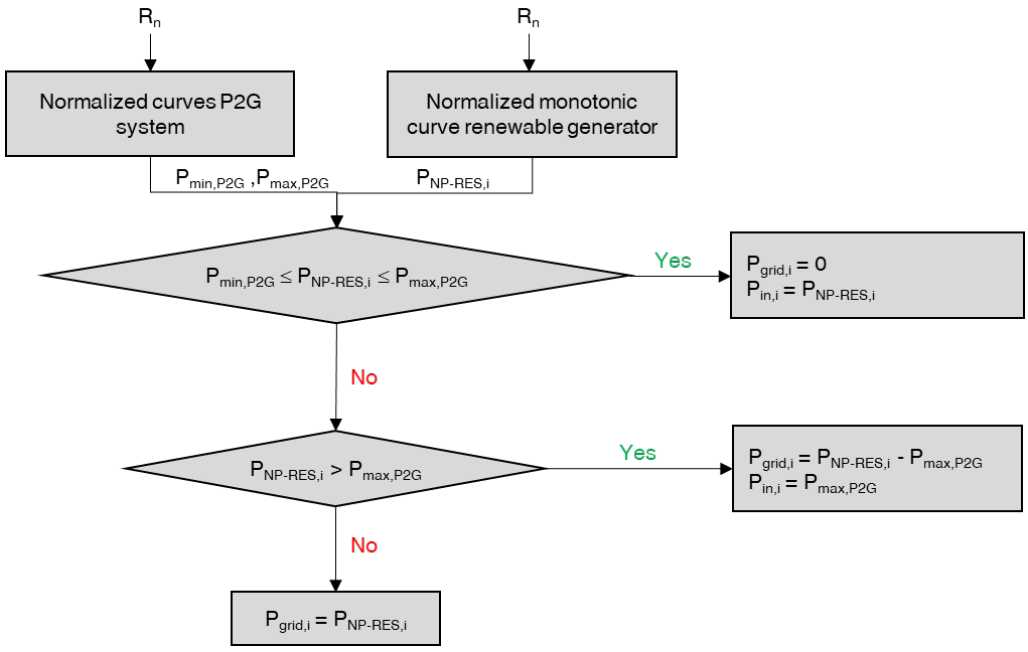

Fig. 5.25. Block diagram of the iterative routine for the management of the energy fluxes.

5.2.2 – Boundary conditions and hypothesis: small-scale dimensional study

In the second case study, reference has been made to the electricity production profile of a specific site. In this case, then, the feasibility of the P2G system on a small scale has been evaluated, with a real NP-RES power plant with a set nameplate power. The selected profile refers to the site's renewable power curve in one year of operation. On the other hand, the same dimensionless curves of the P2G system previously introduced and used in the previous analysis have been considered.

Selected NP-RES generation profile

In this analysis, reference has been made to the electricity production of a wind turbine with a nameplate power equal to 2 MW, installed in Italy (in an Apennines' site), in the year 2019. The electrical generation data, available with a sampling time of 1 hour, are shown in Fig. 5.26; in this figure, the trend of the ramp rate (hourly variation of the generated power, see Fig. 5.26b) is presented too. In this case, the wind production shows recurring variations between the maximum and the minimum power; a seasonality in the production is highlighted, with more production peaks in the winter months and larger periods of low production in the summer months. Sorting the power values in descending order, the monotonic curve of Fig. 5.27 has been derived. In the considered year, this specific plant has produced an amount of electrical energy equal to about 5.8 GWh, with an average power of about 660 kW, corresponding to about 2900 equivalent hours per year.

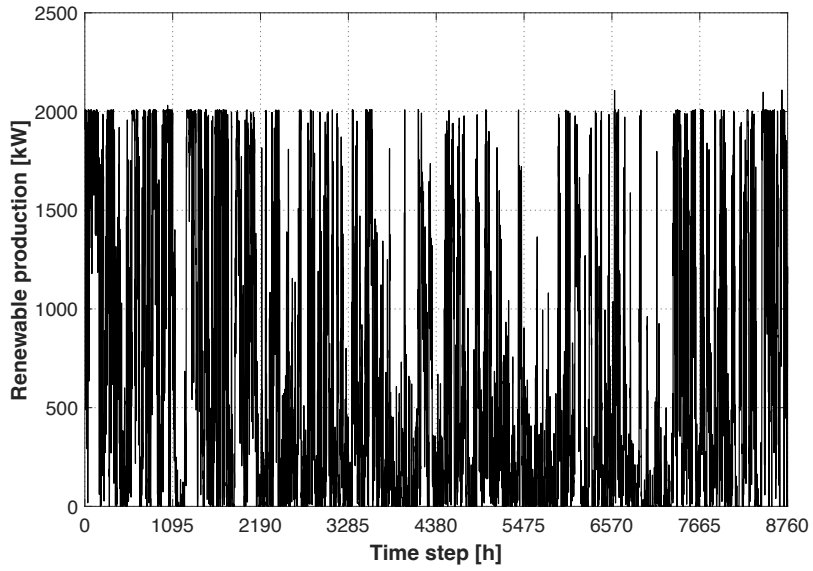

a)

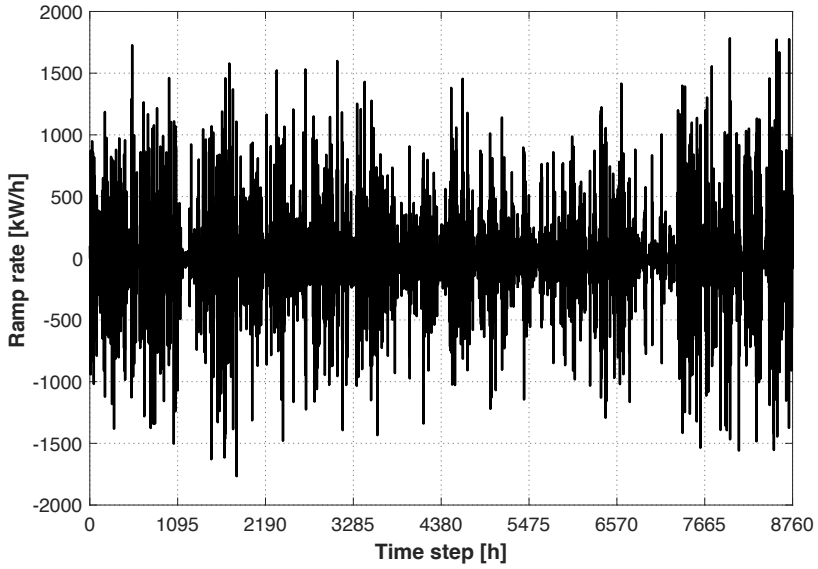

b)

Fig. 5.26. Experimental data of the electrical production for the selected renewable generator, in the year 2019: a) instantaneous electrical generation; b) ramp rate.

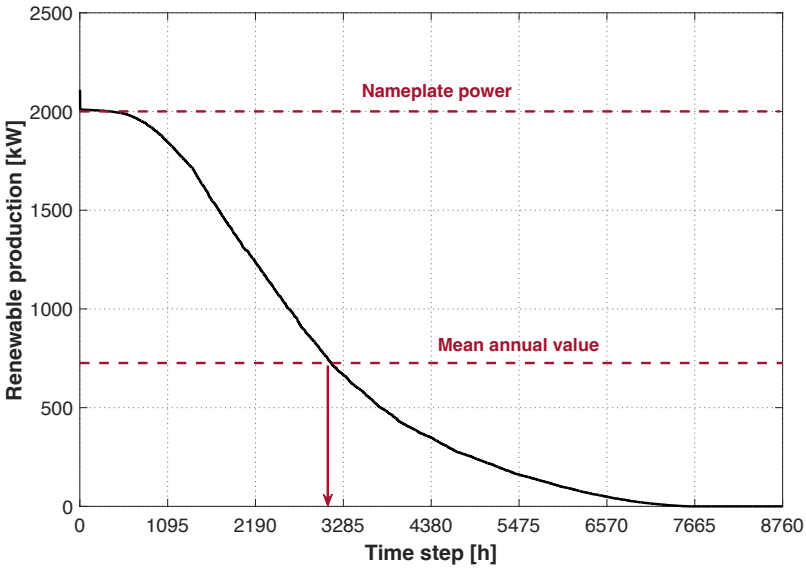

Fig. 5.27. Monotonic curve of the electrical production for the selected renewable generator.

Parametric analysis

In this second study, a parametric analysis with a variable P2G system size has been carried out. The applied methodology and the configurations of the P2G system are the same of the previous analysis, but, in this case, the size of the coupled renewable generator is set. The size of the P2G system varies in a range between 2 MW (corresponding to the power peak value of the renewable plant) and a minimum value of 50 kW. Also in this case, the P2G system operates at a variable load between 50 % and 150 % of the design electrical load and the management strategy (presented in Fig. 5.28) is similar to the simplified method implemented in the previous case study.

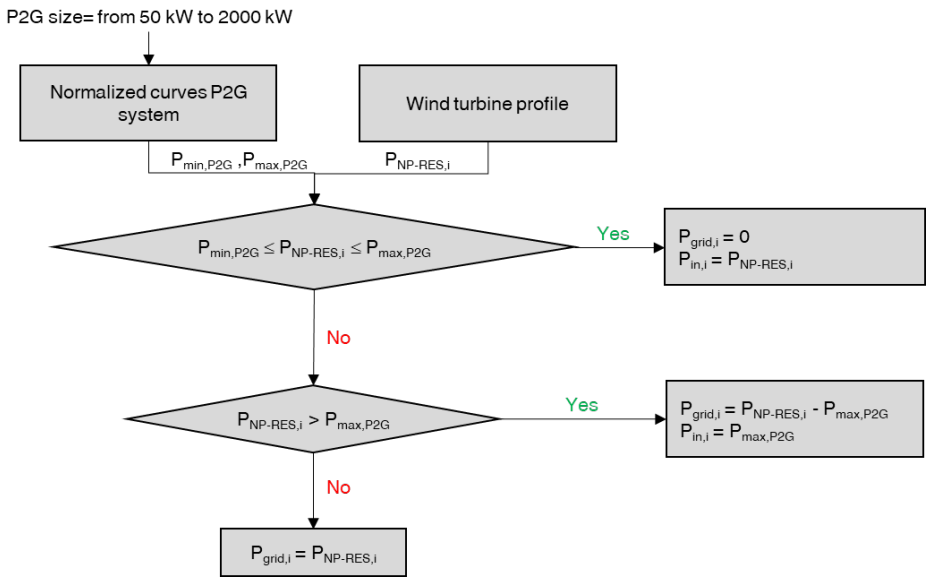

Fig. 5.28. Block diagram of the iterative routine for the management of the energy fluxes.

5.2.3 – Results: large-scale dimensionless study

In this paragraph, the results as a function of the size ratio R, in the case of the large-scale dimensionless study, are shown. At first, the amount of electrical energy produced by NP-RES not stored by the P2G system (equal to: $E_{NP-RES} - E_{in\,P2G}$) has been evaluated. In particular, in Fig. 5.29, the trend of the electrical energy produced by the NP-RES and not used by the P2G system, as a function of the size ratio R, is shown. In both the renewable sources (wind and solar), a trend is observed: in the first part, the considered quantity increases with the increase of the size ratio R, up to a relative maximum point, in correspondence of R equal to about 1 (electrical power size of the P2G system equal to the power peak value of the coupled NP-RES). In this first part of the curve, the renewable generator is too small to allow a full exploitation of the P2G system (the P2G system often receives an input power from the NP-RES lower than its minimum operating limit); as a consequence, the energy produced by the NP-RES, or a large part of it, is introduced into the electric network (or wasted). For values of the size ratio R higher than the relative maximum point, a relative minimum point is observed, corresponding to an R value equal to 3.2 in the case of wind production and to an R value equal to 3.4 in the case of solar production. In the part of the diagram between the relative maximum and minimum points, the amount of unused energy decreases, since the P2G system is always smaller than the size of the renewable generator and, then, the P2G system is able to operate for a number of hours gradually increasing (the hours in which $P_{NP-RES,i} < P_{min,P2G}$ are reduced). If R is equal to values higher than the minimum point (cases with a greater under-sizing of the P2G system), the amount of electricity produced by NP-RES and not used by the P2G system increases (the surplus $P_{NP-RES,i} - P_{max,P2G}$ increases in the hours in which: $P_{NP-RES,i} > P_{max,P2G}$).

The relative minimum point in the case of wind generation shows a lower R with respect to the relative minimum point related to the solar generation (the optimal size of the P2G system is higher in the case of wind generation), since the operating time of the wind generation is higher (see Fig. 5.15 and Fig. 5.16).

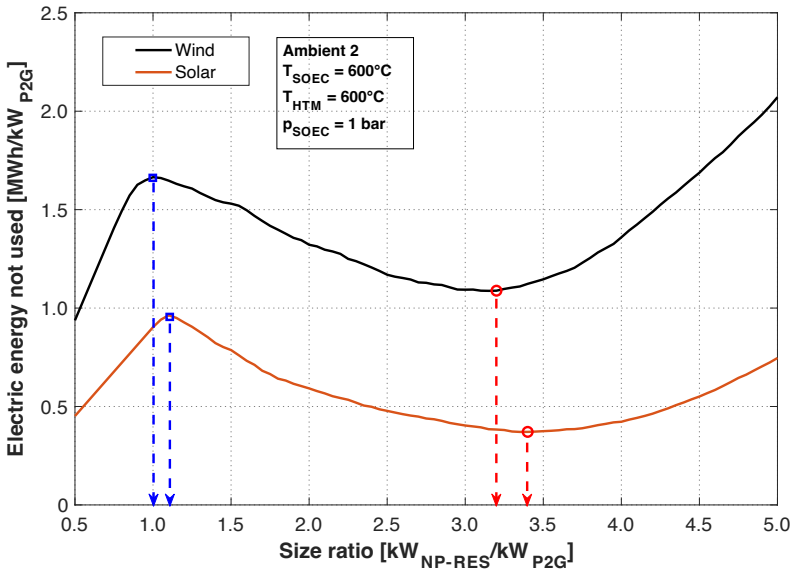

Fig. 5.29. Electrical energy produced by the NP-RES and not used by the P2G system, as a function of the size ratio R (the maximum/minimum points are highlighted).

In Fig. 5.30, the SNG production of the P2G system is presented. An increasing trend of this parameter, as a function of the size ratio R, is observed: the higher the values of R, the smaller the P2G system size in relation to the renewable generator; as a consequence, the amount of electrical energy in input to the P2G system will be higher. Then, the P2G system operates with loads higher than the design value (points of higher SNG production) in more time steps during the year.

In Fig. 5.31, the operating time of the P2G system as a function of the size ratio R is shown. This trend is related to the SNG production and it increases with the increase in the size ratio R. If the P2G system is highly oversized with respect to the coupled renewable generator (for values of R lower than about 1), the P2G system is turned off. The maximum value of the operating time corresponds to $R = 5$ and it is equal to about 6200 h/year in the case of wind generation; in the case of solar generation, the maximum value is lower (equal to about 3000 h/year).

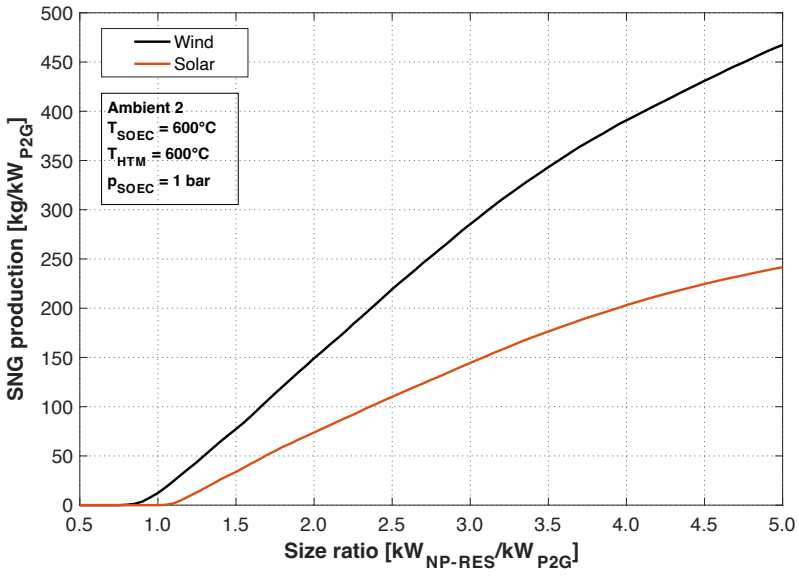

Fig. 5.30. SNG production per unit of installed power, as a function of the size ratio R.

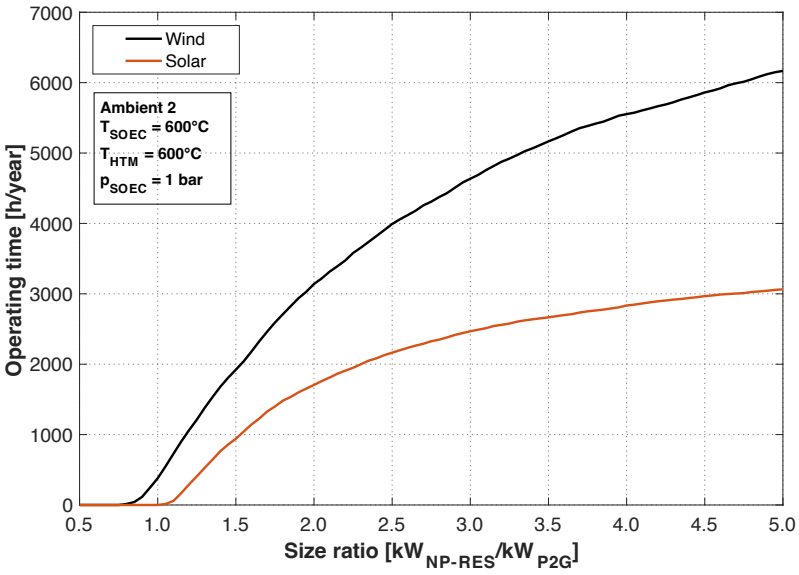

Fig. 5.31. Operating time of the P2G system as a function of the size ratio R.

In Fig. 5.32a, the trends of the $U_{E\,NP-RES}$ factor previously introduced are shown; this factor is defined as:

Eq. 5.2. $$U_{E\,FRNP} = \frac{E_{in\,P2G}}{E_{NP-RES}}$$

This factor represents the share of electrical energy produced by the NP-RES and used by the P2G system: this share is zero at the beginning (P2G system not operative since it is oversized

compared to the renewable generator), then it increases with the increase of the size ratio R, up to a maximum value (equal to about 90 % in the case of wind generation and equal to about 80 % in the case of solar generation) and then it decreases, when the P2G system is undersized. Finally, with the purpose to evaluate the efficiency of the P2G plant as a storage system, it is possible to calculate the utilization and conversion factor of electrical energy, previously defined as:

Eq. 5.3. $$U_{E2F\ NP-RES} = \frac{F_{SNG}}{E_{NP-RES}}$$

This parameter specifies the ability to convert the electric power produced by the NP-RES into fuel and it is affected by the size of the P2G system with respect to the size of the coupled renewable generator. In Fig. 5.32, the trend of $U_{E2F\ NP-RES}$ as a function of the size ratio R is shown. With the exception of the area with R lower than 1, the coupling with both the renewable sources shows an increasing trend of $U_{E2F\ NP-RES}$ up to a maximum point. For the P2G system coupled with a solar source, the maximum value is equal to about 70 % in correspondence of a size ratio of 4, while the P2G system coupled with a wind source shows a maximum value of about 66 % in correspondence of a size ratio equal to 3.7.

For values of R lower than about 1.7, the P2G system coupled with the wind generator shows higher values of $U_{E2F\ NP-RES}$ with respect to the P2G system coupled with a solar generator; when R is greater than 1.7, the situation is the opposite.

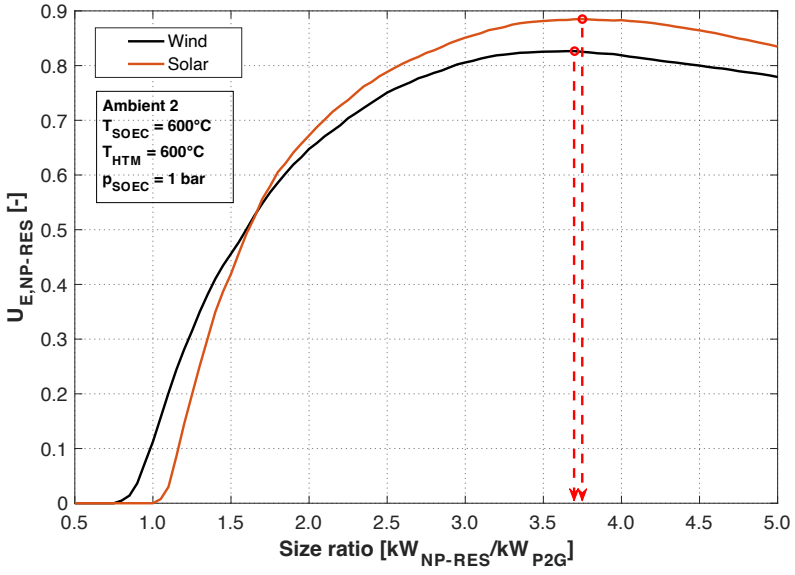

a)

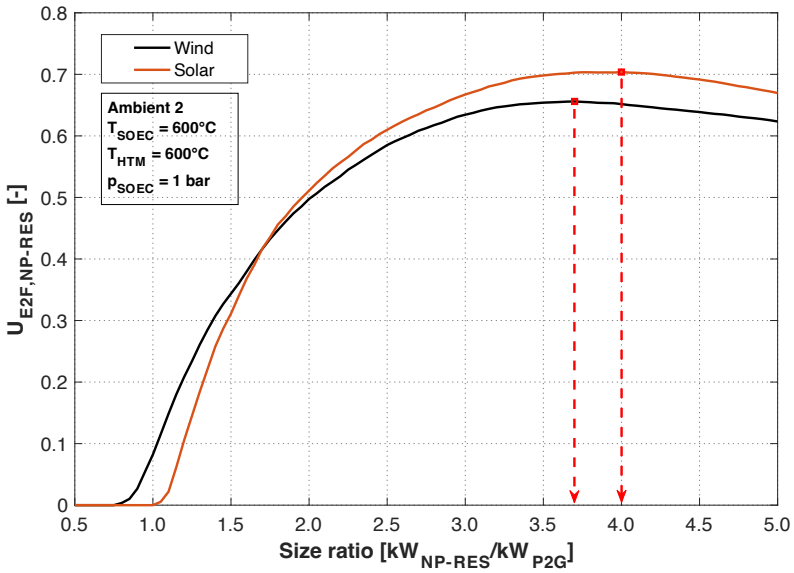

b)

Fig. 5.32. Utilization factors as a function of the size ratio R: a) utilization factor of the NP-RES electric energy; b) utilization and conversion factor electric-to-fuel.

In Tab. 5.4, the values of the main quantities in the point of optimal sizing (point of maximum $U_{E2F\ NP-RES}$), for the two considered renewable sources, are presented.

Instead, in Tab. 5.5 and Tab. 5.6, the results obtained for the four different thermodynamic configurations of the P2G system, respectively, in the case of wind generation with $R = 3.7$ and in the case of solar generation with $R = 4$, are presented. The results show that, with the same renewable source, the energy performance of the P2G system are better in the case of Ambient 2, but with limited differences with respect to the other cases.

Tab. 5.4. Values of the main quantities in the point of optimal sizing, for the two considered renewable sources.

Parameter	**Wind**	**Solar**
Optimal size ratio [$kW_{NP\text{-}RES}/kW_{P2G}$]	3.7	4.0
Electrical energy produced by NP-RES and not used by the P2G system [MWh/kW_{P2G}]	1.2	0.4
SNG production [kg/kW_{P2G}]	363.9	203.2
Operating time [h/year]	5354	2834
$U_{E2F\ NP-RES}$ [-]	0.656	0.704

Tab. 5.5. Annual results for the large-scale dimensionless study in the point of optimal sizing in the case of wind source (R = 3.7 $kW_{NP\text{-}RES}/kW_{P2G}$), for the four considered thermodynamic configurations of the P2G system.

Parameter	Ambient 1	Ambient 2	Pressurized 1	Pressurized 2
P2G operating time - h_{P2G} [h/year]	5354	5354	5241	5255
P2G plant utilization factor - $f_{u\,P2G}$ [%]	61.1	61.1	59.8	60.0
P2G equivalent hours - $h_{eq\,P2G}$ [h]	5623	5623	5444	5465
NP-RES energy available - E_{NP-RES} [MWh/year]	6941	6941	6941	6941
P2G energy input - $E_{in\,P2G}$ [MWh/year]	5731	5736	5727	5728
Energy not used - $E_{Grid/Wasted}$ [MWh/year]	1209	1205	1214	1213
Electricity utilization factor - $U_{E\,NP-RES}$ [%]	82.6	82.6	82.5	82.5
SNG production [t/year]	356	364	318	316
Mean LHV [MJ/kg]	45.2	45.0	48.6	49.1
Electric-to-fuel conversion index - $\eta_{E2F\,P2G}$ [%]	78.0	79.4	75.0	75.2
Total thermal energy externally requested - $Q_{in\,P2G}$ [MWh/year]	219	281	160	245
First law efficiency - $\eta_{I,P2G}$ [%]	75.2	75.7	73.0	72.1
Utilization factor - $U_{E2F\,NP-RES}$ [%]	64.4	65.6	61.9	62.1

Tab. 5.6. Annual results for the large-scale dimensionless study in the point of optimal sizing in the case of solar source (R = 4.0 $kW_{NP\text{-}RES}/kW_{P2G}$), for the four considered thermodynamic configurations of the P2G system.

Parameter	Ambient 1	Ambient 2	Pressurized 1	Pressurized 2
P2G operating time - h_{P2G} [h/year]	2831	2834	2782	2789
P2G plant utilization factor - $f_{u\,P2G}$ [%]	32.3	32.4	31.8	31.8
P2G equivalent hours - $h_{eq\,P2G}$ [h]	3125	3127	3030	3042
NP-RES energy available - E_{NP-RES} [MWh/year]	3612	3612	3612	3612
P2G energy input - $E_{in\,P2G}$ [MWh/year]	3186	3190	3187	3188
Energy not used - $E_{Grid/Wasted}$ [MWh/year]	426	422	424	424
Electricity utilization factor - $U_{E\,NP-RES}$ [%]	88.2	88.3	88.3	88.3
SNG production [t/year]	198	203	177	176
Mean LHV [MJ/kg]	45.2	45.0	48.6	49.1
Electric-to-fuel conversion index - $\eta_{E2F\,P2G}$ [%]	78.0	79.4	75.1	75.2
Total thermal energy externally requested - $Q_{in\,P2G}$ [MWh/year]	116	153	85	134
First law efficiency - $\eta_{I,P2G}$ [%]	75.3	76.0	73.1	72.2
Utilization factor - $U_{E2F\,NP-RES}$ [%]	68.8	70.4	66.2	66.4

5.2.4 – Results: small-scale dimensional study

In this paragraph, the results of the small-scale dimensional study, characterized by the production curve of Fig. 5.26, are presented.

In Fig. 5.33, the trend of the electric energy produced by the wind generator and not used by the P2G system (and then introduced into the electric network or wasted), as a function of the P2G system design size, is shown. In this case, a minimum point is observed, in correspondence of a P2G system design size equal to about 1300 kW; P2G systems with smaller or larger sizes show an increase in the share of electric energy produced by the wind generator and not used by the storage system. The design size of the P2G system in correspondence of the minimum electrical energy introduced into the electric network allows the maximum production of SNG too, as shown in Fig. 5.34; the maximum value of production is equal to about 311 tons of SNG.

In Fig. 5.35, the trend of $U_{E2F\,NP-RES}$ as a function of the P2G system design size is shown; a maximum value of $U_{E2F\,NP-RES}$ equal to about 67 % has been achieved. Finally, the decreasing trend of the operating time as a function of the P2G system design size is shown (Fig. 5.36).

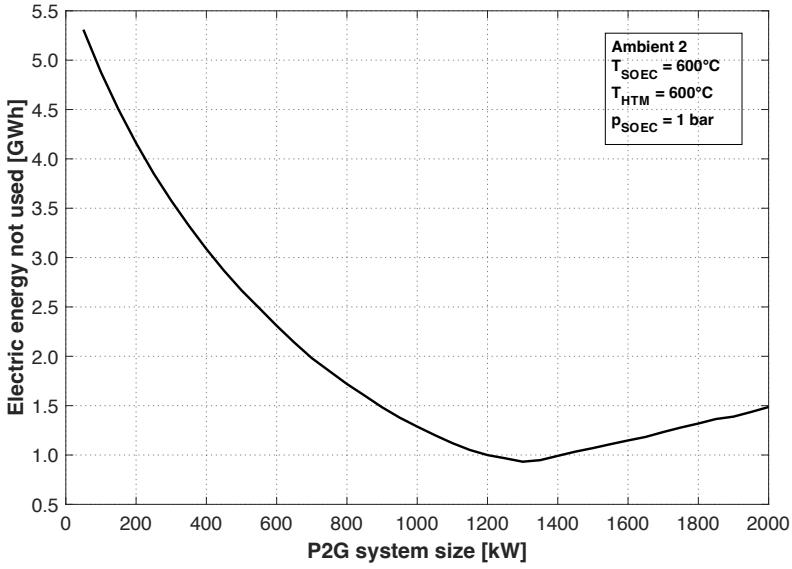

Fig. 5.33. Electric energy produced by the NP-RES and introduced into the electric grid, as a function of the P2G system size.

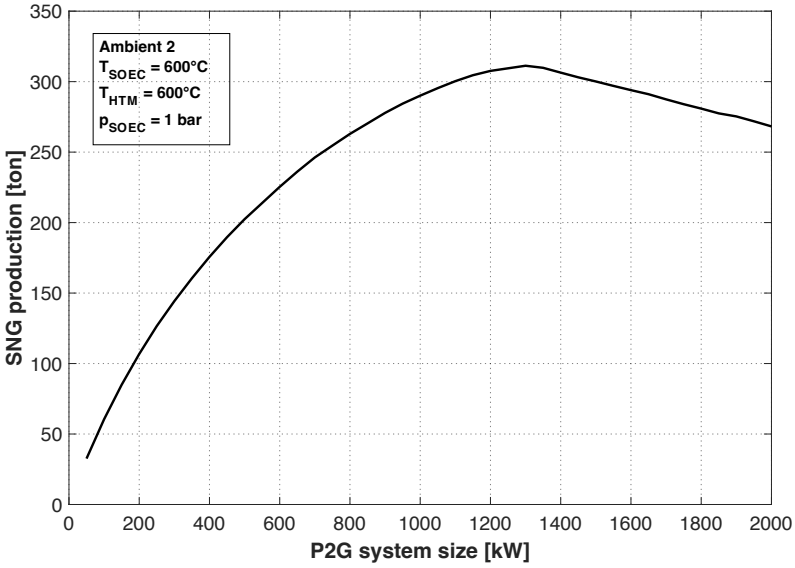

Fig. 5.34. SNG production as a function of the P2G system size.

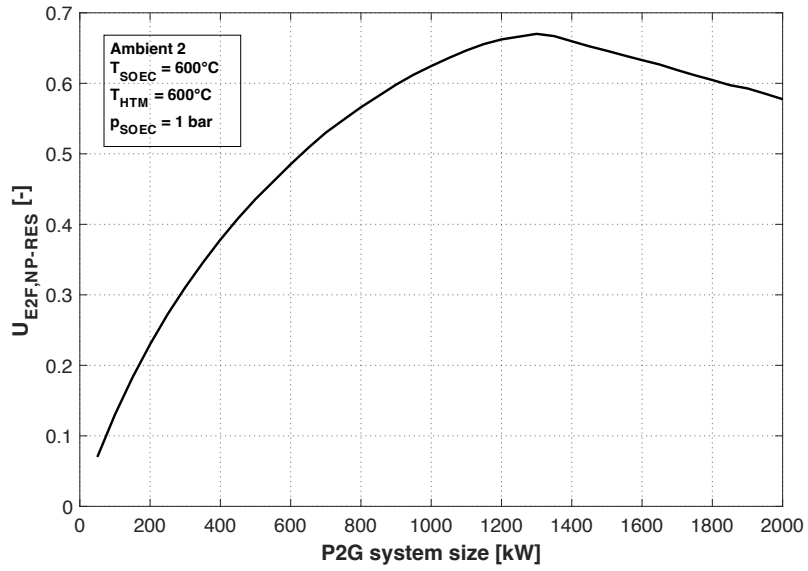

Fig. 5.35. $U_{E2F\ NP-RES}$ as a function of the P2G system size.

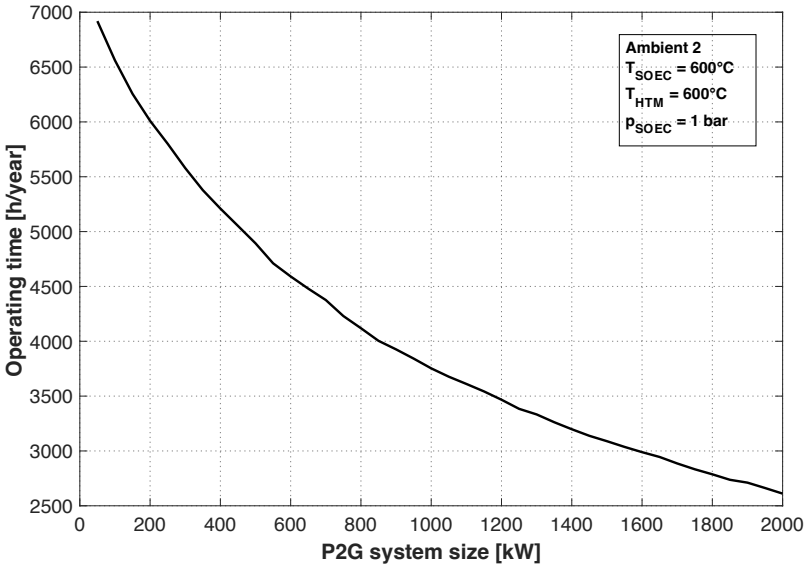

Fig. 5.36. Operating time as a function of the P2G system size.

In this case study, the value of the optimal size ratio R is equal to about 1.5, lower than the values obtained in the previous case study (between 3.5 and 4). This result can be explained by the different monotonic profile of the NP-RES electrical production, if compared to the average profile related to a large territory: in the case of the single NP-RES plant, the number of hours during the year with a production value close to the peak value is greater; a larger size of the P2G system is more advantageous, even if this system operates for fewer hours during the year.

In Tab. 5.7, the main performance parameters for the small-scale dimensional study in the point of optimal sizing of the storage system (1300 kW), for the four consider thermodynamic scenarios, are presented. The corresponding value of the size ratio R between the wind generator and the P2G system is equal to about 1.54 $kW_{NP\text{-}RES}/kW_{P2G}$; the P2G operating time during the year is over 3300 h/year; the electricity utilization factor ($U_{E\ NP-RES}$) is equal to about 84 %, but the utilization factor ($U_{E2F\ NP-RES}$) is in the range of 63 – 67 %, on the basis of the thermodynamic configuration; the most performant configuration is Ambient 2, which is the most performant configuration in the design point too .

Tab. 5.7. Annual results for the small-scale dimensional study in the point of optimal sizing of the storage system (1300 kW), for the four considered thermodynamic configurations of the P2G system.

Parameter	**Ambient 1**	**Ambient 2**	**Pressurized 1**	**Pressurized 2**
P2G operating time - h_{P2G} [h/year]	3332	3333	3332	3332
P2G plant utilization factor - $f_{u\ P2G}$ [%]	38.0	38.1	38.0	38.0
P2G equivalent hours - $h_{eq\ P2G}$ [h]	4783	4783	4635	4651
NP-RES energy available - E_{NP-RES} [MWh/year]	5811	5811	5811	5811
P2G energy input - $E_{in\ P2G}$ [MWh/year]	4875	4879	4876	4875
Energy not used - $E_{Grid/Wasted}$ [MWh/year]	935	932	935	936
Electricity utilization factor - $U_{E\ NP-RES}$ [%]	83.9	84.0	83.9	83.9
SNG production [t/year]	303	311	271	269
Mean LHV [MJ/kg]	45.2	45.0	48.6	49.1
Electric-to-fuel conversion index - $\eta_{E2F\ P2G}$ [%]	78.1	79.8	75.1	75.2
Total thermal energy externally requested - $Q_{in\ P2G}$ [MWh/year]	174	236	125	204
First law efficiency - $\eta_{I,P2G}$ [%]	75.4	76.1	73.2	72.2
Utilization factor - $U_{E2F\ NP-RES}$ [%]	65.5	67.0	63.0	63.1

Chapter 6 – Comparison between hydrogen and synthetic natural gas applications

In this chapter, an innovative comparison between different Power-to-Gas concepts in a microgrid application, considering also Gas-to-Power (G2P) systems and a user demand, is presented. The aim of this section is to compare the behavior of different storage paths when integrated in a real scenario of functioning, with a real renewable production and a real electrical demand. The P2G concepts that have been considered differ on the used energy vector: one line is based on the hydrogen and the other line on the SNG. Firstly, the system has been analyzed from the energetic point of view by means of a developed management strategy. Indeed, setting the electrical demand, the other components' size has been varied in a large range in order to figure out the performance of the overall microgrid on the basis of the different size ratios among the devices.
Then, a decision-making parameter has been defined in order to establish the best solution among the obtained results and then optimize the overall performance. In this section, a novel optimization method has been developed, based on an innovative approach that takes into account the variability of the electricity purchase price.
Finally, in order to generalize the results of the study in a wider context, sensitivity analyses on selected economic parameters have been carried-out. In detail, firstly, the effect of the electricity market cost profile has been considered; in particular, the several profiles considered in the study refer both to historical scenarios and to hypothetical future trends. Then, the impact of the P2G storage system cost has been evaluated; indeed, the operating and maintenance costs have been varied due to the high uncertainty on the price prediction for a technology still in development.
The structure of this section can be summarized as: at first, the considered microgrid, based on different P2G concepts, is introduced; then, the overall process modelling is shown, with a detailed focus on the several sub-sections, and the adopted methodology is presented. Finally, the obtained results are provided and discussed.

6.1 – Microgrid description

In this study, a microgrid based on different P2G concepts has been investigated (see Fig. 6.1). This grid employs a distributed generation based on a Non-Programmable Renewable Energy Source (NP-RES) for the electric power production, that can be represented by wind or photovoltaic generators. This power source is necessary to provide for the electric demand of the load, here represented by the residential power consumption for a group of households, in which also the electric car demands are included. In addition, in order to completely meet

the electrical demand when the renewable generation is not sufficient, the microgrid system is connected to the external electrical grid.

The most innovative sub-section of the microgrid is represented by the P2G section, here depicted in two different concepts on the basis of the energy vector: hydrogen and SNG. This sub-section is integrated with a storage and a G2P system (fuel cell for hydrogen and an engine for the SNG) for the electricity production; due to the renewables' intermittency, when the renewable production exceeds the electrical demand, the surplus is employed by the P2G system to convert reactants (water and, in the case of the SNG, also carbon dioxide) into an energy vector (H_2 or SNG), which is then stored in a tank for later use. When the renewable production is not sufficient to meet the electrical demand, the G2P system can operate as a back-up power source to integrate the electrical production.

The whole model of the presented microgrid has been developed on MATLAB™ environment. In more detail, for the NP-RES production and for the G2P systems, experimental data have been used, while, regarding the electrical demand, realistic patterns of residential power consumption, including electric car demands and validated with metered data, have been employed. In addition, the P2G storage systems have been modelled through the semi-empirical model developed in the previous chapter (see Chapter 3 – The Power-to-Gas model), calibrated by experimental data. The modelling of the several sections will be described in the following paragraph.

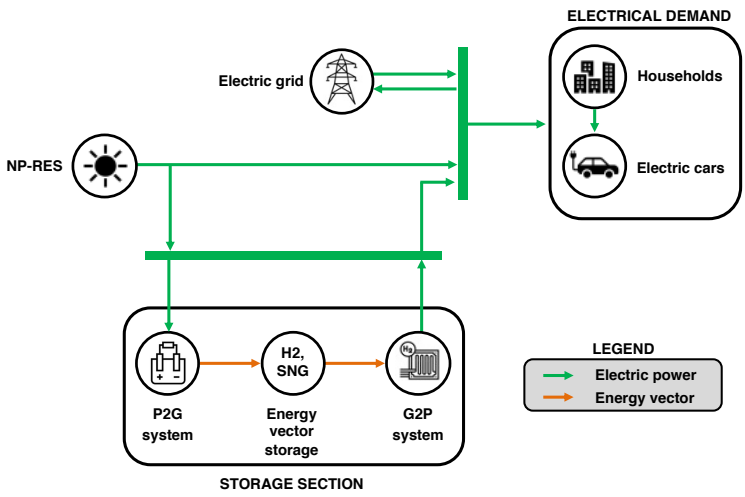

Fig. 6.1. Schematic of the investigated microgrid based on the two considered P2G concepts (H_2 and SNG).

6.2 - Process modelling

6.2.1 - Renewable production

The characteristics of the renewable generation are fundamental in order to assess the microgrid performance. In this study, reference is made to the experimental data from the

Italian Authority for the national electric grid (TERNA [59]), referring to the wind and photovoltaic generation for year 2020 on the whole Italian territory. Indeed, in order to meet the electrical demand, a mixed generation by means of different renewable sources has been considered more reasonable than a single-source production.

The electrical production data have a resolution time equal to 1 hour and they have been normalized with respect to the peak value (see Fig. 6.2) in order to evaluate different generator sizes in the optimization analysis of the whole microgrid; as a consequence, during the optimization the peak value of the renewable production has been shifted in a large range, as it will be described in the next paragraph.

The normalized mixed production (wind and photovoltaic) used in the analysis as electrical input of the microgrid, is shown in Fig. 6.3.

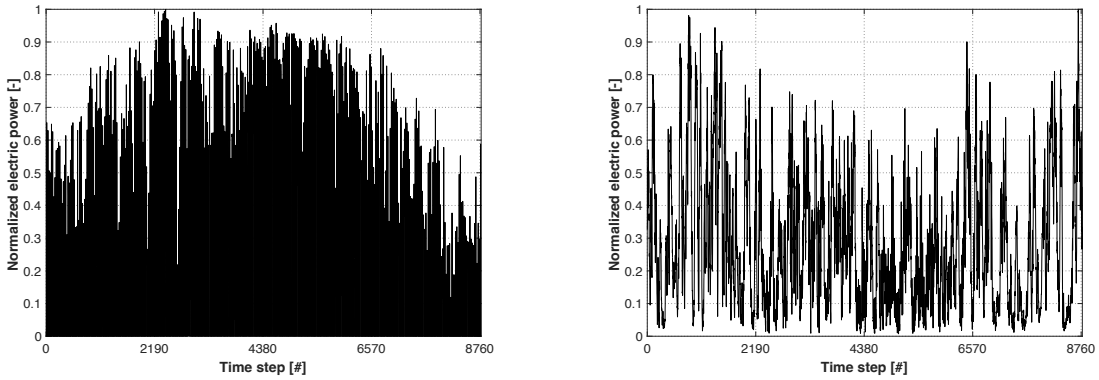

Fig. 6.2. Normalized power production in the year 2020 on the whole Italian territory: a) solar production; b) wind production **[59]**.

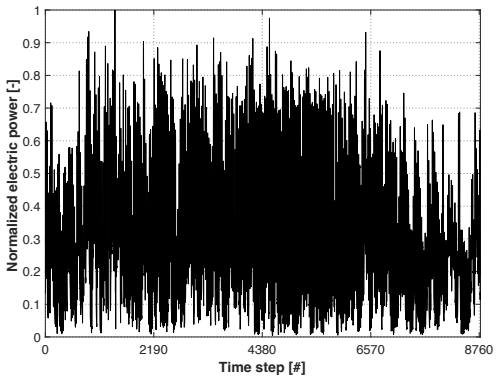

Fig. 6.3. Normalized power production in the year 2020 on the whole Italian territory, referring to a mixed renewable production (wind and photovoltaic) **[59]**.

6.2.2 - Electrical demand

The overall electric power demand for a group of households has been simulated by means of a highly detailed modelling of residential power demand, including Plug-in Electric Vehicles (PEV) charging. Indeed, PEV charging will impact the electric power system in two

main ways. First, the additional demand for recharging PEV batteries, which is now mainly supplied at residential households when vehicles are parked and recharged overnight [62], will impact the overall power demand and add complexity to managing electric power generation, transmission and distribution. Second, PEVs can be seen both as a distributed storage technology or as flexible loads acting like a virtual power plant. Coordinated PEV charging and vehicle-to-grid (V2G) applications hold promise in integrated smart grids as opportunities to facilitate the integration of non-dispatchable renewable energy sources and, in general, improve the operation and reliability of the electric power system. As such, modelling of the impacts of PEV charging behaviour is required to anticipate future needs.

To address these needs, a highly resolved modelling of residential power demand and PEV use – based on a bottom-up approach that quantifies consumer energy-use behaviour and real-world vehicle use – to better assess the aggregate and local impact of uncoordinated PEV charging, has been adopted (by means of the model presented in [63]).

In particular, residential and personal transportation energy needs are modelled in a single framework to capture the entire energy footprint of an individual household, including all appliances, heating, ventilation and air conditioning systems, in-home charging of PEVs and any other electricity needs. These models generate highly resolved electricity consumption profiles (10 min resolution) for individual households and account for in-home recharging of PEVs, simulating real-world vehicle usage.

Residential power demand profiles are generated using the proposed modelling, which produces realistic patterns of residential power consumption, validated against metered data.

To estimate the aggregate impact of uncoordinated in-home PEV charging on the total residential demand, a simulation including 200 residential households (see Fig. 6.4) in the Midwest region of the United States is performed. Characteristics and composition of these households, which include 502 individuals and 348 passenger vehicles, are taken from a representative sample of housing units included in the Residential Energy Consumption Survey [64].

The selected households vary in size and number of occupants and the aggregate power demand of these households (Fig. 6.5) shows a peak equal to about 550 kW and an annual demand equal to about 2 GWh.

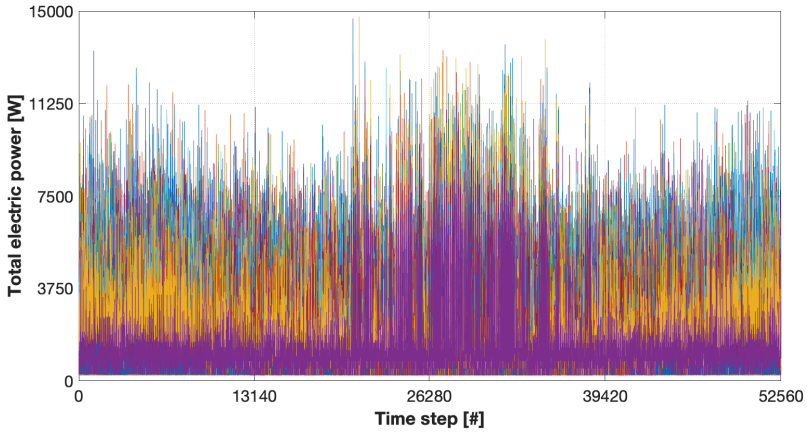

Fig. 6.4. Electric demand for the 200 considered households [63].

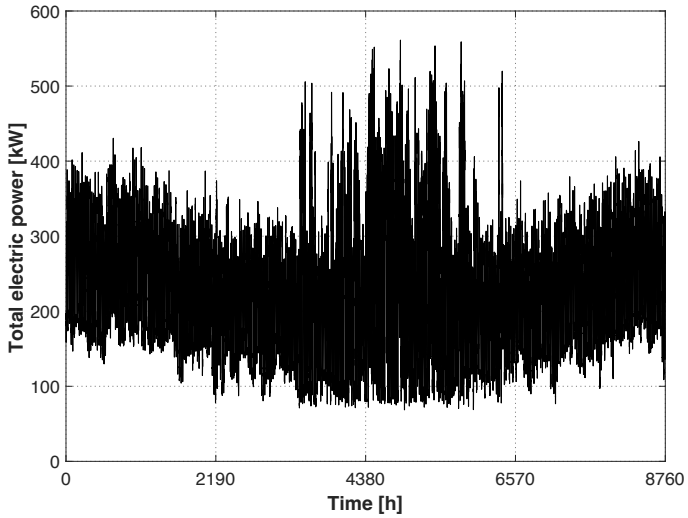

Fig. 6.5. Aggregated electrical demand for household consumers [63].

6.2.3 - Power-to-Gas systems

The Power-to-Gas concepts

The P2G systems evaluated in this study are illustrated in Fig. 6.6. The two considered concepts rely on the developed numerical model (see Chapter 3 – The Power-to-Gas model) and they can be identified on the basis of the final product: hydrogen (Power-to-Hydrogen, PtH_2) and SNG (Power-to-Methane, PtM).

In the case of PtH_2, the CO_2 supply is not considered in the process, while for the PtM process it is directly fed to the Solid Oxide Electrolyzer (SOE) by mixing with the water steam. In the latter case, the hydrogen-rich blend at the outlet of the SOE represents the feed to the methanation reactions; in the concept of this study, the methanation section is divided into an experimental methanator (based on experimental data [27] - [28]) and a conventional methanation section, included in order to improve the methane content in the outlet stream.

The product of this section (a blend of H_2, CO, CO_2, CH_4 and H_2O) is then cooled and separated from the residual water in the upgrading section to obtain a high methane purity. In the case of PtH_2, the stream at the outlet of the SOE bypass the methanation sections and it goes directly into the upgrading section. More details on the processes' concept can be found in Chapter 3 – The Power-to-Gas model.

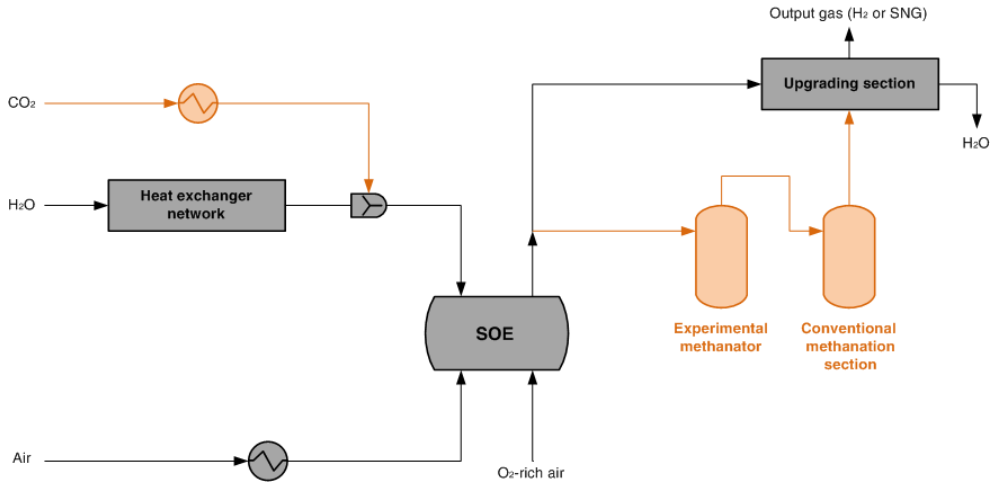

Fig. 6.6. Schematic of the SOE-based P2G systems: black lines for the PtH_2 option and orange lines for the PtM option.

Developed numerical model and assumptions

A numerical model has been developed and calibrated with experimental data in order to predict the performance in off-design conditions; indeed, in order to evaluate the design and part-load thermodynamic performance of the P2G processes, the two considered concepts have been modelled in an integrated tool environment. In more detail, the model has been introduced and described in Chapter 3 – The Power-to-Gas model and it is able to simulate the behaviour of the P2G system in off-design conditions in both the considered concepts.

For the model input, reference is made to the tests performed on a 6-cell SOE short stack [65] - [66] by the Technical Research Center of Finland. The stack has been tested at 700/750/800°C and 1 bar with the anode swept by an air flow of 51.4 sccm/cm² and a cathode feed of 12 sccm/cm². The reactant feed compositions (H_2/H_2O/CO_2, vol. %) are 10/90/00 for the steam electrolysis (SE) tests, and 10/80/10, 10/65/25 and 10/45/45 for the co-electrolysis (CE) tests (both tests have been performed with a set operating pressure of 1 bar). The experimental polarization curves are shown in Fig. 6.7.

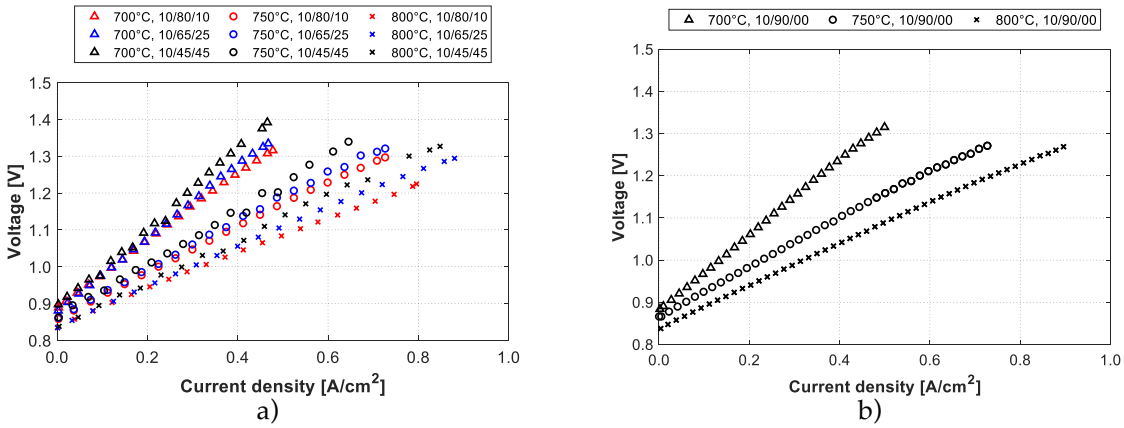

Fig. 6.7. Experimental polarization curves obtained by means of the tests performed by the Technical Research Center of Finland on a 6-cell SOE short stack [65] - [66] operated in: a) co-electrolysis mode; b) electrolysis mode.

In order to calibrate the developed P2G model, these experimental data have been used as input of the numerical model. With this purpose, a comparison between the developed numerical model and a quasi-2D model (1D + 1D) developed by Wang et al. [66] has been proposed; the latter model has been previously calibrated and validated with the same experimental data of this study. With this purpose, for both the models an operating temperature of 700 °C and an operating pressure of 1 bar have been set; the comparison is shown in Fig. 6.8. Good agreement has been reached for all experimental and prediction points under all considered conditions. For tests at this temperature and relatively small and large current density, the prediction accuracy reduces but remains at high level. Nevertheless, it can be concluded that the calibrated model is satisfactory for the purposes of this study.

Regarding the settings of the P2G systems, the operating temperature of the SOE has been set at 700 °C for both the P2G concepts, while for the methanation sections of the PtM configuration it has been considered an operating temperature of 450 °C for the experimental methanator and 200 °C for the conventional section; in both cases, the operating pressure of the whole process has been set at 1 bar. Starting from the SOE design electric power input and accounting also for the compression and auxiliaries' consumption, the P2G off-design operating range has been assumed between – 50 % and + 50 % of the design inlet power.

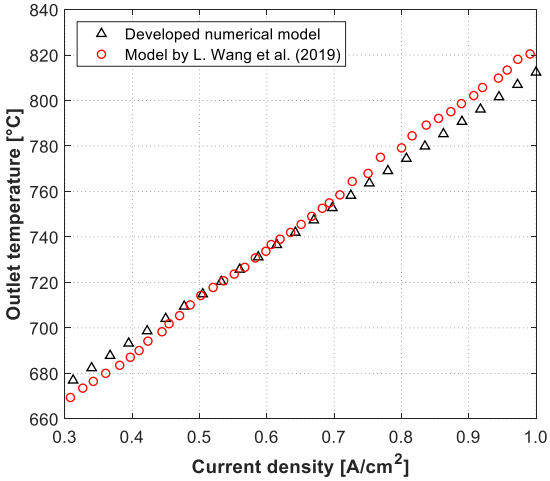

Fig. 6.8. Comparison between the developed numerical model (black triangles) and the quasi-2D (1D+1D) model developed by Wang et al. [66] (red circles), on the evaluation of the SOEC outlet temperature as a function of the current density.

6.2.4 – Gas-to-Power systems

In this study, on the basis of the energy vector of the considered P2G system, a specific G2P system has been taken into account; indeed, two completely different production chains have been evaluated in order to compare different P2G concepts.

If the final product of the P2G system is the SNG, then an engine has been considered. In more detail, the efficiency curve as a function of the load (Fig. 6.9a) refers to the engine Wartsila 6L32 [67], that shows a maximum efficiency of about 42 % for loads higher than the 80 %. Instead, if the final product of the P2G system is the hydrogen, then a fuel cell has been considered. In particular, the used experimental data refer to a Proton Exchange Membrane Fuel Cell (PEMFC) described by Guo et al. in [68], consisting in a commercial module; as shown in Fig. 6.9b, the PEMFC presents a maximum efficiency value of about 62 % at the 20 % of the load.

For the engine a technical minimum of 20 % of the load has been considered, while for the PEMFC this value has been set at 15 %, on the basis of the manufacturer datasheets.

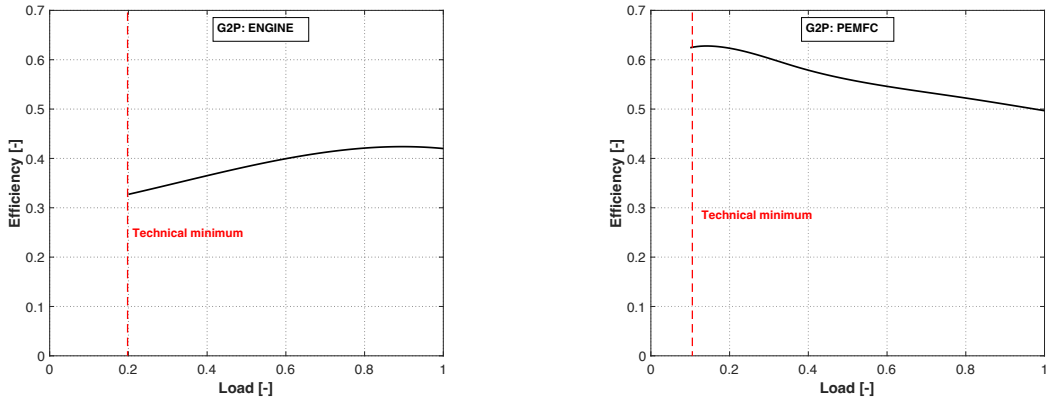

Fig. 6.9. Electrical efficiency as a function of the load for the considered G2P systems: a) engine [67]; b) fuel cell [68].

6.3 - Methodology

In this study, a multi-variable optimization has been carried-out in order to evaluate the best configuration of the overall system. In the first place, an analysis of the whole system, considering variable size ranges for the renewable production, the P2G and the G2P systems has been performed; this first analysis has been necessary in order to figure out the behaviour of the overall system from the energetic point of view and it represents the starting point of the optimization. Indeed, after obtained the performance results of the system, a decision-making criterion is necessary to establish the best configuration; following this way, an optimization based on the electricity price for end-costumers has been carried-out. Finally, in order to generalize the results of the study, sensitivity analyses on selected economic parameters have been carried-out. In particular, firstly, the effect of the electricity market cost profile has been considered, referring both to historical scenarios and to hypothetical future trends. Then, the impact of the P2G storage system cost has been evaluated.

6.3.1 - Multi-variable analysis

In order to analyse the system behaviour from the energetic point of view, a multi-variable analysis has been carried out. In more detail, in this preparatory analysis a large number of solutions has been considered, varying the size of the renewable production and of the P2G and G2P systems. Thus, in order to apply the methodology of this study to a real case study, the local demand has been set to the one shown previously. Instead, the other systems size has been varied in a large range, covering all the solutions from 0 to 3000 kW (the upper limit of the range has been considered reasonable with respect to the user demand size – maximum peak value of about 550 kW – in order to not exclude possible effects related to the size).

In order to evaluate the overall system design, a power management strategy has been proposed to efficiently operate the system and improve the utilization of renewable energy. The aim of the strategy is to ensure that the user demand in the considered microgrid is always met; meanwhile, G2P systems, P2G systems and storages could always work within acceptable operating ranges. The full schematic of the strategy is shown in Fig. 6.10, which presents in detail the dispatch of multiple energy flows in response to renewable power and user demand variation. The operation principles of the power management strategy can be summarized as below:

a) the user demand is met, in order of priority, using the renewable generation; if there is power surplus, it is used by the P2G system for the energy vector production;
b) the residual demand is supplied by the G2P systems;
c) the power from the electric grid is used in order to completely meet the user demand.

These principles maximize the use of the available renewable power, with the G2P system used as a back-up power source to integrate the electricity production when renewable power is not enough. Grid supply is included to completely meet the user demand.
On the basis of the operation principles, the detailed procedure of the power management strategy is described as below:

1) loading of the boundary conditions (renewable production, electrical demand and P2G and G2P systems set-point data) in the code at time t;

2) in the modules of the P2G and G2P systems, the operating limits are evaluated on the basis of the step size and saved;

3) comparing the renewable power to the user demand at time t.

3.1) Renewable power is sufficient to meet the user demand; if the renewable production is higher with respect to the demand, then the surplus is evaluated.

3.1.1) The surplus is less than the lower limit of the P2G system range, then the surplus power is wasted (or introduced into the electric grid).

3.1.2) The surplus is within the operating range of the P2G system, then the surplus is supplied to the latter.

3.1.3) The surplus is higher than the upper limit of the P2G system range, then the P2G system is operated at maximum and the power difference is wasted (or introduced into the electric grid).

3.2) Renewable power is not sufficient to meet the user demand, then the load difference is calculated; evaluating if the storage is sufficient to fill the load difference.

3.2.1) The storage is sufficient, then evaluate if the load difference is within the operating range of the G2P system.

3.2.1a) The required power is lower than the technical minimum of the G2P system, then the renewable production is integrated by the electrical grid.

3.2.1b) The required power is within the operating range of the G2P system, then the renewable production is integrated by the G2P system.

3.2.1c) The required power is higher than the maximum load of the G2P system, then the renewable production is integrated by the electrical grid.

3.2.2) The storage is not sufficient, then the renewable production is integrated by the electrical grid.

4) Calculating the syngas flows at time t and updating the amount of syngas in the storage.

5) Operation of the system at time t is completed, import design parameters and update the data to time $t + 1$; return to Step 1) and repeat the operations.

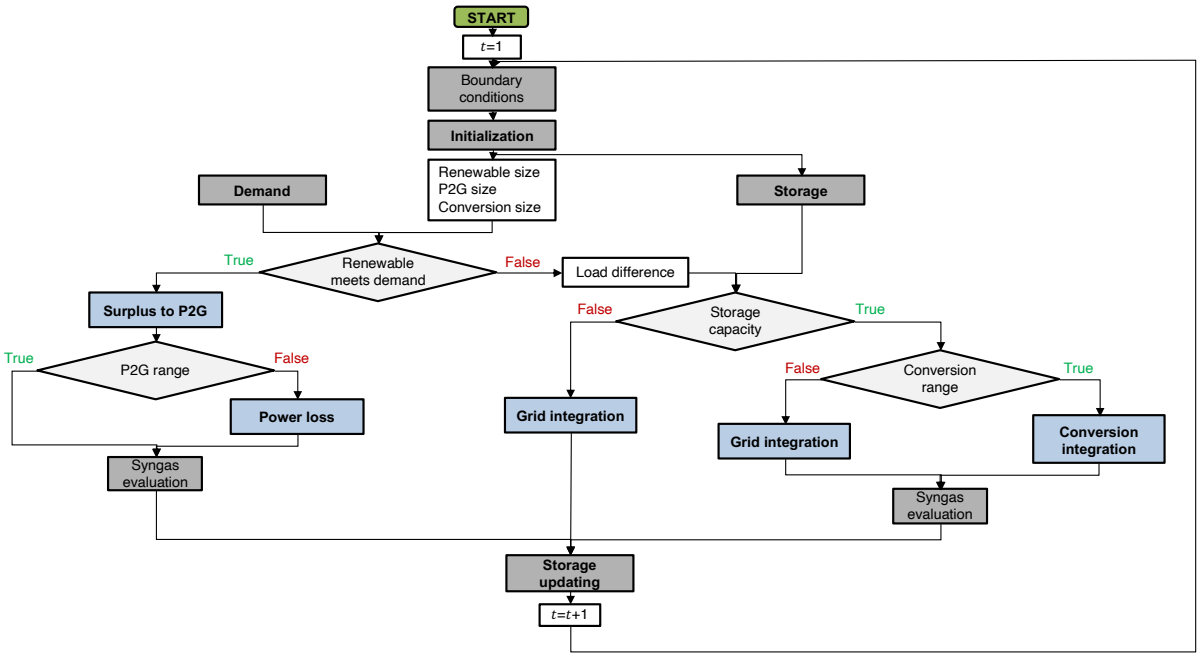

Fig. 6.10. Flowchart of the developed power management strategy.

6.3.2 - Optimization

Once the behavior of the system has been analyzed in a large range of solutions, in order to determine the best configuration, an optimization analysis has been performed. In more detail, the optimization is based on an innovative approach that takes into account the variability of the electricity purchase price. Indeed, in every hour of the year, the electricity purchase price for end-customers is given by the average of zonal prices in the Day-Ahead

Market (venue for the trading of electricity supply offers and demand bids for each hour of the next day), weighted for total purchases. Thus, starting from the electricity price, the overall system has been optimized by means of the evaluation of the revenues and of the costs; the resulting aim is then the maximization of the profit (P) that can be expressed as:

Eq. 6.1. $$P = R - C_{O\&M} - C_{E,grid}$$

where, R [€/year] is the revenue, $C_{O\&M}$ [€/year] is the cost related to the operation and maintenance of the overall system during the year and $C_{E,grid}$ [€/year] is the cost of the electricity purchased by the grid during the year.
Moreover, single terms of the equation can be further specified as:

Eq. 6.2. $$R = \sum_{t=1}^{T} P_{produced,t} \cdot E_{price,t}$$

Eq. 6.3. $$C_{E,grid=} \sum_{t=1}^{T} P_{grid,t} \cdot E_{price,t}$$

Eq. 6.4. $$C_{O\&M} = O\&M_{Renewable} + O\&M_{P2G} + O\&M_{Conversion}$$

where, $P_{produced,t}$ [kW] is the electric power produced by the hybrid system (renewable + G2P system) in the time t and used to meet the demand, $P_{grid,t}$ [kW] is the electric power integrated by the grid in the time t, $E_{price,t}$ [€/kW] is the electricity price in the time t, while the operation and maintenance costs have been divided among the renewable production ($O\&M_{Renewable}$), the P2G system ($O\&M_{P2G}$) and the conversion system ($O\&M_{Conversion}$). In the carried-out analysis a time horizon (T) of one year has been considered.
In this study, regarding the electricity price, reference has been made to the electricity purchase price for end-customers in Italy for the year 2020 (data from the Italian Authority for the electricity market – GME [69]), shown in Fig. 6.11. Instead, regarding the costs, the used data have been selected from the state-of-the-art of the considered technologies and they are shown in Tab. 6.1.

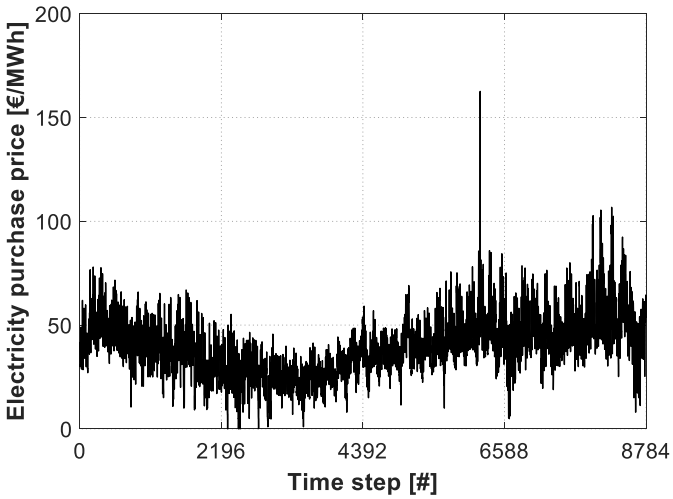

Fig. 6.11. Electricity purchase price for end-customers in Italy for the year 2020 [69].

Tab. 6.1. Operational and maintenance costs per unit of installed power size for the considered technologies.

	Cost [€/kW$_{installed}$/year]
$O\&M_{Renewable}$	10.00 [70]
$O\&M_{P2G}$	84.00 [16]
$O\&M_{G2P,engine}$	9.75 [71]
$O\&M_{G2P,fc}$	39.00 [71]

6.3.3 - Sensitivity analysis

On the basis of the settings and the above assumptions, a sensitivity analysis has been carried-out in order to evaluate the impact of different input parameters on the economic performance of the overall system.

In more detail, firstly, a parametric study acting on the electricity price profile has been considered. Indeed, for this specific analysis, several electricity price profiles have been selected, referring both to actual data in the Italian context and to future trends. At first, reference has been made to the values of electricity purchase price in the last 6 years in Italy (2015 - 2020, see Fig. 6.12); the used data refer to the managing authority of Italian electric markets [69] and they are presented in Fig. 6.13a. These profiles show several differences in the behavior during the year, with peaks of different magnitudes placed in different points in the time period. The minimum values are equal to about 5 €/MWh, while peaks are higher than 150 €/MWh. These extreme values are uncommon during the year; instead, the hourly electricity purchase price varies daily, with variations in the range of 20 - 40 €/MWh. In addition, also the mean electricity price results different for the several years (see Fig. 6.13b), varying from a minimum of 38.92 €/MWh for year 2020 to a maximum of 61.31 €/MWh for year 2018.

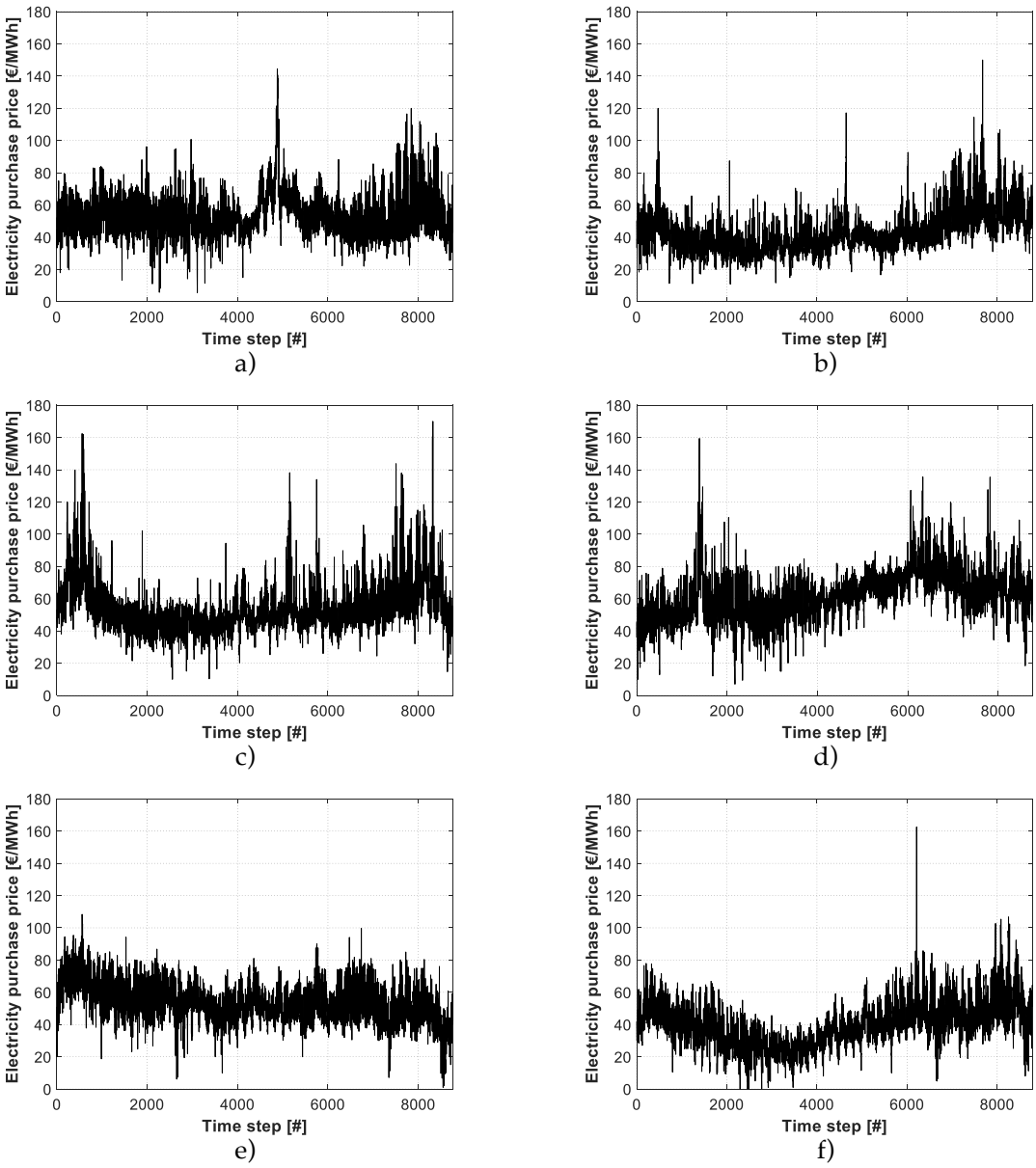

Fig. 6.12. Electricity purchase price variation for end-customers in Italy for the considered years [69]: a) 2015; b) 2016; c) 2017; d) 2018; e) 2019; f) 2020.

Then, in order to generalize the results of the parametric analysis, hypothetical future trends of the electricity purchase price have been taken into account. In particular, considering the monthly mean price trend during the years 2020 - 21 (see Fig. 6.14 [69]), an increasing trend of the values in the last year - at the moment of the thesis writing – is observed, with an annual mean value of about 125 €/MWh. Therefore, three values have been assumed in the analysis, respectively equal to 100 €/MWh, 150 €/MWh and 200 €/MWh; these values can be associated with three possible future scenarios in agreement with the current trend. For the sake of simplicity, in these additional scenarios, the selected electricity price has been assumed as constant during the year of operation.

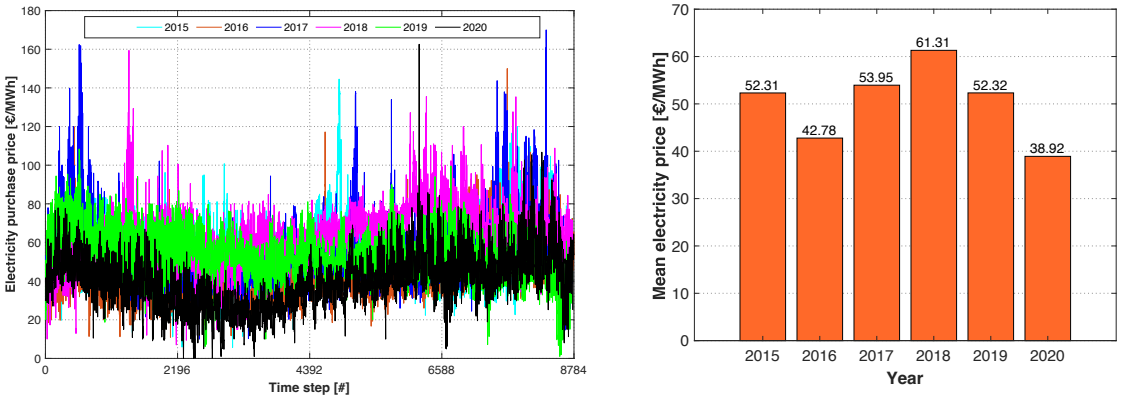

a) b)

Fig. 6.13. Electricity purchase price for end-customers in the years 2015 - 2020 in Italy [69].

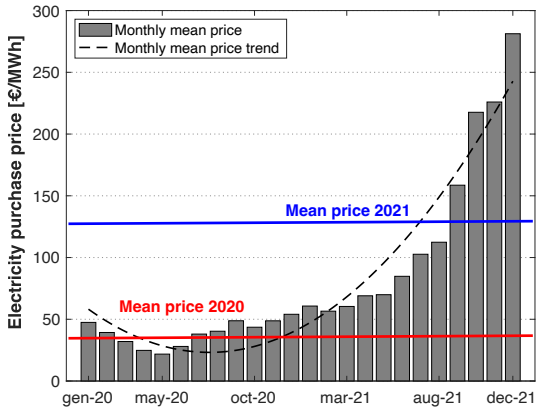

Fig. 6.14. Monthly mean price trend during the years 2020 – 21 [69].

Finally, a further sensitivity analysis, acting on the operating costs, has been carried-out. In particular, the operating and maintenance cost of the P2G system ($O\&M_{P2G}$), which represents the main factor of cost uncertainty, has been varied. In this additional study, a range of values for $O\&M_{P2G}$ has been explored, varying between 84 €/kW$_{P2G}$ (reference data) and 17 €/kW$_{P2G}$ (scenario of a future reduction equal to 80 % of the reference value, in line with the expected costs according to a recent roadmap [5]).

6.4 - Results and discussion

In this section, the results of the carried-out analyses are presented. In more detail, at first the results of the multi-variable analysis are shown, based on the developed management strategy. Then, the obtained results have been optimized on the basis of the variability of the electricity price cost for end-customers. Finally, in order to figure out the effect of specific parameters on the optimization, the results of the sensitivity analysis are presented.

6.4.1 - Multi-variable analysis results

Performance parameters

In order to evaluate and compare the performance of the two considered concepts, several parameters have been considered.

Firstly, the systems have been assessed from the point of view of the energy performance. The first parameter to consider is the energy produced by the hybrid system (renewable generator + G2P system) that is used in order to meet the demand (indicated as E_{hybrid}); this parameter can be considered as the net energy produced by the hybrid system (since the losses are not included).

Related to this parameter, it is the energy supplied by the grid (E_{grid}), given by the difference between the electric demand (E_{demand}) and the production of the hybrid system to meet the demand (E_{hybrid}):

Eq. 6.5. $$E_{grid} = E_{demand} - E_{hybrid}$$

In addition, in order to complete the evaluation of the systems from the energetic point of view, the energy losses have been included too (E_{losses}).

Then, due to the aim to use the produced SNG/H_2 in order to meet the demand, a parameter concerning the productivity of the P2G system has been taken into account; this parameter is the annual mass production of SNG/H_2 by the different P2G system concepts.

Finally, it is possible to characterize the P2G system in terms of plant operating time during the year of operation, in order to assess the operating time (h_{P2G}) and the periods of inactivity.

Results

The results of the introductory multi-variable analysis are shown from Fig. 6.15 to Fig. 6.19, for both the systems based on different P2G concepts. In order to present the results of this section, a G2P size equal to 1000 kW has been set for the figures, otherwise the surfaces would be overlapped. In more detail, in Fig. 6.15 the electric energy produced by the hybrid system (renewable production + G2P system) and used to meet the demand is presented. For both the systems, the production is more affected by the renewable size with respect to the P2G size, since the higher the renewable size, the higher is the possibility to supply the user and then meet the demand. Indeed, for renewable sizes higher than about 1500 kW, the hybrid system is able to completely meet the demand during the year (equal to about 2 GWh) with a negligible integration by the grid; comparing the two P2G concepts, the hydrogen system (Fig. 6.15a) is able to meet the overall demand with renewable sizes lower with respect to the SNG system (Fig. 6.15b), due to the higher efficiency in the syngas production (the hydrogen concept consists of fewer steps – and lower losses – with respect to the SNG concept). The

energy supplied by the electric grid, presented in Fig. 6.16, is affected by the previous results. In this case, the results are quite the opposite: the energy supplied by the grid increases as the renewable size decreases. Indeed, with small sizes of the renewable source the microgrid is not able to meet the demand, since at many times throughout the year the electric production is lower with respect to the demand and the main solution to the user needs is the grid integration. Also in this case, for both the systems (Fig. 6.16a hydrogen, Fig. 6.16b SNG) the energy supplied by the grid is less affected by the P2G size and the hydrogen system shows a higher slope of the surface with respect to the SNG system for small renewable sizes. Regarding the energy wasted by the microgrid, shown in Fig. 6.17, the trend is influenced by the combination of the renewable and the P2G sizes. This parameter shows a peak of about 5 kWh for large renewable productions and small P2G systems: in this case, the renewable source is able to meet the user demand with a large energy surplus in addition, that the P2G system cannot use due to the small operating range. Then, for renewable/P2G size ratios in the range 4 - 5, there is a minimum in the energy wasted: this is the optimum correlation between energy surplus from renewable and the P2G operating range. For large P2G systems, the energy wasted by the microgrid increases since the lower limit of the P2G operating range is higher with respect to the energy surplus given by the renewable source. In Fig. 6.18, the production for both the systems (of hydrogen and SNG, respectively) is presented. In this case, the production is a trade-off between the renewable size and the P2G size, showing a maximum, for both the systems, for large renewable productions and P2G systems of about 1000 kW: for the hydrogen system (Fig. 6.18a) the maximum production is equal to about 420 ton/year, while for the SNG system (Fig. 6.18b) the production is lower and equal to about 270 ton/year. Finally, regarding the P2G system operating time (Fig. 6.19), for both the systems the maximum value is obtained by a trade-off between the renewable generator size and the P2G system size: small P2G systems coupled with large renewable generators are able to operate large periods during the year.

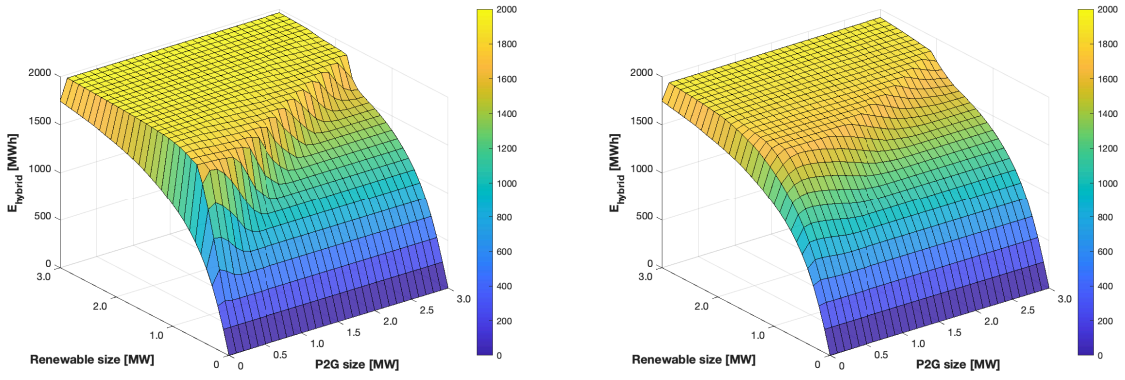

Fig. 6.15. Electric energy produced by the hybrid system (renewable production + G2P system) and used to meet the demand for a set size of the G2P system (1000 kW): a) hydrogen system; b) SNG system.

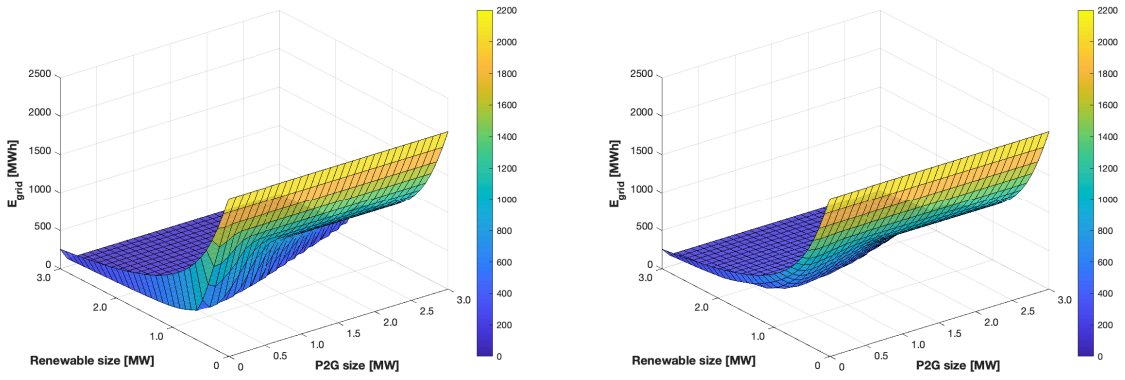

a) b)

Fig. 6.16. Energy supplied by the grid for a set size of the G2P system (1000 kW): a) hydrogen system; b) SNG system.

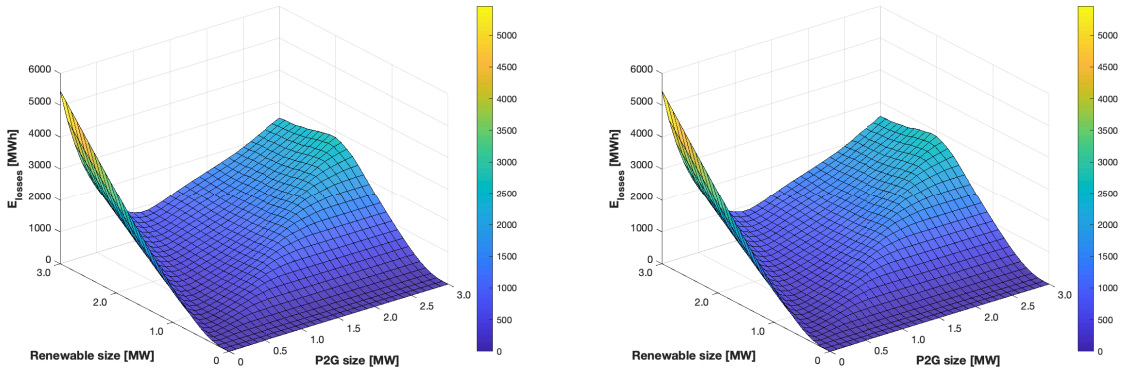

a) b)

Fig. 6.17. Electric energy wasted and then not used by the microgrid for a set size of the G2P system (1000 kW): a) hydrogen system; b) SNG system.

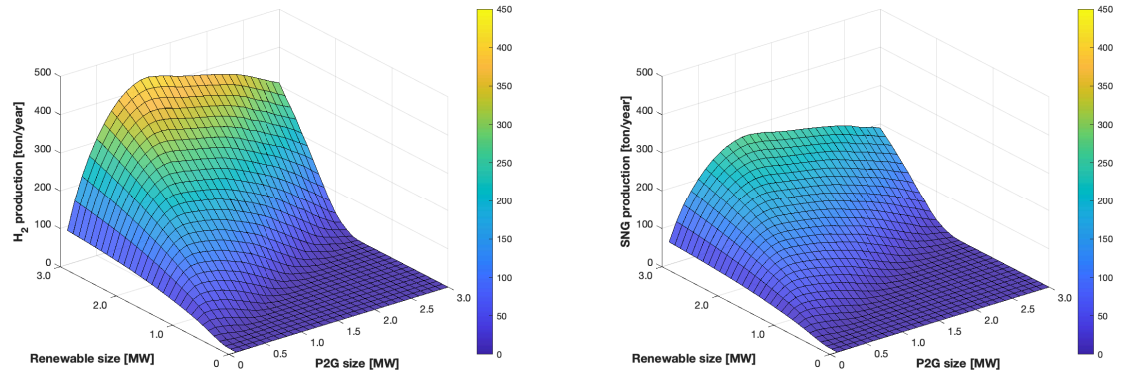

a) b)

Fig. 6.18. Syngas production for a set size of the G2P system (1000 kW): a) hydrogen system; b) SNG system.

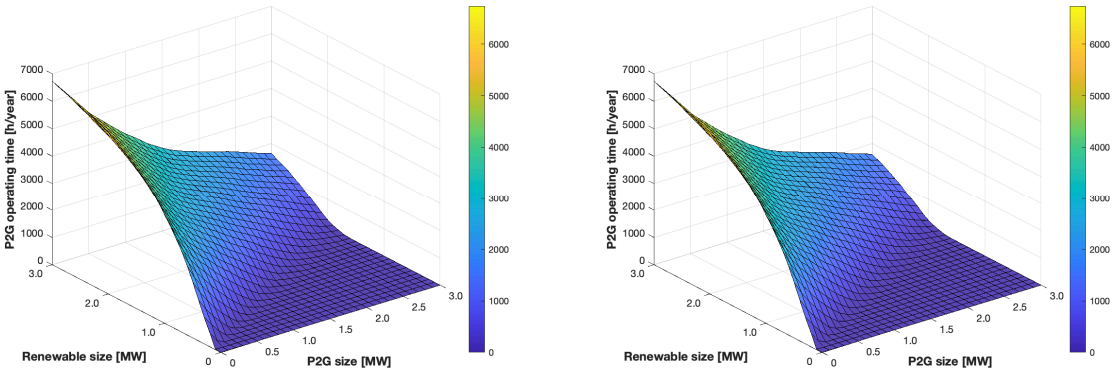

a) b)

Fig. 6.19. Operating time of the P2G system for a set size of the G2P system (1000 kW): a) hydrogen system; b) SNG system.

6.4.2 - Optimization results

In Fig. 6.20, the results of the optimization analysis are shown for the P2G concepts. In this case, in order to present the results of this section, a G2P size equal to the optimum one (400 kW for the hydrogen system and 300 kW for the SNG system) has been set for the figures.

The profit results possible only for a few combinations of renewable/P2G sizes, due to the high costs to be incurred during the year. For the hydrogen system the maximum achievable profit is equal to about 43000 €/year for ratios of size around 1300/100/400 kW (renewable size/P2G size/G2P size); for the SNG system the profit is in line with the hydrogen system, for an optimum configuration of 2400/100/300 kW. Compared to the renewable generator size (the storage and the G2P system sizes are similar for both the concepts), the maximum achievable profit is equal to about 33 €/$kW_{NP\text{-}RES}$·year for the hydrogen concept and equal to about 18 €/$kW_{NP\text{-}RES}$·year for the SNG concept. From these results it's highlighted that, in order to achieve the maximum profit from the presented microgrid, the renewable production must be highly oversized with respect to both the P2G system and the G2P system; in particular, the P2G size, with this approach, must be very small if compared to the renewable source, due to the high costs related to this technology not yet commercial (see Tab. 6.1).

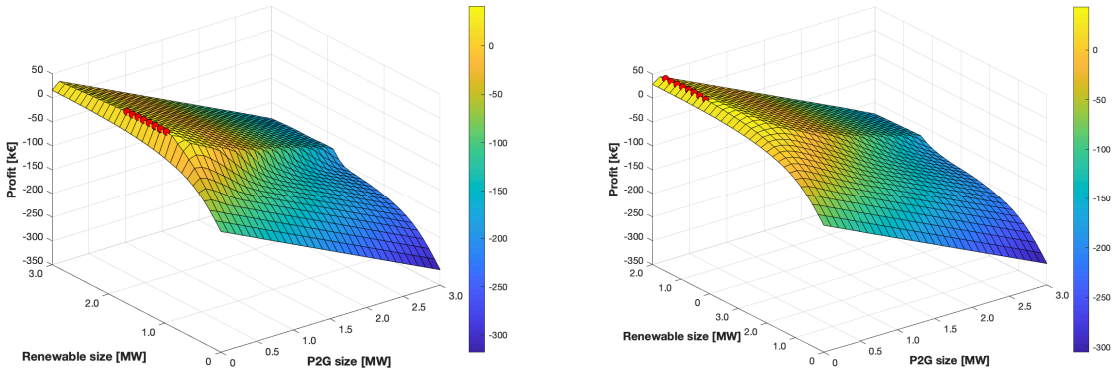

a) b)

Fig. 6.20. The obtained profit from the optimization analysis for a set size of the G2P system (400 kW for the hydrogen system and 300 kW for the SNG system), in which the optimum points are highlighted in red: a) hydrogen system; b) SNG system.

In order to show the relationship between the revenue and the costs, Fig. 6.21 is presented. The revenue, for both the concepts, follows the behavior of the energy produced by the microgrid (see Fig. 6.15) and increases with the increase of the renewable size; this behavior can be explained by Eq. 6.2, in which the revenue is defined as a function of the sum of the products between the energy produced by the microgrid and the electricity price in a specific time. On the contrary, the costs are more affected by the P2G size due to the higher costs of this technology with respect to the other sub-sections (see Tab. 6.1). From the intersection of these two surfaces, only a limited area of points has the possibility to make a profit: indeed, the higher revenue with respect to the costs is the necessary but not sufficient condition to have a positive profit.

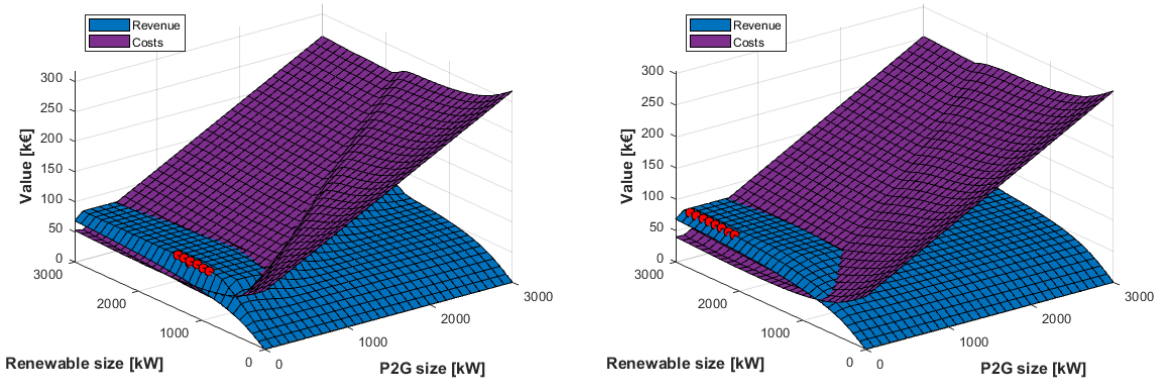

a) b)

Fig. 6.21. Comparison of the revenue and of the costs for a set size of the G2P system (400 kW for the hydrogen system and 300 kW for the SNG system), in which the optimum points are highlighted in red: a) hydrogen system; b) SNG system.

Finally, the instantaneous values of the main performance parameters, considering the optimum solutions, have been presented, respectively for the hydrogen system (Fig. 6.22) and

the SNG system (Fig. 6.23). Regarding the hydrogen concept, the microgrid is able to meet the demand for large periods during the year (E_{hybrid} indicated as *total output* in the figure); as a consequence, the electric energy requested to the grid shows a few peaks only in the periods of the year with a higher demand (during the summer). The energy losses are higher during the central part of the year. Compared to the hydrogen concept, the SNG system is able to meet the demand during the year too; however, this system shows higher losses due to the larger size of the renewable generator with respect to the hydrogen system (2400 kW for the SNG system and 1300 kW for the hydrogen system).

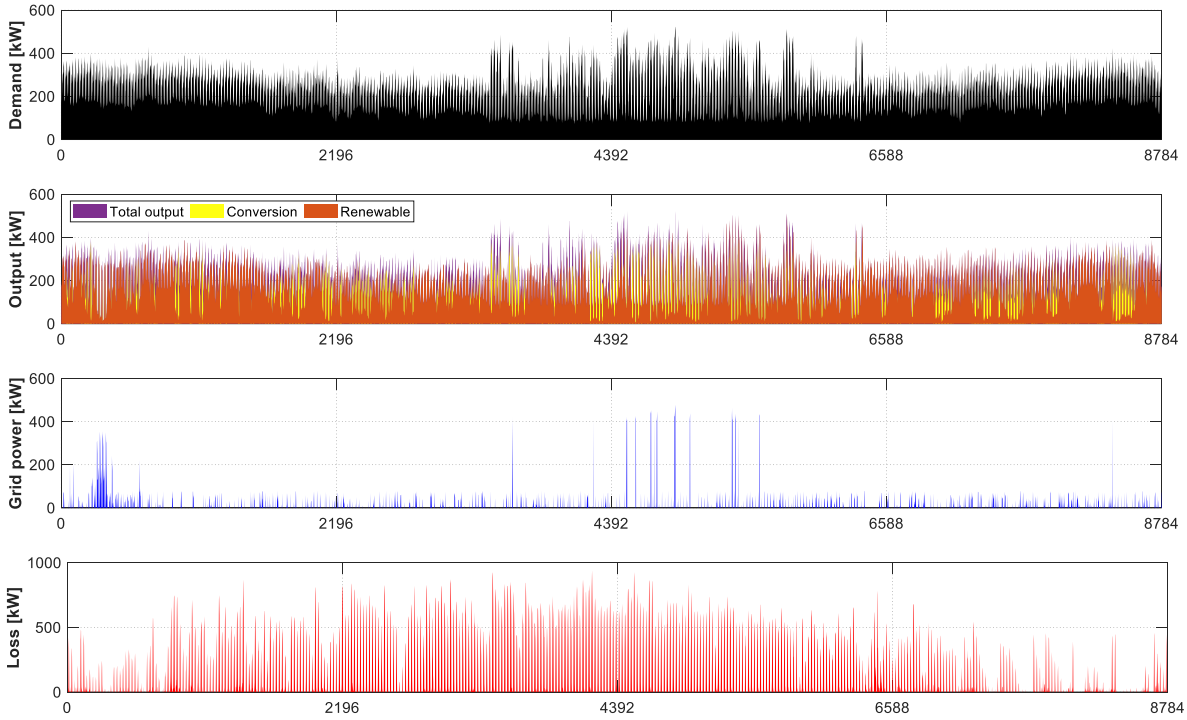

Fig. 6.22. Instantaneous values for the optimum solution during the year, considering the hydrogen system: a) user demand; b) output of the microgrid; c) power requested from the grid; d) energy losses.

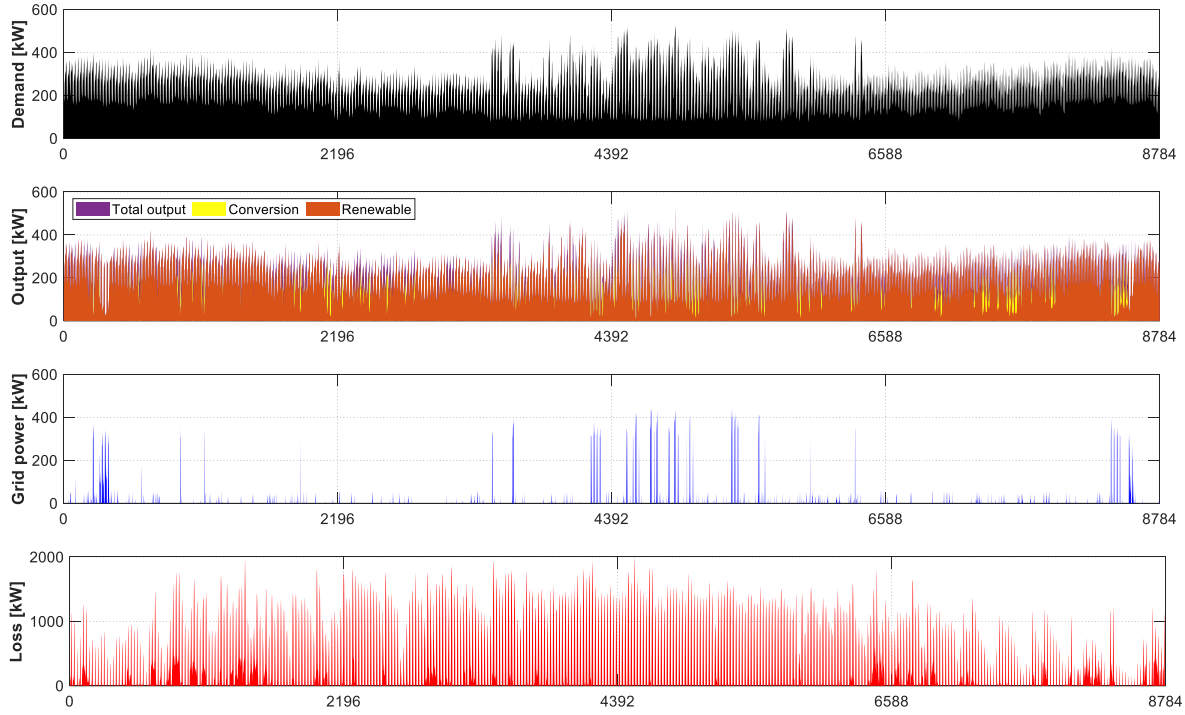

Fig. 6.23. Instantaneous values for the optimum solution during the year, considering the SNG system: a) user demand; b) output of the microgrid; c) power requested from the grid; d) energy losses.

6.4.3 - Sensitivity analysis results

In Fig. 6.24 the comparison between the revenue and the profit in the considered years is shown; in this case, the presented results are related to the optimum solution of each year. The revenue seems to follow the trend of the mean electricity price of each year (see Fig. 6.13b), with a maximum for the hydrogen system (Fig. 6.24a) equal to about 120'000 € in the year 2018 and a minimum of about 76'000 € in the year 2020. Also the SNG system (Fig. 6.24b) shows a similar trend, with a revenue comprised between 75'000 € (year 2020) and 120'000 € (year 2018). Regarding the profit, this parameter is affected by the mean electricity price too; indeed, both the P2G concepts show a maximum in the year 2018, with a value of about 85'000 € for the hydrogen system and of about 90'000 € for the SNG system..

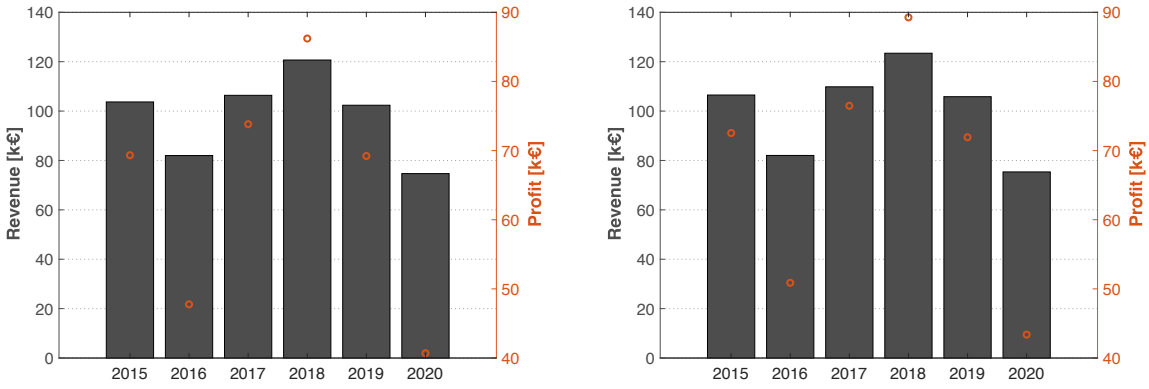

Fig. 6.24. Comparison of the revenue and the profit in the considered years (2015 - 2020) for the optimized configurations, considering the Italian scenario: a) hydrogen system; b) SNG system.

Regarding the costs (Fig. 6.25), the main part is represented by the O&M costs, with a share of about 86 % in the total costs in the considered years for the SNG concept and a share of about 84 % for the hydrogen system. In this case, the costs are less affected by the electricity price variability with respect to the profit and the revenue: indeed, the O&M costs, that represent the main part of the total costs, are not affected by the electricity price but only by the size of the devices (see Eq. 6.4) and by the equivalent hours of functioning. However, as shown in Tab. 6.2, the size of the several sub-sections does not vary significantly in the considered years and the size ratios among the devices tend to be preserved.

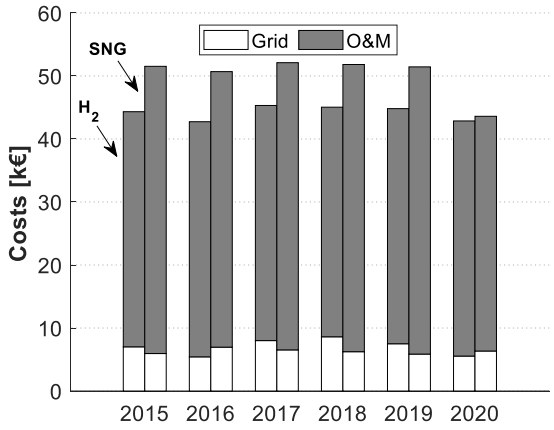

Fig. 6.25. Distribution of the costs in the considered years (2015 - 2020) for the optimized configurations of the considered P2G concepts (hydrogen and SNG), taking into account the Italian scenario.

Tab. 6.2. Optimum configuration sizes in the considered years (2015 - 2020) for the considered P2G concepts (hydrogen and SNG), taking into account the Italian scenario. Sizes are expressed in [kW].

	Hydrogen			SNG		
	Renewable	**P2G**	**G2P**	**Renewable**	**P2G**	**G2P**
2015	1500	100	400	2600	100	400
2016	1300	100	400	2400	100	300
2017	1500	100	400	2600	100	400
2018	1500	100	400	2700	100	400
2019	1500	100	400	2600	100	400
2020	1300	100	400	2400	100	300

In Fig. 6.26 the trend of the profit as a function of the mean annual price of the electricity is presented. The scenarios based on a possible increase of the electricity lead to values of the profit higher with respect to the results obtained in the historical scenarios; for example, an increase of almost an order of magnitude in the economic outputs for a scenario of price equal to 200 €/MWh is observed.

Finally, the results of a further parametric analysis on the effect of the operating costs of the components on the economic performance of the overall system are shown in Fig. 6.27. A hypothetical reduction of the operating and maintenance cost of the P2G section equal to 80 % leads to a decrease in the specific size of both the NP-RES and G2P systems in the case of the SNG system; regarding the H_2 system, the specific sizes tend to be preserved.

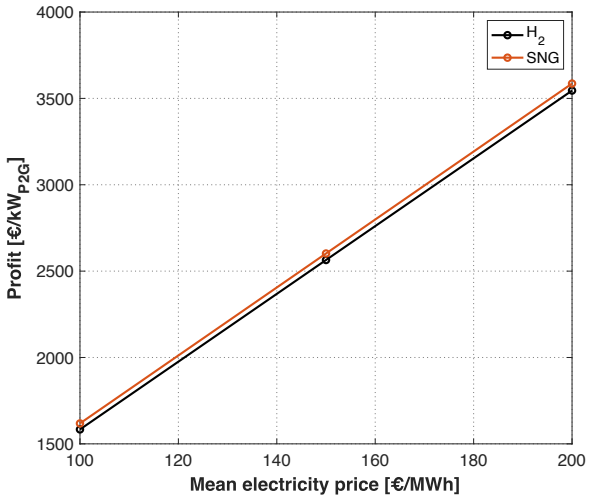

Fig. 6.26. Obtainable profit in correspondence of the economic optimum point for several values of mean electricity price.

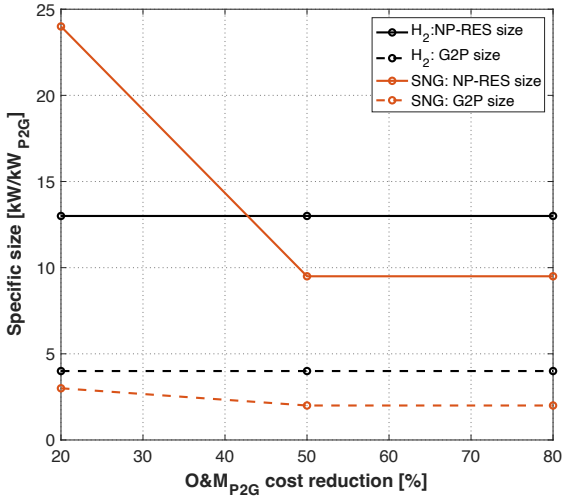

Fig. 6.27. Trend of the NP-RES and G2P system sizes as a function of P2G cost reduction, for the year 2020.

6.5 - Considerations

In this chapter, an innovative comparison between different P2G concepts, in scenario in which also G2P systems and a user demand are considered, has been proposed. The aim of the study is to compare the behavior of different storage paths when integrated in a real scenario of functioning, with a real renewable production and a real electrical demand. The P2G concepts that have been considered differ on the used energy vector: one line is based on the hydrogen and the other line on the SNG. Firstly, the system has been analyzed from the energetic point of view by means of a developed management strategy. Indeed, setting the electrical demand, the other components' size has been varied in a large range in order to figure out the performance of the overall microgrid on the basis of the different size ratios among the devices. Results show that combinations of large renewable generators with undersized storage systems (with respect to the renewable generator) lead to high energy production but high energy losses too.

After the simulation of the whole microgrid, a decision-making parameter has been defined in order to establish the best solution among the obtained results and then optimize the overall performance. In this study a novel optimization method has been developed, based on an approach that takes into account the variability of the electricity purchase price. With this original approach, configurations with a highly oversized renewable source with respect to the storage and the G2P systems show a maximum achievable profit of about 33 €/$kW_{NP\text{-}RES}$·year for the hydrogen concept and equal to about 18 €/$kW_{NP\text{-}RES}$·year for the SNG concept. Finally, in order to evaluate the effect of different economic inputs on the optimization model, a sensitivity analysis has been carried out, showing that the profit is more affected by the mean

electricity price of the year, while the size ratios of the optimum configurations tend to be preserved.

The economic potential of using P2G systems based on methane synthesis is related to:

- the use of an already existing natural gas distribution network; this aspect, due to the increase of the renewable source exploitation, could be advantageous with respect to the development of new electric infrastructures and new distribution networks for the hydrogen;
- possible savings from avoided carbon dioxide emissions.

In addition, it should be highlighted that the potential of the P2G technologies is greater in large areas (regional/national), where the transport and distribution costs are relevant.

Chapter 7 – Conclusion

In order to meet the climate targets, energy production must come mainly from renewable sources. However, power supply from wind and solar will be different than demand at times; energy has therefore to be stored to be made available when needed. As a consequence, the long-term and large-scale storage demand for high energy density, low costs and little self-discharging will be boosted in the near future. One option to these needs is to use the Power-to-Gas technology, which allows to store electric power by producing renewable hydrogen or renewable methane.
In this context, in the PhD research project a particular and innovative P2G system has been developed. This system is composed by a high temperature section and a low temperature section. The high temperature section is composed by two innovative components: 1) a high temperature co-electrolyzer of SOEC technology; 2) a high temperature methanation sub-section, based on an experimental structured catalyst. The low temperature section, instead, has been implemented in order to improve the quality of the produced SNG. In particular, this section is composed by: 1) a low temperature methanation section, based on a conventional catalytic technology; 2) a SNG upgrading section. In addition, a pre-heating section has been implemented in order to achieve significant energy savings by means of internal heat recovery.

As a preliminary step of the research activity, the proposed P2G concept has been introduced and the developed numerical model has been described. The originality of the developed model is represented by the possibility to predict the performance of any P2G process in conditions far from the design point, on the basis of a limited set of experimental data.

In a first approach, a thermodynamic design analysis has been carried out; starting from the obtained results, a selection among the best solutions has been made:

- P-TAIL 850/450/200 case: configuration with SOEC, HTM and LTM operating at ambient pressure, with the SNG pressurization downstream of the last methanation reactor, with different operating temperatures for the key components (the SOEC operating at 850 °C, the experimental methanator at 450 °C and the commercial methanation section at 200 °C); this configuration shows first law efficiency η_I values equal to about 78 % and a methane molar fraction in the produced SNG equal to about 80 %;
- P-TAIL 600/600/200 case: configuration in which the SOEC and the experimental methanator are operated at the same temperature (both at 600 °C); compared to the previous one, this configuration shows higher values from the point of view of the

efficiency parameters η_{E2F}, η_I and η_{II} (the first law efficiency is slightly higher and close to 79 %), but a lower methane molar fraction in the produced SNG is noticed;

- P-SOEC 850/450/200 case: pressurized configuration, with the SOEC operating at 850 °C, the experimental methanator at 450 °C and the commercial methanation section at 200 °C; this configuration shows the highest values in terms of x_{CH4}, but the lowest efficiency values;
- P-SOEC 600/600/200 case: configuration that differs from the previous since the SOEC and the experimental methanator are operated at the same temperature (both at 600 °C); the performance parameters vary with respect to the previous case in the same direction as in the P-TAIL 600/600/200 case with respect to the P-TAIL 850/450/200, but with a greater variation;
- P-LTM 600/600/200 case: intermediate pressure configuration, with the pressurization starting from the low temperature methanation section and the SOEC and the experimental methanator operating at ambient pressure; SOEC and HTM work at 600 °C, while the low temperature methanation section operates at 200 °C; this configuration represents a trade-off solution between the goal of maximizing the efficiency and maximizing the quality of the produced SNG. In addition, this case is in line with one of the aims of the study to identify a single operating temperature for the co-electrolyser and for the experimental methanator (also in this case equal to 600 °C).

In a second approach, by means of the developed calculation model for the simulation of the P2G system in off-design conditions, an analysis on the behaviour of the whole P2G system in variable load conditions has been carried out. The results of this analysis have highlighted that the following parameters affect the energy performance of the P2G system:
1) the ratio between the size of the P2G system and the size of the NP-RES generator;
2) the type of coupled NP-RES generator;
3) the related monotonous production profile.

In particular, it is possible to identify a size ratio *R* that allows to maximize the use of electric energy produced by the NP-RES; with the assumed hypotheses, the optimal value of *R* is equal to about 3.7 (4.0) in the case of the large-scale dimensionless study, considering a wind (solar) source. The operating time of the P2G system, for the considered scenarios, shows values equal to about 5300 h/year and the energy utilization and conversion factor can reach values up to about 70 %. On the other hand, in the case with a single NP-RES generator (small-scale dimensional study) the performance vary on the basis of the production site profile and of the size of the P2G system. In the analysed case, the optimal sizes of the P2G system which allow to maximize the production of SNG and the efficiency are different (higher) with respect to those obtained in the case of the large-scale dimensionless study. The performance in terms

of first law efficiency and of the utilization factor are, instead, similar to the values obtained in the large-scale dimensionless study.

Finally, an innovative comparison between different P2G concepts, in scenario in which also G2P systems and a user demand are considered, has been proposed; this research has been carried out during the PhD period abroad, at the École Polytechnique Fédérale de Lausanne (EPFL) – Valais offices. The aim of the study is to compare the behavior of different storage paths when integrated in a real scenario of functioning, with a real renewable production and a real electrical demand. The P2G concepts that have been considered differ on the used energy vector: one line is based on the hydrogen and the other line on the SNG. Firstly, the system has been analyzed from the energetic point of view by means of a developed management strategy. Results show that combinations of large renewable generators with undersized storage systems (with respect to the renewable generator) lead to high energy production but high energy losses too. Then, a decision-making parameter has been defined in order to identify the best solution among the obtained results and then optimize the overall performance. A novel optimization method has been developed, based on an approach that takes into account the variability of the electricity purchase price. With this approach, configurations with a highly oversized renewable source with respect to the storage and the G2P systems show a maximum achievable profit of about 33 €/$kW_{NP\text{-}RES}$·year for the hydrogen concept and equal to about 18 €/$kW_{NP\text{-}RES}$·year for the SNG concept.
Finally, in order to evaluate the effect of different economic inputs on the optimization model, a sensitivity analysis has been carried out, showing that the profit is more affected by the mean electricity price of the year, while the size ratios of the optimum configurations tend to be preserved.
The economic potential of using P2G systems based on methane synthesis is related to:

- the use of an already existing natural gas distribution network; this aspect, due to the increase of the renewable source exploitation, could be advantageous with respect to the development of new electric infrastructures and new distribution networks for the hydrogen;
- possible savings from avoided carbon dioxide emissions.

In addition, it should be highlighted that the potential of the P2G technologies is greater in large areas (regional/national), where the transport and distribution costs are relevant.

Appendix A

Several performance parameters are considered and used in the analysis. Firstly, the storage system performance can be quantified in terms of energy conversion efficiency, i.e. rate of electric energy converted into chemical energy of the produced SNG. However, with this preliminary approach, thermal needs are not considered. Heat demand represents a key element of the considered high-temperature storage system, and in order to account for this aspect it is necessary to analyse the whole thermodynamic balance, including all the involved input thermal flows. Moreover, due to the presence of variable levels of temperature, it is necessary to evaluate the thermodynamic efficiency of the storage system both via a first-law approach and with a second-law assessment. Finally, in order to introduce the produced SNG into the natural gas distribution network, SNG quality parameters must be also taken into account.
In detail, the performance indicators applied for the P2G analysis are presented in the following list:

- The electric-to-fuel conversion index, defined as follows:

$$\eta_{E2F(LHV)} = \frac{\dot{m}_{SNG} LHV_{SNG}}{P_{e,IN}}$$

where $\dot{m}_{SNG}$ [kg/s] is the mass flow of produced SNG, LHV_{SNG} [kJ/kg] is the lower heating value of the SNG, $P_{e,IN}$ [kW] is the system inlet electric power, including both the SOEC input electric power and the auxiliaries electric power consumption. The electric-to-fuel conversion index has also been evaluated referring to the higher heating value (HHV_{SNG}):

$$\eta_{E2F(HHV)} = \frac{\dot{m}_{SNG} HHV_{SNG}}{P_{e,IN}}$$

- The first law efficiency, defined as follows:

$$\eta_{I(LHV)} = \frac{\dot{m}_{SNG} LHV_{SNG}}{P_{e,IN} + Q_{IN}}$$

where Q_{IN} [kW] is the total amount of input heat required by the process. Also in this case, the first law efficiency has been evaluated referring to the HHV_{SNG}:

$$\eta_{I(HHV)} = \frac{\dot{m}_{SNG} HHV_{SNG}}{P_{e,IN} + Q_{IN}}$$

- The second-law efficiency, defined as follows:

$$\eta_{II} = \frac{\dot{m}_{SNG} \cdot ex_{SNG}}{Ex_{in}} = \frac{\dot{m}_{SNG} \cdot ex_{SNG}}{Ex_{in,f} + Ex_{in,Q} + Ex_{in,Pe}} = \frac{\dot{m}_{SNG} \cdot ex_{SNG}}{\sum \dot{m}_{in} \cdot ex_{in,f} + Ex_{in,Q} + Ex_{in,Pe}}$$

where $Ex_{in,f}$ [kJ] represents the exergy of the system inlet mass streams, $Ex_{in,Q}$ [kJ] the exergy of heat fluxes and $Ex_{in,Pe}$ [kJ] the exergy related to the inlet electric power, while the corresponding mass specific exergy contributions are indicated as ex [kJ/kg]. Exergy represents the maximum useful work possible during a process that brings the system into equilibrium with surroundings environment.
Mass specific exergy of inlet mass streams and outlet produced SNG are calculated as:

$$ex_{in,f} = ex_{in,Ph} + ex_{in,Mix} + ex_{in,Chem}$$

$$ex_{SNG} = ex_{SNG,Ph} + ex_{SNG,Mix} + ex_{SNG,Chem}$$

The above equations include the physical exergy ($ex_{in,Ph}$ and $ex_{SNG,Ph}$), a contribution related to components mixing ($ex_{in,Mix}$ and $ex_{SNG,Mix}$) and a chemical contribution ($ex_{in,Chem}$ and $ex_{SNG,Chem}$). The specific physical exergy is defined as:

$$ex_{Ph} = \Delta h - T_0 \Delta s = (h - h_0) - T_0(s - s_0)$$

where T_0 [K], h_0 [kJ/kg] and s_0 [kJ/kgK] are respectively temperature, specific enthalpy and specific entropy in reference conditions (T_0 = 25 °C, p_0 = 1 bar). Specific exergy of mixing type is defined as:

$$ex_{Mix} = \frac{R_0}{M_m} T_0 \sum_i \left[\ln\left(\frac{1}{y_i}\right) y_i \right]$$

where R_0 represents the universal gas constant [kJ/kmolK], M_m [kg/kmol] the molecular mass of the mixture and y_i [-] the molar fraction of the i-th component of the mixture.
Specific exergy of chemical type can be expressed as:

$$ex_{Chem} = \frac{1}{M_m}\sum_i \left(ex^0_{i,mol} \cdot y_i\right)$$

where $ex^0_{i,mol}$ [kJ/kmol] is the specific molar exergy related to a reference physical state of the i-th component.
Finally, the exergy related to a generic thermal input (Q) is defined as follows:

$$Ex_{in,Q} = Q\left(1 - \frac{T_0}{T}\right)$$

where T [K] is the considered final heating temperature level at which Q is available.

- Quality of the produced SNG. In order to consider that the produced SNG can contain several components besides methane, the following additional SNG quality parameters are monitored:

  - total output methane mass flow rate;
  - volume fraction of methane and residual species in the produced SNG;
  - LHV and HHV of the SNG;
  - Wobbe Index (WI), indicator of interchangeability of fuel gases with respect to natural gas, defined as:

$$WI = \frac{HHV}{\sqrt{\rho_{SNG}/\rho_{air}}}$$

where, ρ_{SNG} and ρ_{air} are respectively the density of the produced SNG and of the air [kg/Sm^3], both evaluated at standard conditions. ρ_{air} has been set to a value equal to 1.22 kg/Sm^3.

- Heat recovery indices. In the several considered configurations, in order to increase the overall performance of the system, thermal recoveries have been introduced. Since during the simulations the temperature and pressure levels vary, the heat exchanges in the heat exchangers will be different from case to case and, as a consequence, it has been necessary to introduce indices in order to take into account the heat recovery. In particular, the following parameters have been considered: the thermal power introduced from an external source ($Q_{IN,TOT}$), given by the sum of the heat necessary to heat up the water and the carbon dioxide; the total thermal power required by the P2G system ($Q_{requested}$); the

thermal power recovered by the heat exchangers in the preheating section ($Q_{recovered}$). These quantities are linked to each other through the following relationship:

$$Q_{requested} = Q_{IN,TOT} + Q_{recovered}$$

Finally, in order to evaluate the efficiency of the heat recovery, the index of recovery (IR) has been introduced, defined as follows:

$$IR = \frac{Q_{recovered}}{Q_{requested}}$$

References

[1] T. CABUZEL, '2030 Climate Target Plan', *Climate Action - European Commission*, Sep. 11, 2020. https://ec.europa.eu/clima/policies/eu-climate-action/2030_ctp_en (accessed Oct. 05, 2021).

[2] M. Karimi, H. Mokhlis, K. Naidu, S. Uddin, and A. H. A. Bakar, 'Photovoltaic penetration issues and impacts in distribution network – A review', *Renew. Sustain. Energy Rev.*, vol. 53, pp. 594–605, Jan. 2016, doi: 10.1016/j.rser.2015.08.042.

[3] M. A. Eltawil and Z. Zhao, 'Grid-connected photovoltaic power systems: Technical and potential problems—A review', *Renew. Sustain. Energy Rev.*, vol. 14, no. 1, pp. 112–129, Jan. 2010, doi: 10.1016/j.rser.2009.07.015.

[4] C. Jung, D. Taubert, and D. Schindler, 'The temporal variability of global wind energy – Long-term trends and inter-annual variability', *Energy Convers. Manag.*, vol. 188, pp. 462–472, May 2019, doi: 10.1016/j.enconman.2019.03.072.

[5] 'Innovative large-scale energy storage technologies and Power-to-Gas concepts after optimisation Roadmap for large-scale storage base PtG conversion in the EU up to 2050', *STORE&GO*. https://www.storeandgo.info/publications/press-articles/ (accessed Oct. 05, 2021).

[6] Ş. Kılkış, G. Krajačić, N. Duić, M. A. Rosen, and M. A. Al-Nimr, 'Advances in integration of energy, water and environment systems towards climate neutrality for sustainable development', *Energy Convers. Manag.*, vol. 225, p. 113410, Dec. 2020, doi: 10.1016/j.enconman.2020.113410.

[7] M. Greiml, F. Fritz, and T. Kienberger, 'Increasing installable photovoltaic power by implementing power-to-gas as electricity grid relief – A techno-economic assessment', *Energy*, vol. 235, p. 121307, Nov. 2021, doi: 10.1016/j.energy.2021.121307.

[8] W. Wei and G. Jinlong, 'Methanation of carbon dioxide: an overview', *Front. Chem. Sci. Eng.*, vol. 5, no. 1, pp. 2–10, Mar. 2011, doi: 10.1007/s11705-010-0528-3.

[9] S. F. Cannone, A. Lanzini, and M. Santarelli, 'A Review on CO2 Capture Technologies with Focus on CO2-Enhanced Methane Recovery from Hydrates', *Energies*, vol. 14, no. 2, p. 387, Jan. 2021, doi: 10.3390/en14020387.

[10] S. Anwar, F. Khan, Y. Zhang, and A. Djire, 'Recent development in electrocatalysts for hydrogen production through water electrolysis', *Int. J. Hydrog. Energy*, vol. 46, no. 63, pp. 32284–32317, Sep. 2021, doi: 10.1016/j.ijhydene.2021.06.191.

[11] O. Schmidt, A. Gambhir, I. Staffell, A. Hawkes, J. Nelson, and S. Few, 'Future cost and performance of water electrolysis: An expert elicitation study', *Int. J. Hydrog. Energy*, vol. 42, no. 52, pp. 30470–30492, Dec. 2017, doi: 10.1016/j.ijhydene.2017.10.045.

[12] Y. Zheng *et al.*, 'A review of high temperature co-electrolysis of H_2O and CO_2 to produce sustainable fuels using solid oxide electrolysis cells (SOECs): advanced materials and technology', *Chem. Soc. Rev.*, vol. 46, no. 5, pp. 1427–1463, 2017, doi: 10.1039/C6CS00403B.

[13] M. Gruber *et al.*, 'Power-to-Gas through thermal integration of high-temperature steam electrolysis and carbon dioxide methanation - Experimental results', *Fuel Process. Technol.*, vol. 181, pp. 61–74, Dec. 2018, doi: 10.1016/j.fuproc.2018.09.003.

[14] B. Meier, F. Ruoss, and M. Friedl, 'Investigation of Carbon Flows in Switzerland with the Special Consideration of Carbon Dioxide as a Feedstock for Sustainable Energy Carriers', *Energy Technol.*, vol. 5, no. 6, pp. 864–876, Jun. 2017, doi: 10.1002/ente.201600554.

[15] Z. Li, H. Zhang, H. Xu, and J. Xuan, 'Advancing the multiscale understanding on solid oxide electrolysis cells via modelling approaches: A review', *Renew. Sustain. Energy Rev.*, vol. 141, p. 110863, May 2021, doi: 10.1016/j.rser.2021.110863.

[16] 'technology_data_for_renewable_fuels.pdf'. Accessed: Oct. 06, 2021. [Online]. Available: https://ens.dk/sites/ens.dk/files/Analyser/technology_data_for_renewable_fuels.pdf

[17] L. Wang, M. Pérez-Fortes, H. Madi, S. Diethelm, J. V. herle, and F. Maréchal, 'Optimal design of solid-oxide electrolyzer based power-to-methane systems: A comprehensive comparison between steam electrolysis and co-electrolysis', *Appl. Energy*, vol. 211, pp. 1060–1079, Feb. 2018, doi: 10.1016/j.apenergy.2017.11.050.

[18] M. Liao, C. Liu, and Z. Qing, 'A Recent Overview of Power-to-Gas Projects', in *2020 IEEE 4th Conference on Energy Internet and Energy System Integration (EI2)*, Wuhan, China, Oct. 2020, pp. 2282–2286. doi: 10.1109/EI250167.2020.9346826.

[19] S. Rönsch *et al.*, 'Review on methanation – From fundamentals to current projects', *Fuel*, vol. 166, pp. 276–296, Feb. 2016, doi: 10.1016/j.fuel.2015.10.111.

[20] B. Nastasi, S. Mazzoni, D. Groppi, A. Romagnoli, and D. Astiaso Garcia, 'Solar power-to-gas application to an island energy system', *Renew. Energy*, vol. 164, pp. 1005–1016, Feb. 2021, doi: 10.1016/j.renene.2020.10.055.

[21] M. Momeni, M. Soltani, M. Hosseinpour, and J. Nathwani, 'A comprehensive analysis of a power-to-gas energy storage unit utilizing captured carbon dioxide as a raw material in a large-scale power plant', *Energy Convers. Manag.*, vol. 227, p. 113613, Jan. 2021, doi: 10.1016/j.enconman.2020.113613.

[22] B. Xiong, J. Predel, P. Crespo del Granado, and R. Egging-Bratseth, 'Spatial flexibility in redispatch: Supporting low carbon energy systems with Power-to-Gas', *Appl. Energy*, vol. 283, p. 116201, Feb. 2021, doi: 10.1016/j.apenergy.2020.116201.

[23] J. Liu, W. Sun, and J. Yan, 'Effect of P2G on Flexibility in Integrated Power-Natural Gas-Heating Energy Systems with Gas Storage', *Energies*, vol. 14, no. 1, p. 196, Jan. 2021, doi: 10.3390/en14010196.

[24] W. Wang, C. Cheng, X. Liu, J. Liu, C. Long, and W. Chen, 'Research on the electricity-gas coupling system with P2G to absorb surplus hydropower', *E3S Web Conf.*, vol. 300, p. 01016, 2021, doi: 10.1051/e3sconf/202130001016.

[25] J. zhai, Y. Li, F. Li, and X. Zhou, 'Effect of P2G on Suppression of New Energy Fluctuations and Carbon Capture and Dynamic Simulation of Gas Pipeline', *IOP Conf. Ser. Earth Environ. Sci.*, vol. 657, p. 012061, Feb. 2021, doi: 10.1088/1755-1315/657/1/012061.

[26] E. Giglio, A. Lanzini, M. Santarelli, and P. Leone, 'Synthetic natural gas via integrated high-temperature electrolysis and methanation: Part I—Energy performance', *J. Energy Storage*, vol. 1, pp. 22–37, Jun. 2015, doi: 10.1016/j.est.2015.04.002.

[27] A. Vita, C. Italiano, L. Pino, P. Frontera, M. Ferraro, and V. Antonucci, 'Activity and stability of powder and monolith-coated Ni/GDC catalysts for CO2 methanation', *Appl. Catal. B Environ.*, vol. 226, pp. 384–395, Jun. 2018, doi: 10.1016/j.apcatb.2017.12.078.

[28] C. Italiano, J. Llorca, L. Pino, M. Ferraro, V. Antonucci, and A. Vita, 'CO and CO2 methanation over Ni catalysts supported on CeO2, Al2O3 and Y2O3 oxides', *Appl. Catal. B Environ.*, vol. 264, p. 118494, May 2020, doi: 10.1016/j.apcatb.2019.118494.

[29] M. Lo Faro, S. C. Zignani, S. Trocino, V. Antonucci, and A. S. Aricò, 'New insights on the co-electrolysis of CO2 and H2O through a solid oxide electrolyser operating at intermediate temperatures', *Electrochimica Acta*, vol. 296, pp. 458–464, Feb. 2019, doi: 10.1016/j.electacta.2018.11.079.

[30] V. Eveloy and T. Gebreegziabher, 'A Review of Projected Power-to-Gas Deployment Scenarios', *Energies*, vol. 11, no. 7, Art. no. 7, Jul. 2018, doi: 10.3390/en11071824.

[31] C. Wulf, J. Linßen, and P. Zapp, 'Review of Power-to-Gas Projects in Europe', *Energy Procedia*, vol. 155, pp. 367–378, Nov. 2018, doi: 10.1016/j.egypro.2018.11.041.

[32] M. A. Laguna-Bercero, 'Recent advances in high temperature electrolysis using solid oxide fuel cells: A review', *J. Power Sources*, vol. 203, pp. 4–16, Apr. 2012, doi: 10.1016/j.jpowsour.2011.12.019.

[33] H. T. A/S (HQ), 'SNG | Methanation | Catalytic methanation | Haldor Topsoe'. https://www.topsoe.com/processes/sng/methanation (accessed Oct. 07, 2021).

[34] 'Aspen HYSYS | Process Simulation Software | AspenTech'. https://www.aspentech.com/en/products/engineering/aspen-hysys (accessed Oct. 07, 2021).

[35] Y. Redissi and C. Bouallou, 'Valorization of Carbon Dioxide by Co-Electrolysis of CO2/H2O at High Temperature for Syngas Production', *Energy Procedia*, vol. 37, pp. 6667–6678, 2013, doi: 10.1016/j.egypro.2013.06.599.

[36] X. Sun, M. Chen, S. H. Jensen, S. D. Ebbesen, C. Graves, and M. Mogensen, 'Thermodynamic analysis of synthetic hydrocarbon fuel production in pressurized solid oxide electrolysis cells', *Int. J. Hydrog. Energy*, vol. 37, no. 22, pp. 17101–17110, Nov. 2012, doi: 10.1016/j.ijhydene.2012.08.125.

[37] M. Samavati, M. Santarelli, A. Martin, and V. Nemanova, 'Thermodynamic and economy analysis of solid oxide electrolyser system for syngas production', *Energy*, vol. 122, pp. 37–49, Mar. 2017, doi: 10.1016/j.energy.2017.01.067.

[38] C. M. Stoots, J. E. O'Brien, J. S. Herring, and J. J. Hartvigsen, 'Syngas Production via High-Temperature Coelectrolysis of Steam and Carbon Dioxide', *J. Fuel Cell Sci. Technol.*, vol. 6, no. 1, p. 011014, Feb. 2009, doi: 10.1115/1.2971061.

[39] J. P. Stempien, O. L. Ding, Q. Sun, and S. H. Chan, 'Energy and exergy analysis of Solid Oxide Electrolyser Cell (SOEC) working as a CO2 mitigation device', *Int. J. Hydrog. Energy*, vol. 37, no. 19, pp. 14518–14527, Oct. 2012, doi: 10.1016/j.ijhydene.2012.07.065.

[40] S. D. Ebbesen, J. Høgh, K. A. Nielsen, J. U. Nielsen, and M. Mogensen, 'Durable SOC stacks for production of hydrogen and synthesis gas by high temperature electrolysis', *Int. J. Hydrog. Energy*, vol. 36, no. 13, pp. 7363–7373, Jul. 2011, doi: 10.1016/j.ijhydene.2011.03.130.

[41] M. A. Ancona *et al.*, 'Renewable Energy Storage System Based on a Power-to-Gas Conversion Process', *Energy Procedia*, vol. 101, pp. 854–861, Nov. 2016, doi: 10.1016/j.egypro.2016.11.108.

[42] J. H. Jensen, J. M. Poulsen, and N. U. Andersen, 'Converting even low grade coal to clean Substitute Natural Gas (SNG) is not only feasible but highly attractive from the perspectives of the environment, security of energy supply, use of available (domestic) resources and economics.', p. 5, 2011.

[43] M. A. Ancona *et al.*, 'Thermal integration of a high-temperature co-electrolyzer and experimental methanator for Power-to-Gas energy storage system', *Energy Convers. Manag.*, vol. 186, pp. 140–155, Apr. 2019, doi: 10.1016/j.enconman.2019.02.057.

[44] S.-W. Kim *et al.*, 'Reactions and mass transport in high temperature co-electrolysis of steam/CO2 mixtures for syngas production', *J. Power Sources*, vol. 280, pp. 630–639, Apr. 2015, doi: 10.1016/j.jpowsour.2015.01.083.

[45] C. Graves, S. D. Ebbesen, and M. Mogensen, 'Co-electrolysis of CO2 and H2O in solid oxide cells: Performance and durability', *Solid State Ion.*, vol. 192, no. 1, pp. 398–403, Jun. 2011, doi: 10.1016/j.ssi.2010.06.014.

[46] M. T. Mehran *et al.*, 'Production of syngas from H2O/CO2 by high-pressure coelectrolysis in tubular solid oxide cells', *Appl. Energy*, vol. 212, pp. 759–770, Feb. 2018, doi: 10.1016/j.apenergy.2017.12.078.

[47] 'Snam home page'. https://www.snam.it/en (accessed Oct. 07, 2021).

[48] 'MATLAB - MathWorks'. https://uk.mathworks.com/products/matlab.html (accessed Oct. 07, 2021).

[49] M. T. Mehran *et al.*, 'Production of syngas from H2O/CO2 by high-pressure coelectrolysis in tubular solid oxide cells', *Appl. Energy*, vol. 212, pp. 759–770, Feb. 2018, doi: 10.1016/j.apenergy.2017.12.078.

[50]'Aicart - 2014 - Modélisation et validation expérimentale d'un co-é.pdf'.

[51]M. Manno, 'Materiale didattico di supporto al corso di Macchine 4', p. 155.

[52]H. I. H. Saravanamuttoo, G. F. C. Rogers, and H. Cohen, *Gas Turbine Theory*. Pearson Education, 2001.

[53]R. Kurz, S. Ohanian, and M. Lubomirsky, 'On Compressor Station Layout', Feb. 2009, pp. 1–10. doi: 10.1115/GT2003-38019.

[54]V. Dossena, G. Ferrari, and P. Gaetani, *Macchine a fluido*. Milano: CittàStudi edizioni, 2015.

[55]D. Beevers, 'Pumped hydro storage plants with improved operational flexibility using constant speed Francis runners', *Appl. Energy*, p. 9, 2015.

[56]R. Kurz and K. Brun, 'Process Control for Compression Systems', presented at the ASME Turbo Expo 2017: Turbomachinery Technical Conference and Exposition, Aug. 2017. doi: 10.1115/GT2017-63005.

[57]E. I. Koytsoumpa and S. Karellas, 'Equilibrium and kinetic aspects for catalytic methanation focusing on CO2 derived Substitute Natural Gas (SNG)', *Renew. Sustain. Energy Rev.*, vol. 94, pp. 536–550, Oct. 2018, doi: 10.1016/j.rser.2018.06.051.

[58]M. A. Ancona *et al.*, 'Numerical prediction of off-design performance for a Power-to-Gas system coupled with renewables', *Energy Convers. Manag.*, vol. 210, p. 112702, Apr. 2020, doi: 10.1016/j.enconman.2020.112702.

[59]'Terna Driving Energy - Terna spa'. https://www.terna.it/en (accessed Oct. 07, 2021).

[60]M. A. Ancona *et al.*, 'Off-Design Performance Evaluation of a LNG Production Plant Coupled With Renewables', in *Volume 9: Oil and Gas Applications; Supercritical CO2 Power Cycles; Wind Energy*, Phoenix, Arizona, USA, Jun. 2019, p. V009T27A017. doi: 10.1115/GT2019-90495.

[61]'GSE'. https://www.gse.it/ (accessed Oct. 07, 2021).

[62]J. G. Smart and S. D. Salisbury, 'Plugged In: How Americans Charge Their Electric Vehicles', Idaho National Lab. (INL), Idaho Falls, ID (United States), INL/EXT-15-35584, Jul. 2015. doi: 10.2172/1369632.

[63]M. Muratori, 'Impact of uncoordinated plug-in electric vehicle charging on residential power demand', *Nat. Energy*, vol. 3, no. 3, pp. 193–201, Mar. 2018, doi: 10.1038/s41560-017-0074-z.

[64]'Residential Energy Consumption Survey (RECS) - Energy Information Administration'. https://www.eia.gov/consumption/residential/ (accessed Oct. 07, 2021).

[65]M. Kotisaari, O. Thomann, D. Montinaro, and J. Kiviaho, 'Evaluation of a SOE Stack for Hydrogen and Syngas Production: a Performance and Durability Analysis', *Fuel Cells*, vol. 17, no. 4, pp. 571–580, Aug. 2017, doi: 10.1002/fuce.201600166.

[66]L. Wang *et al.*, 'Power-to-methane via co-electrolysis of H2O and CO2: The effects of pressurized operation and internal methanation', *Appl. Energy*, vol. 250, pp. 1432–1445, Sep. 2019, doi: 10.1016/j.apenergy.2019.05.098.

[67]‘Wärtsilä 32 - diesel engine’. https://www.wartsila.com/marine/build/engines-and-generating-sets/diesel-engines/wartsila-32 (accessed Oct. 07, 2021).
[68]Y.-F. Guo, H.-C. Chen, and F.-C. Wang, ‘The development of a hybrid PEMFC power system’, *Int. J. Hydrog. Energy*, vol. 40, no. 13, pp. 4630–4640, Apr. 2015, doi: 10.1016/j.ijhydene.2015.01.169.
[69]‘GME - Gestore dei Mercati Energetici SpA’. https://mercatoelettrico.org/En/default.aspx (accessed Oct. 07, 2021).
[70]‘Renewable Power Generation Costs 2020’, p. 180, 2020.
[71]‘technology_data_catalogue_for_el_and_dh_-_0009.pdf’.